CONTENTS

NASA Technical Paper 1531

Dynamic Response of a Mach 2.5 Axisymmetric Inlet and Turbojet Engine With a Poppet-Valve-Controlled Inlet-Stability Bypass System When Subjected to Internal and External Airflow Transients

Bobby W. Sanders

JANUARY 1980

NASA

NASA Technical Paper 1531

Dynamic Response of a Mach 2.5 Axisymmetric Inlet and Turbojet Engine With a Poppet-Valve-Controlled Inlet-Stability Bypass System When Subjected to Internal and External Airflow Transients

Bobby W. Sanders
Lewis Research Center
Cleveland, Ohio

National Aeronautics
and Space Administration

**Scientific and Technical
Information Office**

1980

CONTENTS

SUMMARY

The throat of a Mach 2.5, mixed-compression inlet with 40-percent internal supersonic-area contraction was fitted with a stability bypass system that was designed to provide a large, stable airflow range. With this bypass system the inlet can operate near the optimum performance condition without being susceptible to inlet unstart as a result of small variations in inlet airflow. In previous research programs with the inlet attached to a coldpipe, pressure-activated poppet-valve control of the stability bypass airflow resulted in very large stable margins. As a further evaluation of this control system, the inlet was tested on a turbojet engine. Inlet-stability bypass performance was determined for several transient airflow disturbances, both internal and external. Internal airflow was varied by transient pulses in overboard-bypass-door area, power lever angle, and primary nozzle area. Propulsion system response to a compressor stall was also determined. External airflow was varied by means of a flat gust plate located upstream of the inlet. For reference, data were also included for a conventional fixed exit controlling the stability bypass bleed airflow.

At a free-stream Mach number of 2.5 the poppet-valve-controlled stability bypass system can provide greater inlet stability than a conventional bleed system. The addition of the stability bypass system to the inlet did not adversely affect the engine performance. Limited unstarted-inlet bleed performance data are presented.

INTRODUCTION

At flight speeds above Mach 2.0 an inlet with a mixture of internal and external compression allows optimum performance by supplying the engine with high-pressure airflow while maintaining minimum drag. In mixed-compression inlets, maintaining the terminal shock at the inlet throat gives the highest pressure recovery and least distortion at the engine entrance. However, mixed-compression inlets have an undesirable airflow characteristic known as "unstart," which may occur when the terminal shock is placed too near the inlet throat. A slight transient reduction in airflow can cause the terminal shock to move forward of the throat, where it is unstable and is abruptly expelled ahead of the inlet cowling. This shock expulsion, or unstart, rapidly reduces mass flow and pressure recovery and greatly increases drag. Inlet buzz, compressor stall, or combustor blowout may also occur. Obviously, an inlet unstart is extremely undesirable because of its effects not only on the propulsion system itself, but also on

the aircraft's aerodynamic qualities. If an unstart does occur, complex mechanical variations of the inlet geometry are required to reestablish the design operating conditions. An engine relight sequence will also be necessary if blowout occurs.

Both external airflow disturbances (such as atmospheric turbulence) and internal airflow disturbances (such as reduced engine airflow demand) can cause the inlet to unstart. For an internal disturbance the inlet should provide a margin in corrected airflow below the optimum without incurring unstart. This margin is defined as the stable airflow operating range. Conventional mixed-compression inlets can be designed to have a limited stable range that is provided by the ability of the performance bleed system to increase its airflow as the terminal shock moves upstream into the throat bleed region. With fixed bleed exit areas, this limited stable range may not be adequate to absorb many airflow transients encountered by a typical supersonic propulsion system. A larger stable airflow range is currently provided for these inlets by operating them supercritically, with a resultant loss in their performance. Since any loss in inlet performance is reflected directly as a loss in propulsion-system thrust and efficiency, supercritical operation should be avoided.

The necessary system stability can be provided without compromising steady-state performance (i.e., pressure recovery and distortion) by redesigning the inlet. The throat bleed system can be replaced with an inlet-stability bypass system capable of removing large amounts of airflow (ref. 1). (The nomenclature for the throat airflow-removal system has been changed since ref. 1 was published from throat-bypass system to inlet-stability bypass system.) This system prevents unstarts by removing airflow from the inlet throat to compensate for reduced diffuser-exit airflow demand. As shown in reference 1, inlet-stability bypass airflow can be greatly increased without removing prohibitive amounts of airflow during normal operation if the stability bypass exit area can be controlled to maintain a relatively constant pressure in the bypass plenum. This stability bypass exit area control can be provided by pressure-activated valves (such as the poppet valve in ref. 2) at the bypass exit. The valves respond to small pressure increases in the bleed plenum induced by upstream movement of the terminal shock. References 3 to 6 show that the poppet valves of reference 2 can operate automatically to provide large, stable airflow margins for the inlet. The effectiveness of several stability bleed systems (e.g., distributed porous; distributed educated slot; and forward-slanted slot) is discussed in references 1, 3, and 6 to 10.

During the initial research on inlet-stability bypass bleed concepts and bypass airflow-control valves, the inlet was attached to a coldpipe, choked-exit-plug system. This test configuration allows the various concepts to be evaluated. However, the final merit of a concept can only be judged by integrating it into a complete propulsion system. Therefore, an inlet incorporating a stability bypass system and attached to a J85-GE-13 turbojet engine was tested in the Lewis 10- by 10-Foot Supersonic Wind Tunnel to evalu-

ate its performance, both steady state and dynamic. The inlet was a Mach 2.5, mixed-compression type with 40 percent of the supersonic-area contraction occurring internally.

During the investigation, data were obtained for two types of stability bypass exits: a small, conventional fixed exit (downstream of a small or large bypass plenum); and self-activated poppet valves. Both steady-state and transient data were recorded. Internal airflow disturbances were obtained by reducing overboard-bypass-door area, power lever angle, or primary-nozzle area. External airflow was varied by changing the angle of attack of a large flat gust plate upstream of the inlet. A control system was used for fast inlet restart and engine relight when the inlet unstarted. Limited steady-state bleed performance data were obtained at a free-stream Mach number of 2.5 with the inlet unstarted.

U.S. customary units were used in designing the test model and recording and computing the experimental data. These units were converted to the International System of Units (SI) for this report.

APPARATUS AND PROCEDURE

General Description

An NASA-designed supersonic inlet on a General Electric model J85-GE-13 turbojet engine was tested in the Lewis 10- by 10-Foot Supersonic Wind Tunnel at the following nominal free-stream conditions: Mach number 2.5; total pressure, 9.4 N/cm^2; total temperature, 302 K; Reynolds number, 4.3×10^6 (based on the cowl-lip diameter); and specific-heat ratio, 1.4. The engine operated from windmill to 90-percent corrected speed. When data were being taken with the engine running, the tunnel was operating on its propulsion cycle. In this cycle, the airflow downstream of the test section is vented to the atmosphere rather than recirculated as in the aerodynamic cycle. Figure 1 shows the engine and inlet, with nacelle, installed in the wind tunnel.

Inlet Model

A Mach 2.5, axisymmetric, mixed-compression inlet with 40 percent of the design supersonic-area contraction occurring internally was used in this investigation. The inlet was attached to a cylindrical nacelle 0.635 meter in diameter in which a J85-GE-13 engine or a coldpipe, choked-exit-plug assembly could be installed. For this study, only the engine was used. At the design Mach number, sizing the inlet to match the J85-GE-13's airflow requirements resulted in a 47.32-centimeter inlet capture diameter. The inlet was started by translating the centerbody. A flight version of this inlet with 40-

percent internal contraction would require a collapsing centerbody for starting and off-design operation (ref. 4).

Some basic inlet design details are presented in figure 2. Local theoretical airflow conditions on the cowl and centerbody, inlet contours, and diffuser-area variation are shown for the inlet design Mach number and spike position. A computer program (ref. 11) that incorporated the method of characteristics was used to design the supersonic diffuser. A two-cone surface with half-angles of 10° and 18.5° provided the initial supersonic compression. The internal oblique shock from the cowl lip was canceled at its impingement point on the centerbody by turning the surface. The remaining supersonic compression was isentropic to obtain an average theoretical supersonic throat Mach number of 1.30 with an inviscid recovery of 0.9855. At the design centerbody position, the geometric throat was at an x/R_c of 3.26. (See appendix B for definition of symbols.) Downstream of the geometric throat, the inlet included a throat region with 1° equivalent conical expansion and a main subsonic diffuser with an overboard bypass system The diffuser-centerbody boundary layer was controlled by vortex generators that were located in the diffuser at an axial distance ratio of 3.965 (fig. 3). Details of the vortex generator design are shown in figure 4. The overall inlet length at design - (cone tip to compressor face) was 7.88 cowl-lip radii. Internal surface coordinates of the inlet in terms of the cowl-lip radius are presented in table I. The inlet design characteristics are discussed more completely in reference 12.

Bleed regions were located in the throat on the inlet cowl and centerbody surfaces. The forward-cowl bleed flow (not used during this part of the program) was dumped directly overboard, as shown in figure 5. Stability bypass flow (used to give the inlet a large stable range) was removed through the stability bypass entrance, on the cowl side of the throat. It was then directed through the cowling to the pressure-activated poppet valves and on to the stability bypass coldpipes (figs. 3 and 5). Centerbody bleed flow was ducted through hollow support struts to the centerbody bleed coldpipes (fig. 3). Each stability bypass and centerbody bleed coldpipe housed a choked-plug assembly.

When the choked-plug assemblies were controlling the stability bypass flow by forming a choked exit at the downstream end of the pipes, the pressure-activated poppet valves in the bypass flow circuit (fig. 3) were set wide open so as not to interfere with the rear choke point. When the pressure-activated poppet valves were controlling the stability bypass flow, the choked-plug assemblies were set wide open and the choke point moved forward to place the effective minimum exit area at the valve station.

The subsonic portion of the inlet diffuser incorporated two remotely controlled bypass systems: a fast-acting overboard bypass, and a slow-acting ejector bypass for engine and nozzle cooling airflow. For this investigation the ejector bypass was closed. Engine cooling airflow was supplied from an external source. Cascades were installed in the entrance to the overboard bypass cavity during a previous test program to eliminate resonance (ref. 13).

As shown in the figures, a bulky cowl was used on the test model so that major changes could easily be made to the inlet-stability bypass system and associated ducting during the wind tunnel tests. It was not representative of flight hardware. Figure 6 shows how an inlet-stability bypass system can be packaged within the low-external-cowl-drag profile essential for supersonic flight.

Stability Bypass Entrance and Bleed Region Configuration

The stability bypass configuration used in this test program (fig. 7) was the same as configuration NF of reference 1. As figure 7 shows, all the bleed regions were composed of rows of normal holes arranged in a concentrated, staggered pattern to provide uniform circumferential bleeding of the boundary layer. The distributed, porous hole pattern of 0.3175-centimeter-diameter holes on 0.4763-centimeter centers gave a nominal porosity of 40 percent. Fifteen rows of bleed holes were used as the stability bypass entrance. Reference 1 indicates that this stability bypass system can provide an inlet stability margin of 28.4 percent from a high-performance-match operating condition if constant pressure is maintained in the stability bypass plenum to inlet unstart. The available forward- and aft-cowl bleeds were sealed; the centerbody bleed provided a performance bleed mass-flow ratio of about 0.025 at the inlet-engine match condition.

Pressure-Activated Poppet Valves

The stability bypass flow was controlled by 16 pressure-activated poppet valves located circumferentially within the inlet cowl at the exit of the small stability bypass plenum (figs. 8 and 9). Valves installed in the inlet cowl are shown in figure 8(a) and details of valve mechanical design, in figure 8(b). The poppet valve is essentially a floating piston with a trapped volume at a preset internal pressure on one side of the piston. This piston is activated by differential pressure. The valve chamber pressure was controlled during the test by connecting the valve to an external air supply. (In flight, suitable valve chamber pressure could be supplied by a probe and a pressure regulator could be used if necessary. The poppet-valve system and its variations are described in a United States patent (ref. 2).) The valve chamber pressure was set to just close it during normal inlet operation, that is, with the inlet operating at a high pressure recovery and with the terminal shock at the downstream edge of the stability bypass entrance. Under these conditions, if an airflow disturbance caused the terminal shock to move upstream over the stability bypass entrance, the pressure in the bypass plenum would exceed the internal valve pressure and thus cause the valve to open and bypass flow to occur. Valve control of the stability bypass flow resulted in an effective bypass

plenum volume of about 0.01 to 0.02 cubic meter, smaller than the bleed plenum volume of 0.40 cubic meter for the choked-plug system, which was almost equal to the main-duct volume of 0.42 cubic meter.

The poppet valve was simply designed solely to demonstrate the feasibility of constant-pressure control in a stability bypass plenum. The design allowed the poppet valve to open fully when the pressure on the valve face (stability bypass total pressure P_{sb}) was increased about 20 percent. The actual valve performance, as determined on a bench test stand and reported in reference 5, is shown in figure 8(c) in nondimensional form. The reference pressure $P_{sb, ref}$ was the lowest supply pressure that caused the airflow to just choke at the valve attachment bulkhead opening. The reference mass flow $m_{pv, ref}$ was the theoretical airflow through the bulkhead opening at this reference pressure (flow coefficient of 1.0). The valve was indeed quite sensitive to pressure until the airflow choked at the valve attachment opening. This choke point was reached with a 25-percent increase in the pressure at which the valve began to open.

In flight, many perturbations of the inlet shock into the throat region would probably be quite rapid. To absorb such perturbations, the poppet valve had to be fast acting. For the research programs reported in references 3 and 5, a movable valve-head assembly was therefore designed to minimize weight (fig. 8(b)). For the design valve-head weight of 0.20 kilogram, the valve natural frequency was estimated at about 12 hertz at the pressure levels encountered during the test.

A feasibility study of self-acting, inlet-stability bleed valves - including vortex valves, sliding louver valves, and poppet valves - for the NASA YF-12 supersonic research airplane is reported in reference 14. The results of this study show that only poppet valves provide the flow capacity and dynamic response required for a good stability bypass system. A bench test evaluation of the poppet valves for the YF-12 is reported in reference 15. Basically, the valve design was the same as for the poppet valves used in this study.

Steady-state operation of the poppet valves installed in this inlet-stability bypass system has been successful (refs. 3 to 5). However, with some of the stability bypass entrance configurations of reference 5 the valves oscillated when operating partly open. (In some of these configurations the valves did not oscillate when they were moving in response to a transient, including transients with periods of about 20 seconds. In flight, the valves would probably never be open in a steady-state situation but would be moving in response to a transient and would thus not oscillate.) Because the 16 valves oscillated in unison at a frequency of 44 hertz, it was concluded that the valve and bleed-plenum system was acting like a second-order dynamic system, since it was operating well beyond the valve natural frequency of 12 hertz. Adding a linear potentiometer to measure valve position during the bench test eliminated the oscillations except at very high pressures. (Thus, ref. 5 concluded that a small amount of properly applied friction might

eliminate the oscillation.

Poppet-valve oscillation was not observed during the present investigation.

Engine Description

A sketch of the engine installed with the other test hardware is presented in figure 10. The General Electric J85-13 is an afterburning turbojet with a high thrust-weight ratio. The engine has an eight-stage, axial-flow compressor coupled to a two-stage turbine. It has controlled compressor interstage bleed, variable inlet guide vanes, a throughflow annular combustor, and an afterburner (not used in this test) with a variable-area primary exhaust nozzle. The engine inlet diameter is 40.8 centimeters.

The compressor variable geometry consists of interstage bleed valves on stages 3 to 5 and inlet guide vanes. The guide vanes and valves are linked together and, on the standard engine, are controlled by the main fuel control as a function of the engine corrected speed. During this investigation the compressor variable geometry and power lever angle were controlled either by a computer or manually. The primary-nozzle area, which is normally controlled by the afterburner fuel control, was also controlled either by a computer or manually for this test.

The inlet performance for an engine stall condition was assessed by stalling the compressor by slowly closing the primary-nozzle area while maintaining a constant speed. So that the turbine temperature limit would not be exceeded during this procedure, a reduced-area, first-stage turbine stator was installed. Then, at any point on the compressor map, the turbine was matched to the compressor at a lower turbine-inlet temperature.

Upstream Airflow Variation Device

A flat gust plate was used to vary the inlet, local, free-stream airflow (figs. 10 and 11). With the inlet and the flat gust plate both at 0° angle of attack (fig. 11(a)), the local conditions at the inlet were not changed from the free-stream conditions. Increasing the plate angle of attack decreased the local Mach number and increased the inlet angle of attack (fig. 11(b)).

Instrumentation

Static-pressure distributions were measured along the top centerlines of the cowl and centerbody at the axial locations given in table II. Subsonic diffuser and bleed pres-

sure instrumentation is shown in figures 12 and 13. Stability-bypass-bleed total pressure was measured by two total-pressure rakes just downstream of the open bleed at an x/R_c of 4.051. Pressures from these rakes were averaged to determine the stability-bypass-bleed recovery. Centerbody and overboard-bypass-plenum pressures were measured by single tubes (fig. 13).

Overall inlet total-pressure recovery and distortion were determined from six, 10-tube total-pressure rakes (fig. 12) at the diffuser exit (inlet station 2). Each rake consisted of six equal-area-weighted tubes, with additional tubes at the extreme equal-area-weighted tubes in positions corresponding to an 18-tube area-weighted rake. The compressor-face instrumentation and a calibration curve were used to determine engine airflow, as described in appendix A. Two piezoelectric transducers (D8 and D9) were located at the compressor face (fig. 12). (Dynamic instrumentation locations are given in table III.).

The compressor discharge pressure was measured by 16 steady-state, total-pressure probes mounted in four rakes as shown in figure 14. One probe (D10) measured both steady-state and transient pressures: A piezoelectric transducer was flush mounted to the inside of the tube 15.2 centimeters downstream of the probe entrance, and the tube was extended to the steady-state recording system so that the tube operated like an infinite line.

One dynamic total-pressure probe and eight dynamic static-pressure taps were placed along the inlet duct as shown in figures 12 and 15. Outputs of the strain-gage absolute-pressure transducers in the cowl-lip static-pressure tap (S1) and the throat total-pressure probe (S2) were used in ratio form (S1/S2) to sense inlet unstart. The additional absolute pressure transducer (S3) was used to indicate the terminal shock position for computer control (fig. 16 and ref. 16). The remaining six piezoelectric transducers (D1 to D6) were flush mounted on the surface.

Turbine discharge temperature T_5 was measured by eight thermocouples that were installed by the engine manufacturer and wired in parallel to give an average reading. The engine speed was measured by a magnetic pickup that sensed the tooth passage of a rotating gear attached to the customer-power takeoff shaft from the engine gearbox. Combustion flame was sensed by a photodiode. The positions of the inlet centerbody, the overboard bypass doors, and the pressure-activated poppet valves were determined from potentiometer measurements.

RESULTS AND DISCUSSION

Basic Inlet Stability Data

The steady-state performance of the inlet configuration that was used in this test program has been reported in reference 1. Although the development of an effective stability bypass entrance configuration and the required bypass-plenum exit configuration is described in references 1 to 5, a few of the basic performance plots are presented and briefly discussed in this report.

Steady-state performance of the inlet configuration is shown in figure 17. Stability bypass performance is shown in figure 17(a), where the bypass total-pressure recovery is given as a function of the bypass mass-flow ratio. The dashed curves represent the performance envelope of the distributed, porous, stability bypass configuration, which was the same as configuration NF of reference 1. These curves represent the minimum (supercritical) and maximum (minimum stable) mass flows that were obtained for a series of fixed bleed exits on the stability bypass system. Data for one fixed exit are shown (circular symbols). These data were generated by reducing the inlet diffuser-exit airflow from supercritical (minimum stability bypass airflow) and causing the terminal shock to move upstream until unstart occurred. Bypass airflow was maximum just before inlet unstart. This mode of operation gave loci (dashed curves) of supercritical and minimum stable bypass airflows. The bypass performance with the poppet valves as a exit control, also shown in figure 17(a), was obtained in a similar manner.

Inlet performance is presented in figure 17(b) by a standard plot of total-pressure recovery as a function of mass flow. Inlet recovery as a function of diffuser-exit airflow is shown in figure 17(c). In references 1 and 5 an airflow index was used to develope a stability index envelope for a stability bypass system. However, since specific bypass-exit-area controls have been selected for this study (fixed exit or poppet valve), the data in figure 17(c) better indicate the stability effectiveness of each exit control. Inlet stability could be assessed by the change in diffuser-exit corrected airflow between the operating condition and the point just before the inlet unstarted. Since an inlet-engine match recovery of 0.90 was selected for this investigation, this recovery will be used to illustrate the steady-state stability. The percentage change in corrected airflow from this operating point to the minimum stable condition is the stability index. Therefore, for these data, stability indices were 5.0 and 25.6 for the fixed-exit and poppet-valve controls, respectively. The superiority of the poppet-valve control is quite evident from figure 17.

The ability of the inlet with stability bypass systems to absorb internal airflow transients is illustrated in figure 18. These data were for the inlet with a choke plate at the compressor-face station to simulate an engine-installed configuration. The smallest transient-stability indices (capability of absorbing transients in diffuser airflow) were

obtained for a small bypass-plenum volume and small exit area. This small plenum volume was the same plenum volume used with the poppet valves. Basically, the small-plenum data represent the capability of a conventional inlet to absorb an internal airflow transient. The change in transient-stability index between the small- and large-plenum data indicates the improved transient-absorbing capability of a stability bypass system connected to a small fixed exit through a large plenum. The large-plenum and stability bypass system could absorb very large transients, for example, above 35 percent of the engine corrected airflow for a transient pulse frequency $1/\tau$ of 20 seconds^{-1}. At lower pulse frequencies the capability of the large plenum was rather limited and approached the capability of the small plenum at $1/\tau$ of 1 second^{-1}. The poppet-valve-controlled system had a large transient-stability index, or capability of absorbing very large transients in diffuser airflow, at all pulse frequencies. It could absorb at least 30 percent of the diffuser-exit airflow at all test frequencies (fig. 18).

Propulsion System Response to Internal Airflow Disturbances

Transient airflow disturbance data are presented in two parts: inlet response and engine response. Part (a) of each figure shows the inlet response, which includes inlet throat pressures (transducers D1 to D5), diffuser static pressure (D6), stability-bypass-plenum pressure (D7), overboard-bypass area A_{by}, and inlet centerbody position x_{cb}. Part (b) of each figure shows the engine response, which includes engine speed N, combustor flame sensor, combustor spark source, turbine-exit temperature T_5, power lever angle PLA, primary-nozzle area A_8, compressor pressures (D8, D9, and P_3/P_2), and the inlet unstart ratio S1/S2. An increase in any of these parameters is indicated when the trace moves toward the top of the figure.

Reductions in overboard-bypass-door area. - The inlet and engine response to a single sine-wave pulse reduction in overboard-bypass-door area is presented in figure 19 for a small-fixed-exit bleed configuration. The initial match conditions were an inlet recovery of 0.907 and a corrected engine speed of 84.8 percent. At this match inlet recovery, the terminal shock was just downstream of the stability-bypass-bleed region, at about the same inlet station as the inlet throat transducer D5 (fig. 15). Any reduction in the airflow demand in the subsonic diffuser would cause the terminal shock to move upstream from this match location toward inlet unstart. The forward movement of the terminal shock would cause the local static pressure on the inlet throat surface to increase since the airflow downstream of the terminal shock is subsonic. In figure 19, the reduction in overboard bypass airflow is indicated by the reduction in bypass area A_{by}. The increase in static pressure is evident from the trace for transducer D4 in figure 19. Higher bleed-region surface pressure resulting from the terminal shock

movement also increases bleed-plenum pressure, as reflected by the trace for transducer D7. For a small-fixed-exit-area bleed configuration as in figure 19, a small reduction in subsonic diffuser airflow moves the terminal shock upstream and influences all the throat pressure transducers. Because transducer D1 was just upstream of the open, porous bleed region, any large pressure rise on this transducer would indicate that the terminal shock was upstream of the bleed in an unstable region and that the inlet would unstart. The trace for transducer D1 in figure 19(a) shows a slight pressure rise as a result of the bypass transient. Therefore, the terminal shock was near the unstart condition. The trace for transducer D7 indicates an increase in plenum pressure recovery of 0.195 (0.195 P/P_0 per line times 1.0 line). This increase in pressure was equal to the increase in steady-state pressure recovery from supercritical to minimum stable conditions in figure 17. The inlet would unstart if a slightly larger reduction in diffuser airflow was experienced. During this transient, engine operation was not significantly affected (fig. 19(b)).

Figure 20 shows how the inlet with the poppet-valve exit control on the stability bypass responded for the same-amplitude overboard-bypass disturbance as the fixed-exit control (fig. 19). The traces for transducers D1 to D5 of these two figures show how well the stability bypass and poppet valves retarded the upstream movement of the terminal shock. Transducers D1 to D3 for the small-fixed-exit system of figure 19 show pressure increases that are not evident for the poppet-valve system of figure 20. Since the poppet valves are a nearly constant pressure control, only a small rise in plenum pressure (D7) would open the poppet valves slightly and allow stability bypass airflow to exhaust overboard to compensate for the reduced subsonic diffuser airflow.

Each control - small, fixed exit area and poppet valves - responded to a larger amplitude overboard-bypass-area reduction, as shown in figures 21 and 22 The larger overboard-bypass-area reduction caused the inlet with the small-fixed-exit bleed system to unstart (fig. 21). This unstart is evident in the figure as the first sudden drop in the inlet pressures. Again, the terminal shock was initially at transducer D5. The upstream movement of the terminal shock is indicated by the increase from the initial match pressure levels for transducers D5 to D1.

The inlet unstart of figure 21 resulted in an engine stall and combustor blowout. The hammershock from the stall shows up in most of the pressure traces of figure 21 as a sharp pressure increase just after the initial unstart pressure drop. The combustor blowout on inlet unstart shows up as the change in the combustor flame sensor trace (fig. 21(b)) from a fluctuating signal to a steady-state signal. The large drop in compressor-face total pressure (D9) and the lag in the compressor discharge pressure because of the large combustor volume show up as a significant initial rise in the compressor pressure ratio CPR (fig. 21(b)) immediately after inlet unstart. The hammershock pressure rise at the compressor face shows up as a sharp drop in CPR followed by an increase when the effects of the hammershock have disappeared.

When the unstart sensor sensed inlet unstart (fig. 21(b)), the propulsion system control performed a set of predetermined procedures: The control began inlet restart by extending the inlet centerbody, at the maximum rate, to a position just beyond the minimum required extension for restart. The point of inlet restart is quite evident from the return of the unstart sensor trace to its level before unstart. Correlating this trace with the centerbody translation trace (fig. 21(a)) indicates that the inlet did restart just before the maximum extension was reached. After inlet restart, the control retracted the centerbody, at the maximum rate, to the initial design position. The control also began firing the combustor spark plug at about two sparks per second. The traces for the spark and flame sensor (fig. 21(b)) show that the combustor relighted on the second spark at about 0.4 second after inlet unstart. During this cycle the power lever angle and exhaust nozzle area were not varied. Upon unstart, the command signal to the overboard-bypass doors, which had been a scheduled, single sine-wave pulse, was switched to the output of a control loop. This output varied the bypass to maintain a predetermined inlet duct pressure during the restart cycle. The reduction in engine speed and turbine-inlet temperature as a result of engine stall and combustor blowout can be seen in figure 21(b).

When the reduction in inlet overboard-bypass-door area that caused the inlet unstart of figure 21 was duplicated for the inlet with poppet valves, the inlet did not unstart (fig. 22(a)). As in figure 20 the poppet valves opened to allow the airflow to exit overboard to compensate for the reduction in diffuser-airflow requirement. Because only the downstream edge of the bleed region (transducer D4) had a significant pressure rise, the poppet valves obviously allowed the disturbance to be absorbed without excessive terminal shock movement. Poppet-valve data in which the overboard-bypass door area was varied from the match condition to a closed position are presented in figure 22(b). For these data the doors were commanded to move in a sine-wave pulse toward the closed position. The flat on the A_{by} trace in the center of the pulse disturbance indicates that the doors were completely closed. These data are like those in figure 22(a). The inlet could not be forced to unstart by reducing overboard bypass airflow for the poppet-valve configuration because bypass airflow was insufficient.

Inlet unstart data resulting from a slow manual reduction in overboard-bypass-door area for large- and small-plenum configurations with small-fixed-exit-area bleed controls are shown in figures 23 to 25. These data show very little effect of plenum size on the response of the inlet and engine during the unstart-restart cycle. The data traces show that the propulsion system can be restarted-relighted rapidly (less than 1.5 sec).

Reductions in power lever angle. - The inlet and engine responded to power-lever-angle reductions as shown in figures 26 to 31. The poppet-valve control responded to single sine-wave pulse reductions in the power lever angle as shown in figures 26 and 27. Although the flame sensor trace in each figure shows a large change, blowout did not occur. Reducing power lever angle decreased fuel flow, which in turn decreased engine

speed. Lower engine speed required less diffuser airflow. Therefore, the terminal shock moved upstream in the inlet to compensate for this airflow reduction, as shown by the trace for transducer D4. Then the poppet valves opened to retard the shock movement.

Although the power-lever-angle reduction of figure 27 was twice that of figure 26, the response in the inlet was about the same. Again, as in the overboard-bypass-area reduction data, the inlet could not be unstarted by reducing subsonic diffuser airflow through a decrease in power lever angle. Even when the engine speed was reduced to idle, the poppet-valve-controlled inlet did not unstart.

Steady-state stability bypass data for engine speeds from match speed to idle are shown in figure 28. The mass-flow ratios for the poppet-valve stability bypass sytem were determined by subtraction (appendix A). The ratios obtained were adjusted slightly to put the inlet-engine match condition on the supercritical bleed characteristic, as it should be. As shown by the tailed symbol, engine idle was obtained well within the minimum stable limit of the stability bypass system. The valve characteristic varied between the curve from reference 5 and the data for this test program because of initial valve plenum pressure. For this test program the valve plenum pressure was adjusted to be about 0.01 in pressure recovery above the match stability-bypass-plenum pressure. Therefore, fairing the data in figure 28 indicates that a slight increase in stability plenum recovery of about 0.01 was required before the poppet valves started to open. This slight valve plenum overpressure was used to eliminate valve reaction to extremely small airflow variations and to thus eliminate the valve instability problem of reference 5. Also, extending the poppet-valve data of figure 28 shows that the reduced capacity for airflow removal because of the slight overpressure would be about 0.01 in mass-flow ratio. This is a relatively small amount when the large capacity of the poppet-valve system is considered.

Similar data for the fixed-exit bleed configuration are presented in figure 29. The stability-bypass-airflow characteristic obtained by varying the power lever angle was the same as that for the fixed exit (fig. 17(a)) obtained during an earlier coldpipe investigation. Unlike the results for the poppet valves in figure 28, figure 29 shows that reducing power lever angle and consequently diffuser airflow for the fixed-exit configuration did result in an inlet minimum stable condition (solid symbol). Any additional reduction in power lever angle from the inlet minimum stable position would cause an inlet unstart. Response data for an inlet unstart caused by further reducing power lever angle are presented in figure 30. The traces just before unstart represent the steady-state performance at the minimum stable condition. The inlet unstart caused compressor stall and combustor blowout.

Data for the fixed-exit controlled bleed system when it was subjected to the same disturbance as the poppet-valve-controlled bleed system of figure 26 are presented in figure 31. This pulse reduction in power lever angle caused the inlet with the fixed-

exit-controlled system to unstart. The inlet unstart caused compressor stall and combustor blowout. The inlet was restarted in about 0.2 second, and the engine was relighted about 0.3 second later. Comparing these data with the data of figure 26, which had a similar amplitude disturbance for the poppet-valve control, and with the data of figure 27, which had a larger amplitude disturbance, again indicates the advantage of a poppet-valve bleed control in a supersonic inlet: The poppet-valve-controlled bleed system absorbed the transient with the least variation from normal system operation. The fixed-exit-controlled inlet experienced inlet unstart, which caused engine stall and combustor blowout.

Reductions in primary-nozzle area. - The response of the propulsion system with poppet-valve-controlled stability bleed to a pulse reduction in primary-nozzle area and consequently a reduction in required diffuser airflow is presented in figure 32. The results are like those for the overboard-bypass-area and power-lever-angle reductions. The poppet valves opened to absorb the reduction in diffuser airflow requirement and thus prevent inlet unstart.

The response of the propulsion system with poppet-valve-controlled stability bleed to a compressor stall is shown in figure 33. The compressor was stalled by slowly closing the primary-nozzle area manually to backpressure the engine while manually varying the power lever angle to maintain a constant engine corrected speed of 90.1 percent. Compressor stall also was attempted at the nominal, test, match engine speed of just over 87 percent, but the turbine-inlet temperature limit was reached before the engine stalled. Steady-state compressor performance for these two engine speeds is shown in figure 34. In figure 33(b) the primary-nozzle-area trace A_8 appears to indicate a constant nozzle area before compressor stall because of the very slow manual closing of the exhaust nozzle. Stall hammershock shows up as the large initial pressure spike on all pressure transducer traces in figure 33(a). In figure 33(b) blowout occurred at the same time that the compressor pressure ratio indicated a stall. The inlet unstart sensor indicated an inlet unstart about 0.01 second later. After stall a command (scram) to completely open the nozzle and to chop the fuel flow was given by the control system. Engine relight was not attempted. The poppet valves opened in response to the pressure rise in the stability bypass plenum but did not have the capacity to absorb the airflow transient associated with an engine stall. After stall and the resulting inlet unstart, the poppet valves closed and remained closed until the inlet was restarted and the centerbody was being retracted to the design position. During centerbody retraction after inlet restart, the poppet valves opened briefly in response to a pressure rise in the stability-bypass-bleed region, as indicated by the traces for transducers D2 to D4.

Compressor stall affects a system with fixed-exit-area inlet bleed control as shown in figure 35. Steady-state compressor performance is presented in figure 36. The compressor was stalled at the same engine speed and by the same procedure as for the poppet-valve controlled system of figure 33. Upon stall the combustor blew out, the

inlet unstarted, and the system was scrammed to a safe condition. However, the pressure transients were much greater for the fixed-exit-area-controlled system than for the poppet-valve-controlled system: The hammershock initially caused a larger pressure rise, the drop in pressure just after unstart was greater, and the pressure variation for the throat transducers was larger.

Propulsion System Response to External Airflow Disturbances

The propulsion system responded to disturbances in external airflow as shown in figures 37 to 44. External airflow variations that reduce inlet free-stream Mach number and/or increase angle of attack can induce inlet unstart. For some supersonic inlets, local overcompression of the airflow upstream of the throat region to a subsonic condition causes unstart. When the inlet is operating at an angle of attack, this overcompression (choking) occurs on the leeward side of the inlet. Reference 1 indicates that local overcompression can be delayed to larger angles of attack by locating bleed forward in the supersonic diffuser in the overcompression region and by removing airflow in a large axial region on the cowl with additional bleed airflow removal. Reference 17 indicates that reducing inlet free-stream Mach number produces an overcompression on the inlet surface like that obtained near unstart angle-of-attack operation. The overcompression again appears forward of the throat and circumferentially encompasses the entire inlet flow field.

External airflow was varied by pulsing (single sine wave) the flat-gust-plate angle of attack (fig. 11) upstream of the inlet. Increasing the plate angle of attack from 0° lowered the local Mach number and increased the local airflow angle into the inlet - for a combination of changes in external airflow. For a change in Mach number only, the propulsion system would have to be cycled through the same angle of attack as the plate.

For this test the inlet diffuser dynamic pressure instrumentation was on the side ($\varphi = 90^{\circ}$) of the inlet. Therefore, increasing the flat-gust-plate angle, which caused a local downflow into the inlet, resulted in the dynamic-pressure instrumentation being between the windward ($\varphi = 0^{\circ}$) and the leeward ($\varphi = 180^{\circ}$) sides of the inlet. The inlet throat transducers do show a local pressure increase because the disturbance was largely due to Mach number reduction, but they do not show the maximum pressure rise in the inlet since the combination of Mach number and angle of attack would produce the maximum change on the leeward side. The poppet valve in this region of high local pressure was not instrumented, and hence the individual valve response in each circumferential region is not known because valve operation differs due to the asymmetry in the flow field. The overall response of the inlet and engine system was obtained, however, and these data indicate some significant results.

The poppet-valve-controlled and fixed-exit-area-controlled systems responded to an identical external disturbance as presented in figures 37(a) and 38, respectively. Even though transducers D1 to D5 were on the side of the inlet, the traces indicate that the disturbance increased local surface pressure. This pressure increase resulted from Mach number variation and may be decreased slightly on the side of the inlet by the angle-of-attack operation. Although for these data the engine ignition was initiated before the external disturbance, engine ignition was not required for the conditions of figures 37(a) and 38 since the inlet did not unstart and cause combustor blowout.

For a larger flat-gust-plate angle the fixed-exit-area control allows an inlet unstart (fig. 39), but the poppet-valve control does not (fig. 37(b)). The poppet-valve trace of figure 37(b) shows little or no response to the disturbance although the poppet valves on the leeward (high pressure) side of the inlet must have opened and relieved some of the overcompression that caused the fixed-exit-area-controlled system (fig. 39) to unstart. Data that are presented in figures 39 and 21 show an inlet unstart resulting from an internal airflow disturbance had more severe pressure variations than an unstart resulting from an external airflow disturbance. As shown by the combustor flame sensor trace of figure 39(b), the engine did not blow out when the inlet unstarted. The available data also indicate that the compressor did not stall: The traces show no evidence of a stall hammershock pressure rise. The hammershock influence on the pressure transducers, compressor pressure ratio, and inlet unstart sensor and the very large drop in the diffuser pressures (D6, D8, and D9) associated with a stall in figure 21 are not present in figure 39.

An additional increase in the flat-gust-plate angle (to 1.4°) caused an inlet unstart for the poppet-valve-controlled system, as shown in figure 40. The instrumented poppet valve opened on unstart and then closed until it opened and closed when retracting the centerbody after inlet restart. Figure 40(b) shows that compressor stall and combustor blowout did occur as a result of inlet unstart. Compare these traces with those of figure 39. In figure 40 the hammershock and the very large diffuser pressure drop just after unstart that are associated with stall are evident. Because relight occurred 0.1 second after blowout, engine operation was affected for only a very short time. In figure 41, another inlet unstart from an external disturbance (created by manually varying the flat-gust-plate angle) for the poppet-valve-controlled system did not stall the engine or blow out the combustor. Similar data for the large-plenum, small-fixed-exit bleed configuration show that for one case (fig. 42) stall and blowout did not occur but for the other case (fig. 43) they did. Relight was not attempted in this case. For inlet-engine systems with poppet-valve controls and large-plenum, small-fixed-exit-area controls, inlet unstart from an external disturbance (the flat gust plate) caused stall and blowout for about half of the test points (figs. 38 to 43). For an inlet-engine system with truely conventional, small-plenum, small-fixed-exit-area controls (fig. 44), inlet unstart from an external disturbance always caused stall and blowout. After blowout, engine relight

was more difficult with this control configuration than with the other two. In the first attempt, engine relight occurred 4.2 seconds after combustor blowout. But, when the conditions were duplicated and the engine did not relight after 6 seconds, the attempt was canceled.

The poppet-valve control configuration that was used for this investigation was basically designed to provide the inlet with a large, stable airflow range for internal airflow disturbances. Consequently, the inlet bleed was in the throat region and not necessarily where it would provide the greatest tolerance to external (e.g., angle of attack) disturbances. Nevertheless, the poppet-valve exit control did provide more tolerance to external disturbances (e.g., 16 percent in angle of attack) than a more conventional fixed-exit-area bleed system. For greater tolerance to angle-of-attack disturbances, forward-cowl bleed (fig. 7) should also be used. Reference 1 has shown that forward-cowl bleed capability would increase steady-state, unstart angle of attack from 4.46° to 7.6° if a constant pressure was maintained in the bleed plenum. An additional poppet-valve exit control would be needed for the angle-of-attack system. These valves would shut off the forward-cowl bleed until angle-of-attack or free-stream Mach number changes caused the local pressure increase that would activate them.

Steady-State Stability-Bypass-Bleed Performance

Most researchers have concentrated on investigations that define bleed systems for acceptable, on-design, started-inlet performance. Therefore, very little information on unstarted-inlet bleed performance has been published. Attempts to minimize the number of unstarts have resulted in accepting less than optimum performance (supercritical operation) and in research evaluations of such concepts as the stability bypass system. Because, under certain conditions, unstarts will still occur, the performance and capabilities of bleed systems with the inlet in an unstarted condition should be a part of all inlet performance studies.

Started- and unstarted-inlet bleed performance are shown in figures 45 to 47. Cowl surface pressure distributions for selected data from figure 45 are presented in figure 48. The unstarted-inlet data from figure 45 represent the inlet buzz limits for several centerbody positions. Attempting to operate beyond the unstarted bleed limit curve for a given centerbody position resulted in inlet buzz. These curves show that, when the inlet was in an unstarted condition, the stability-bypass-bleed system was capable of removing large amounts of airflow before the inlet buzz limit was reached. Design centerbody position data (θ_{ℓ} of 25.27°) indicate that the unstarted buzz limit was between the started-inlet supercritical and minimum stable bleed curves. The unstarted-inlet bleed capacity before buzz increased when the centerbody was translated upstream toward the the restart centerbody position (θ_{ℓ} of 22.63°). For this investigation the inlet throat

area was increased by upstream centerbody translation. However, similar trends in unstarted-inlet bleed performance would probably be obtained for inlet configurations in which the centerbody was collapsed to effect inlet restart.

In an unstarted condition the inlet may operate in a stable mode at any point below the bleed characteristic curve for a given centerbody position. The specific operating condition below the bleed characteristic curve was a function of the overboard-bypass-area variation as shown in figure 46. For these data the engine was windmilling and the diffuser airflow demand was varied by the overboard bypass doors. At diffuser-exit airflows larger than that represented by an overboard-bypass-area ratio of 0.1886, the bleed airflow could vary from zero to any value along the bleed characteristic curve for the specific bypass-area ratio. The specific stability-bleed airflow rate would be determined by the bleed-plenum exit area. However, any overboard-bypass-area ratio reduction below 0.1886 required some bleed airflow to maintain an operating condition below the buzz limit curve. For example, if the overboard-bypass-area ratio was reduced from 0.1886 to 0.1696, a minimum of about 0.0273 stability-bypass-bleed, mass-flow ratio was required to prevent buzz. Further reducing the overboard-bypass-area ratio to 0.1358 required a mass-flow ratio of about 0.145 to prevent buzz.

In a sense, the stability system can perform the same basic function during an unstarted condition that it was designed to provide with the inlet started. When the inlet was started, the stability bypass system allowed the diffuser airflow to vary over a large range without inducing an inlet unstart. When the inlet was unstarted, as shown in figure 46, proper control on the stability bypass system could also compensate for a large variation in diffuser airflow before inlet buzz was obtained. Unstarted-inlet bleed characteristics for various overboard bypass areas at the extended centerbody positions have trends like those in figure 46 for the design centerbody position. At the extended positions the overboard bypass could be reduced even more than at design because of the large stability bleed capacity before buzz, as shown in figure 45. For example, the overboard-bypass-area ratio could be reduced to 0.066 at maximum bleed for a θ_ℓ of 23.28° (fig. 45). The stability-bypass-bleed mass-flow ratio at this condition was 0.221.

Extending the centerbody affects started-inlet, stability bypass performance at the inlet design Mach number of 2.5, as shown in figure 47. At the off-design centerbody positions only the minimum stable bleed characteristic curves are presented. These data indicate that the bleed capability increased slightly for a small extension of the centerbody, to a θ_ℓ of 24.30°. Further extending the centerbody toward the inlet restart position reduced the bleed capacity at the larger bleed flow rates below that for the design centerbody position. However, in general, the minimum stable stability-bleed capability at the extended centerbody positions was about the same as the capability at design.

The capability of the large inlet stability-bleed airflows during inlet unstart could be combined with modern computer inlet control to improve system control during the

unstart-restart cycle. During this cycle the present research computer inlet control retains a closed-loop pressure control on the bypass doors in an attempt to avoid buzz and to maintain acceptable compressor-face pressure recovery without high distortion. This control can often command large variations in bypass door area over short time periods. Since overboard bypass doors usually react rather slowly (particularly on flight hardware), a compromise is necessary for an optimum inlet control. However, proper integration of a controlled stability bypass system with the computer inlet controls may require that the bypass doors operate over only a small area range during most of the unstart. The bypass doors would thus make only minor airflow adjustments, and the stability bypass system would handle most of the airflow.

The combined system might operate in the following manner: During started-inlet operation the stability bypass system would provide the inlet with a large stability margin. The stability valves would open in response to diffuser airflow changes. But, if an airflow disturbance exceeded the poppet-valve airflow tolerance, an inlet unstart would occur. The poppet valves would begin to close when the inlet unstarted because of the sudden, extreme pulse decrease in cowl surface pressure. This pressure pulse would be very short (0.05 sec for the inlet configuration of this investigation); then the local pressure would increase enough to activate the poppet valves if the subsonic diffuser airflow were controlled at a proper level. To set this level, the bypass-door exit area would be kept as close to match as possible but large enough to maintain the unstarted-inlet operation within the stability-bypass-bleed buzz limit characteristic (fig. 45).

Current control systems could provide such bypass airflow control since only small variations in bypass door area would be required. When the centerbody is extended to almost the inlet restart position, the stability bypass system can handle more airflow. Therefore, the bypass door area could be reduced as the centerbody is extended (fig. 45). The door area should not be less than the match area because this area would be required upon restart. Since the bypass doors would be at or near the match area at restart, they would not demand large airflows and would not contribute to supercritical operation.

Several factors would contribute to reducing stability-bypass-bleed airflow at inlet restart and thus result in less supercritical operation. At the point of restart when the local conditions would shift from subsonic to supersonic, the bleed airflow would be reduced rather suddenly because of the sharp reduction in flow coefficient. The poppet-valve bleed control would also close because of a drop in local surface pressure and consequently plenum pressure. During centerbody retraction and settling out of the inlet to normal conditions, any small variation that might cause the terminal shock to move upstream would cause the stability bypass system to function and prevent reoccurrence of inlet unstart.

SUMMARY OF RESULTS

The throat of a Mach 2.5, mixed-compression inlet with 40-percent internal supersonic-area contraction was fitted with a inlet-stability bypass system designed to provide the inlet with a large, stable airflow range. This system allows the inlet to be operated near the optimum performance condition without being susceptible to inlet unstart as a result of small variations in inlet airflow. Previous research programs with the inlet on a coldpipe have shown that pressure-activated poppet-valve control of the stability bypass airflow results in very large, stable airflow margins for the inlet. For further evaluation of the inlet and stability system, the inlet was tested on a turbojet engine. Inlet and engine responses were determined for several transient airflow disturbances, both external and internal. For reference, data were obtained with a conventional fixed exit controlling the bypass airflow. Limited unstarted-inlet bleed performance data were also obtained. The test was conducted in the Lewis 10- by 10-Foot Supersonic Wind Tunnel at a Mach number of 2.5 with the following results:

1. The poppet-valve-controlled inlet-stability bypass system had no adverse effects on the performance of the inlet or engine.

2. The inlet with a poppet-valve stability bypass exit control retarded the upstream movement of the terminal shock. It thus prevented unstart for internal airflow disturbances that had caused unstart for the inlet configuration with conventional, fixed, performance-bleed exits.

3. With the inlet operating at a high performance condition for an inlet-engine match, the poppet-valve stability bypass control prevented the inlet from unstarting for all downstream disturbances except an engine stall. For example, the poppet-valve stability bypass system could absorb the reduction in subsonic diffuser airflow caused by reducing the engine speed from the match condition to idle.

4. During an inlet unstart after an engine stall, the pressure fluctuations in the inlet with poppet-valve stability bypass exit control were not as severe as for the small-fixed-exit-area control.

5. The poppet-valve exit control prevented inlet unstart for external airflow disturbances 16 percent larger than that which caused inlet unstart for the fixed-exit control configuration.

6. When the poppet-valve-controlled inlet unstarted as a result of an external airflow disturbance, the longest time required for the inlet restart - engine relight sequence was 1.5 seconds. In general, this time was dictated by engine relight since inlet restart required about 0.2 second.

7. Some of the inlet unstarts that resulted from external airflow disturbances did not cause the engine to stall and the combustor to blow out. In the one inlet unstart for the poppet-valve-controlled system in which stall and blowout did occur, the engine was relighted in less than 0.1 second and the inlet was restarted about 0.15 second later.

8. When the inlet was in an unstarted condition, the stability bypass system could remove large amounts of airflow before inlet buzz occurred. For example, at the design centerbody position, the stability-bypass-bleed, unstarted buzz limit was between the started supercritical and minimum stable bypass characteristic curves.

9. Extending the centerbody with the inlet unstarted increased the airflow removal capability of the stability bypass system before the inlet buzz limit was reached.

Lewis Research Center,
National Aeronautics and Space Administration,
Cleveland, Ohio, July 26, 1978,
505-04.

APPENDIX A

ENGINE AND POPPET-VALVE AIRFLOWS

Engine corrected airflow and stability bypass mass flow were determined by the following procedures.

Engine Airflow

It is very difficult to measure engine airflow either in a wind tunnel or in flight. Therefore, the engine is usually extensively calibrated in a static test facility before, and perhaps after, the propulsion test program. But a different approach to obtaining the engine airflow was used in this investigation.

During the coldpipe investigation of this inlet (ref. 1) the airflow calculated from compressor-face instrumentation was compared with the airflow measured by the choked-exit plug system. From this calibration the compressor-face-calculated airflow can be corrected during an engine test to accurately represent engine airflow. The compressor-face-calculated airflow $W_{corr,cf}$ and the choked-exit-plug-measured airflow $W_{corr,cep}$ are compared in figure 49.

Compressor-face airflow was calculated by the following equation:

$$W_{corr,cf} = \frac{16.102\left(\frac{m_{cf}}{m_0}\right)A_i\left(\frac{A^*}{A}\right)_0}{\frac{P_{cf}}{P_0}}$$

where A_i is the inlet capture area of 0.1757 m^2; P_{cf}/P_0 is the compressor-face, total-pressure recovery (also P_2/P_0); $(A^*/A)_0$ is the area ratio for the free-stream Mach number; and m_{cf}/m_0 was determined from

$$\frac{m_{cf}}{m_0} = \frac{P_{cf}A_{cf}\left(\frac{A^*}{A}\right)_{cf}}{P_0A_i\left(\frac{A^*}{A}\right)_0}$$

where A_{cf} is the annulus flow area at the compressor-face rake station of 0.1177 m^2 and where

$$\left(\frac{A^*}{A}\right)_{cf} = f(M_{cf})$$

(The compressor-face Mach number M_{cf} was determined from the average static and total pressures at the rake station.)

As shown in figure 49, the calculated compressor-face corrected airflow was larger than the actual corrected airflow as determined by the choked plug. Therefore, during the engine test program, the engine corrected airflow ($W_{corr,2}$ or $W_{corr,cep}$) was obtained by applying the calibration curve in figure 49 to measured compressor-face airflows $W_{corr,cf}$. If engine mass-flow m_2/m_0 is required, the corrected airflow equation and the value for $W_{corr,2}$ are used to obtain the correct value.

Stability Bypass Poppet Valve Airflows

The stability bypass mass-flow ratio was determined by subtraction, as follows:

$$\frac{m_{sb}}{m_0} = \frac{m_i}{m_0} - \frac{m_2}{m_0} - \frac{m_{by}}{m_0} - \frac{m_{cb}}{m_0}$$

where m_i/m_0 is the capture mass-flow ratio (1.0 for the inlet cruise Mach number), m_2/m_0 was determined from the calibration curves for the engine-face rake station, and m_{by}/m_0 and m_{cb}/m_0 were measured values of overboard bypass and centerbody mass flows.

APPENDIX B

SYMBOLS

A	flow area, m^2
A_c	cowl-lip capture area, 0.1757 m^2
A_8	primary-nozzle area, m^2
CO	converging-vortex generator pair
CPR	compressor pressure ratio, P_3/P_2
DI	diverging-vortex generator pair
f	pulse frequency, $1/\tau$, sec^{-1}
H	annulus or rake height at local diffuser station, cm
h	distance from inlet surface, cm
M	Mach number
m	mass flow, kg/sec
m_0	free-stream mass flow based on A_c, kg/sec
m/m_0	mass-flow ratio
N	engine speed, rpm
N^*	rated engine speed, 16 500 rpm
$N/N^*\sqrt{\theta_2}$	corrected engine speed
P	total pressure, N/m^2
ΔP	fluctuating component of local pressure
p	static pressure, N/m^2
PLA	power lever angle (throttle), deg
R_c	inlet cowl-lip radius, 23.66 cm
r	radius, cm
SI	stability index, $\left(1 - \frac{W_{corr,\,min\ s,\,2}}{W_{corr,\,op,\,2}}\right) \times 100$
SI_t	transient stability index, $\left(1 - \frac{W_{corr,\,t,\,min\ s,\,2}}{W_{corr,\,op,\,2}}\right) \times 100$

T	total temperature, K
W	weight flow rate, kg/sec
W_{corr}	corrected airflow, $W\sqrt{\theta}/\delta$, kg/sec
x	axial station, cm
x_{cb}	centerbody position measured from $M_0 = 2.5$ design cone tip position, cm
x/R_c	axial distance ratio, inlet radii
α	angle of attack, deg
δ	$P/(10.13\times10^4\ N/m^2)$
θ	T/288.2 K
θ_ℓ	cowl-lip position parameter, $\tan^{-1}\left(\frac{1}{\frac{x}{R_c}}\right)$
τ	transient pulse width, sec
φ	circumferential position, deg

Subscripts:

av	average
b	bleed
bp	bleed plenum
by	overboard bypass
cb	inlet centerbody
cf	compressor face
cep	choked exit plug
e	exhaust
fp	flat plate
ℓ	local
max	maximum
min	minimum
min s	minimum stable inlet operating point
op	inlet operating point
pv	poppet valve
pvi	poppet valve internal

ref	reference
sb	stability bypass
t	transient
uns	unstart
0	free-stream
2	compressor-face station
3	compressor discharge station
5	turbine-exit station
8	exhaust station (primary nozzle)

REFERENCES

1. Sanders, Bobby W.; and Mitchell, Glenn A.: Throat-Bypass Bleed Systems for Increasing the Stable Airflow Range of a Mach 2.50 Axisymmetric Inlet with 40-Percent Internal Contraction. NASA TM X-2779, 1973.

2. Mitchell, Glenn A.; and Sanders, Bobby W.: Airflow Control System for Supersonic Inlets. U.S. Patent 3,799,475, Mar. 1974.

3. Sanders, Bobby W.; and Mitchell, Glenn A.: Increasing the Stable Operating Range of a Mach 2.5 Inlet. AIAA Paper 70-686, June 1970.

4. Bowditch, David N.; et al.: Supersonic Cruise Inlets. Aircraft Propulsion. NASA SP-259, 1971, pp. 283-312.

5. Mitchell, Glenn A.; and Sanders, Bobby W.: Pressure-Activated Stability-Bypass-Control Valves to Increase the Stable Airflow Range of a Mach 2.5 Inlet with 40-Percent Internal Contraction. NASA TM X-2972, 1974.

6. Mitchell, Glenn A.; and Sanders, Bobby W.: Poppet Valve Control of a Throat Stability Bypass to Increase the Stable Airflow Range of a Mach 2.5 Inlet with 60-Percent Internal Contraction. NASA TM X-3297, 1975.

7. Shaw, Robert J.; Mitchell, Glenn A.; and Sanders, Bobby W.: Forward-Slanted Slot Throat Stability Bypass to Increase the Stable Airflow Range of a Mach 2.5 Inlet with 60-Percent Internal Contraction. NASA TM X-2973, 1974.

8. Shaw, Robert J.; Mitchell, Glenn A.; and Sanders, Bobby W.: Distributed Porous Throat Stability Bypass to Increase the Stable Airflow Range of a Mach 2.5 Inlet with 60-Percent Internal Contraction. NASA TM X-2974, 1974.

9. Shaw, Robert J.; Mitchell, Glenn A.; and Sanders, Bobby W.: Distributed Educated Throat Stability Bypass to Increase the Stable Airflow Range of a Mach 2.5 Inlet with 60-Percent Internal Contraction. NASA TM X-2975, 1974.

10. Mitchell, Glenn A.; Sanders, Bobby W.; and Shaw, Robert J.: Throat Stability-Bypass Systems to Increase the Stable Airflow Range of a Mach 2.5 Inlet with 60-Percent Internal Contraction. NASA TM X-2976, 1974.

11. Anderson, Bernhard H.: Design of Supersonic Inlets by a Computer Program Incorporating the Method of Characteristics. NASA TN D-4960, 1969.

12. Wasserbauer, Joseph F.; and Choby, David A.: Performance of a Bicone Inlet Designed for Mach 2.5 with Internal Distributed Compression and 40-Percent Internal Contraction. NASA TM X-2416, 1972.

13. Coltrin, Robert E.; and Calogeras, James E.: Supersonic Wind Tunnel Investigation of Inlet-Engine Compatibility. AIAA Paper 69-487, June 1969.

14. Blausey, G. C.; Coleman, D. M.; and Harp, D. S.: Feasibility Study of Inlet Shock Stability System of YF-12. (Sp-1964, Lockhead Aircraft Corp.) NASA CR-134594, 1972.

15. Dustin, Miles O.; and Neiner, George H.: Evaluation by Step Response Tests of Prototype Relief Valves Designed for YF-12 Inlet Stability Bleed System. NASA TM X-3262, 1975.

16. Cole, Gary L.; Neiner, George H.; and Crosby, Michael J.: An Automatic Restart Control System for an Axisymmetric Mixed-Compression Inlet. NASA TN D-5590, 1969.

17. Choby, David A.: Tolerance of Mach 2.50 Axisymmetric Mixed-Compression Inlets to Upstream Flow Variations. NASA TM X-2433, 1972.

18. McLafferty, George M.; and Ranard, E.: Pressure Losses and Flow Coefficients of Slanted Perforations Discharging from Within a Simulated Supersonic Inlet. R-0920-1, United Aircraft Corp., 1958.

19. Syberg, J.; and Hickcox, T. E.: Design of a Bleed System for a Mach 3.5 Inlet. NASA CR-2187, 1973.

TABLE I. - INLET COORDINATES

(a) Centerbody

Axial distance from centerbody tip, x/R_c	Inlet cowl-lip radius ratio, r/R_c
0	0
10^o Conical section	
1.0323	0.1820
18.5^o Conical section	
2.7620	0.7608
2.800	.7696
2.850	.7794
2.900	.7874
2.950	.7937
3.000	.7986
3.050	.8025
3.100	.8045
3.150	.8043
3.200	.8030
3.250	.8015
3.300	.8000
3.350	.7982
3.400	.7964
3.450	.7944
3.500	.7925
3.550	.7906
3.600	.7886
3.650	.7862
3.700	.7834
3.750	.7798
3.800	.7757
3.850	.7711
3.900	.7655
3.950	.7590
4.000	.7513
4.050	.7426
4.100	.7330
4.150	.7230
4.200	.7133
4.250	.7036
4.300	.6924
4.350	.6810
4.400	.6692
4.450	.6577
4.500	.6455
4.550	.6330
4.600	.6205
4.650	.6085
4.700	.5960
4.750	0.5825
4.800	.5700
4.850	.5573
4.900	.5448
4.950	.5320
5.000	.5195
5.050	.5075
5.100	.4983
5.150	.4895
5.200	.4805
5.250	.4715
5.300	.4622
5.350	.4534
5.400	.4444
5.450	.4352
5.500	.4264
5.550	.4175
5.600	.4085
5.650	.3995
5.700	.3900
5.750	.3815
5.800	.3732
5.850	.3650
5.900	.3566
5.950	.3488
6.000	.3412
6.050	.3339
6.100	.3266
6.150	.3196
6.200	.3130
6.250	.3068
6.300	.2985
6.350	.2910
6.400	.2845
6.450	.2780
6.500	.2716
6.550	.2655
6.600	.2597
6.650	.2545
6.700	.2501
6.750	.2464
6.800	.2430
6.850	.2410
6.900	.2400
6.950	.2396
7.000	.2394
Cylinder	
7.8858	0.2394

(b) Cowl

Axial distance from centerbody tip, x/R_c	Inlet cowl-lip radius ratio, r/R_c
2.117	1.0000
2.150	1.0028
2.200	1.0070
2.250	1.0111
2.300	1.0154
2.350	1.0193
2.400	1.0228
2.450	1.0261
2.500	1.0290
2.550	1.0317
2.600	1.0340
2.650	1.0360
2.700	1.0373
2.750	1.0382
2.800	1.0386
2.850	1.0386
2.900	1.0381
2.950	1.0370
3.000	1.0356
3.050	1.0337
3.100	1.0320
3.150	1.0304
3.200	1.0290
3.250	1.0275
3.300	1.0262
3.350	1.0251
3.400	1.0239
3.450	1.0227
3.500	1.0215
3.550	1.0204
3.600	1.0192
3.650	1.0176
3.700	1.0160
3.750	1.0144
3.800	1.0124
3.850	1.0100
3.900	1.0071
3.950	1.0037
4.000	1.0000
4.050	.9955
4.100	.9908
4.150	.9858
4.200	.9808
4.250	.9756
4.300	.9702
4.350	.9659
4.400	.9595
4.450	.9538
4.500	.9481
4.550	.9426
4.600	0.9374
4.650	.9324
4.700	.9276
4.750	.9232
4.800	.9191
4.850	.9153
4.900	.9120
4.950	.9087
5.000	.9050
5.050	.9044
5.100	.9049
5.150	.9058
5.200	.9071
5.250	.9086
5.300	.9102
5.350	.9118
5.400	.9132
5.450	.9145
5.500	.9157
5.550	.9166
5.600	.9173
5.650	.9177
5.700	.9179
Cylinder	
6.1747	0.9179
Bypass gap	
6.7847	0.8868
6.800	.8865
6.850	.8855
6.900	.8846
6.950	.8837
7.000	.8823
7.050	.8805
7.100	.8785
7.150	.8760
7.200	.8734
7.250	.8707
7.300	.8677
7.350	.8654
7.400	.8639
7.450	.8631
7.500	.8627
7.550	.8623
7.600	.8621
Cylinder	
7.8858	0.8621

TABLE II. - COWL AND CENTERBODY STATIC-

PRESSURE TAP LOCATIONS

[Top centerline.]

(a) Cowl

Axial distance from centerbody tip, x/R_c	Axial distance from centerbody tip, x/R_c
2.684	3.380
2.807	3.434
2.859	3.489
2.894	3.564
2.930	3.639
2.964	3.714
2.999	3.950
3.038	4.192
3.066	4.519
3.101	4.847
3.136	5.202
3.170	5.529
3.205	6.119
3.240	6.742
3.275	7.311
3.310	
3.345	

(b) Centerbody

Axial distance from centerbody tip, x/R_c	Axial distance from centerbody tip, x/R_c
2.308	3.389
2.670	3.441
2.751	3.489
2.802	3.543
2.834	3.586
2.858	3.629
2.893	3.671
2.963	3.714
3.030	3.795
3.102	3.875
3.140	3.951
3.173	4.192
3.210	4.519
3.247	4.847
3.285	5.202
3.317	7.311
3.353	

TABLE III. - DYNAMIC INSTRUMENTATION LOCATIONS

Probe	Description	Reference figure	Comments
D1	Cowl static pressure	15	Inlet dynamics
D2	↓	↓	↓
D3			
D4			
D5		↓	
D6	↓	13	
D7	Stability-bypass-plenum total pressure	15	
D8	Compressor-face static pressure	12	
D9	Compressor-face total pressure	12	↓
D10	Compressor-exit total pressure	14	Used to obtain compressor pressure ratio
S1	Cowl static pressure	15	(Inlet unstart sensor
S2	Inlet throat total pressure	15	pickups)
S3	Terminal shock position sensor	15	Analog computer

Figure 1. - Bottom view of model installed in 10- by 10-Foot Supersonic Wind Tunnel.

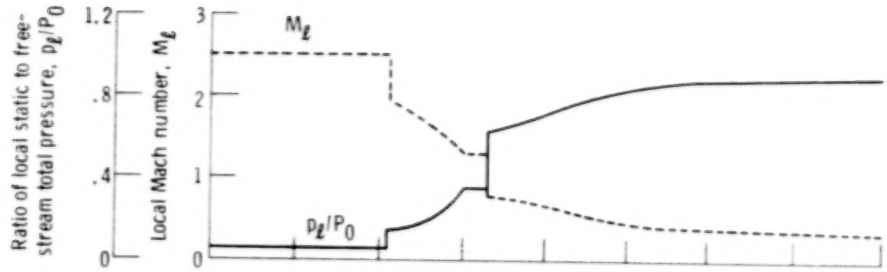

(a-1) Cowl surface conditions.

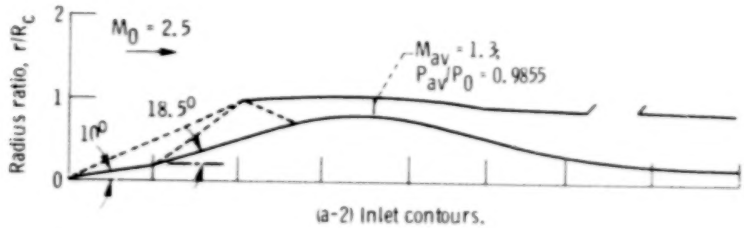

(a-2) Inlet contours.

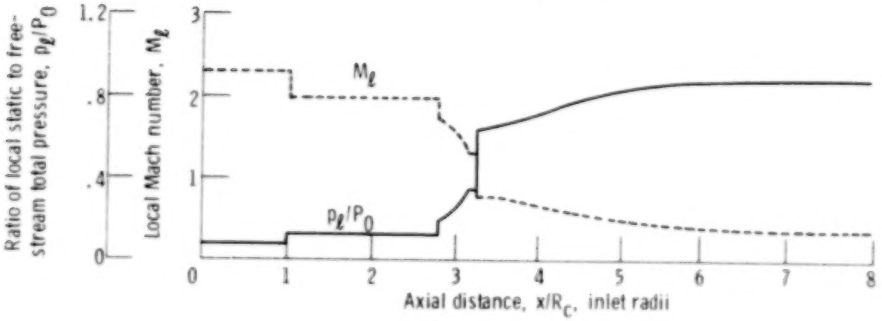

(a-3) Centerbody surface conditions.

(a) Inlet dimensions and airflow conditions. Free-stream Mach number, M_0, 2.5.

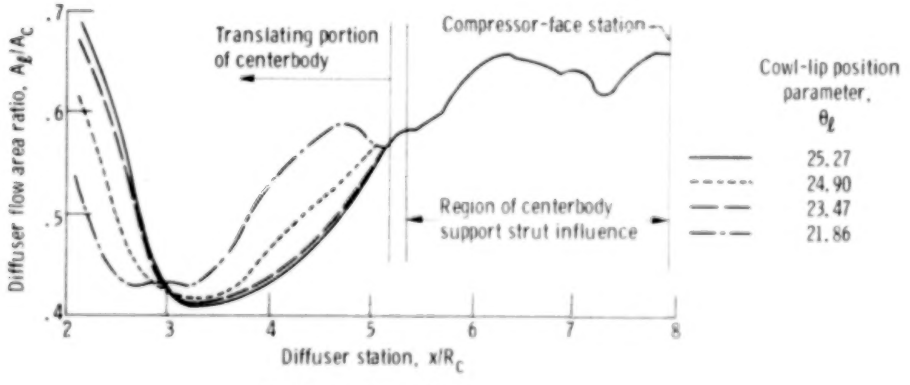

(b) Diffuser area variation.

Figure 2. - Aerodynamic details. Cowl-lip position parameter, θ_ℓ, 25.27°.

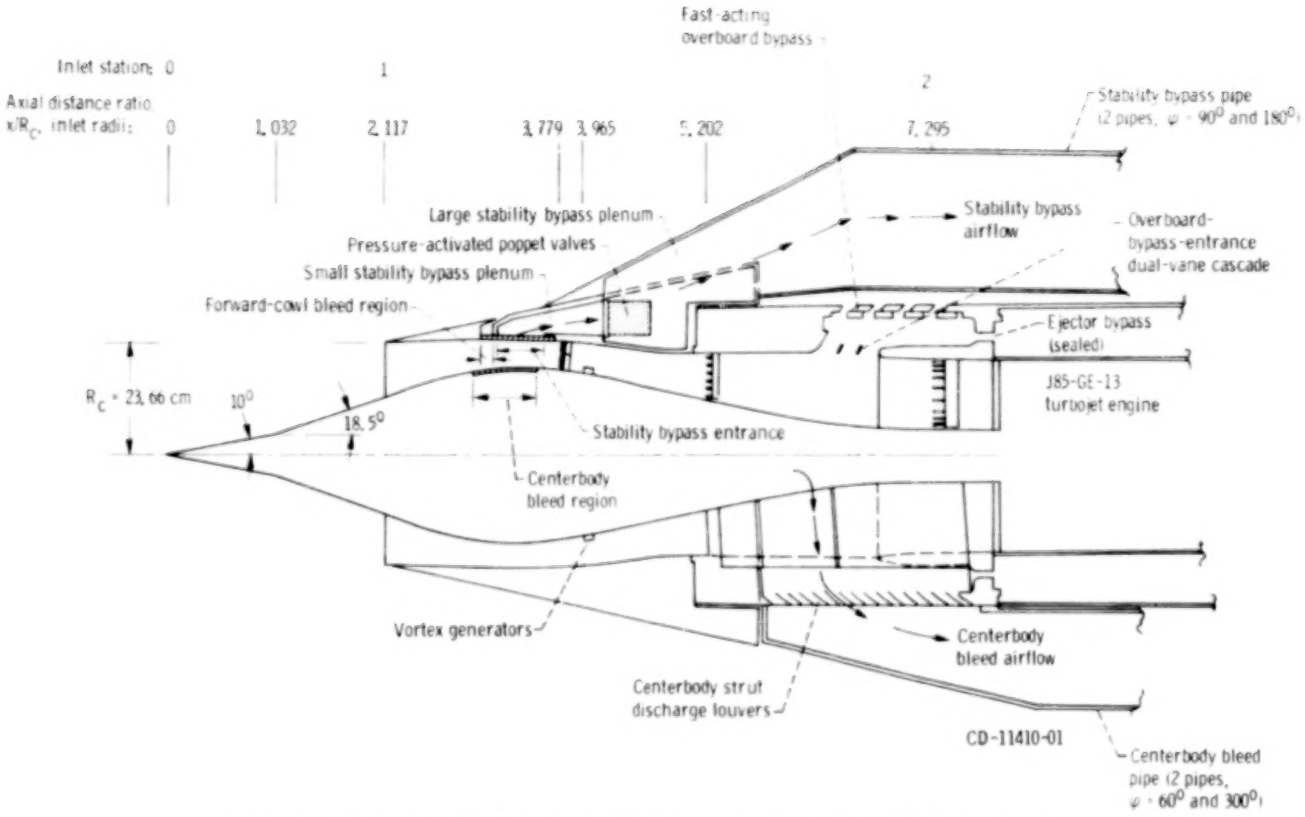

Figure 3. - Inlet details. (Pipes for ducting bleed airflow are not shown in true circumferential positions.)

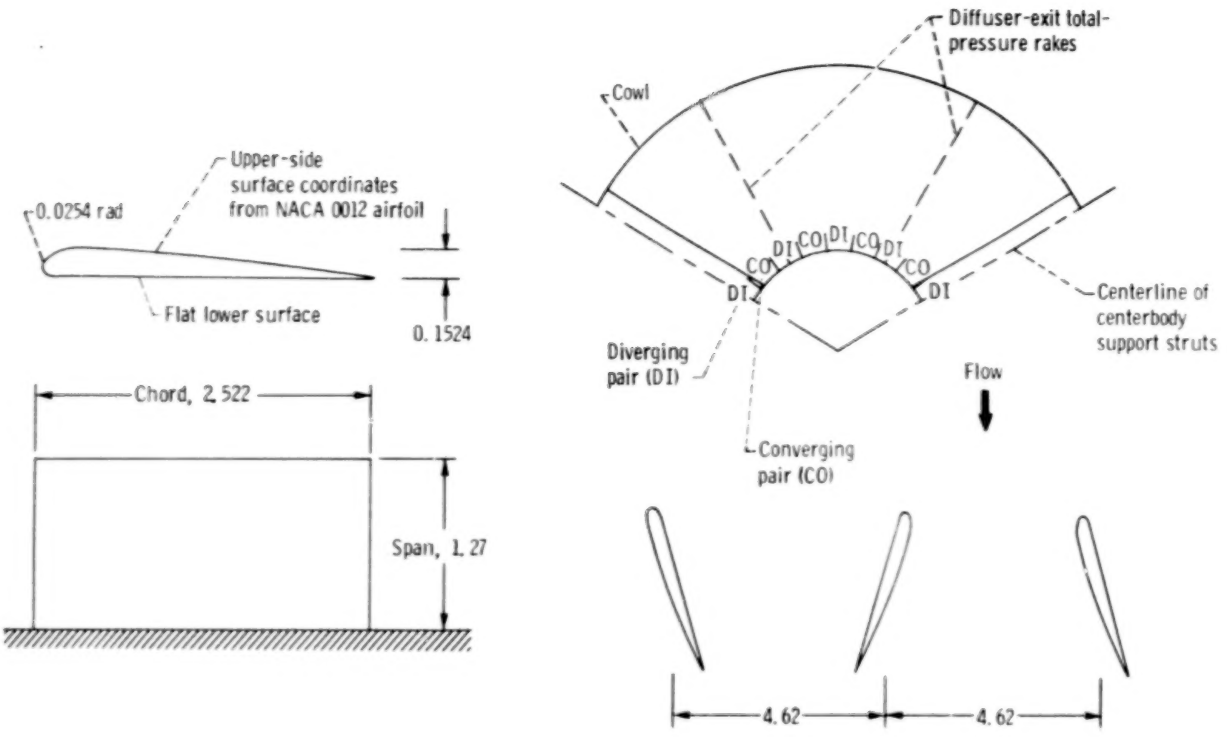

Figure 4. - Vortex generator design. (Dimensions are in cm.)

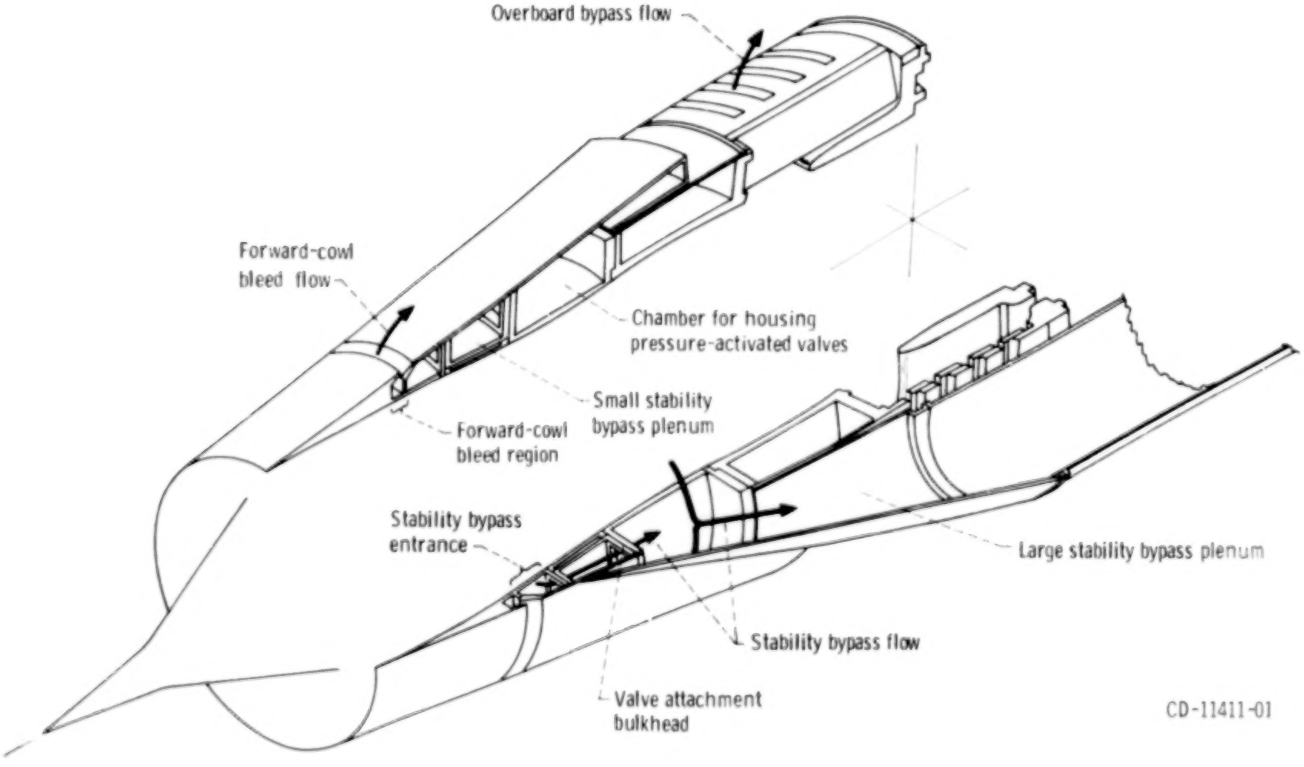

Figure 5. - Sketch of inlet cowl showing cowl bleed and bypass ducting.

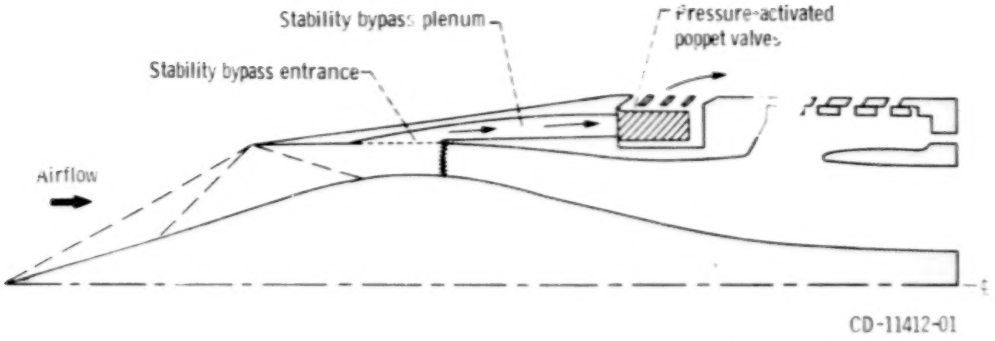

Figure 6. - Possible arrangement of flight inlet incorporating a poppet-valve-controlled inlet-stability bypass system.

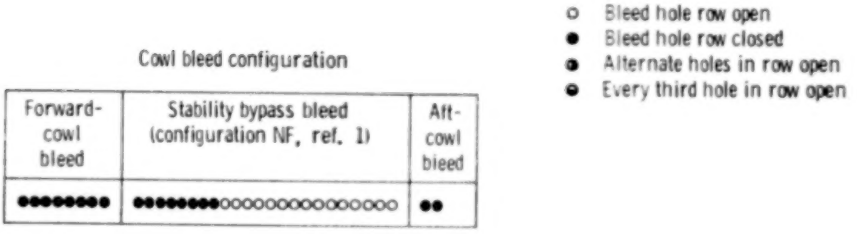

- Bleed hole row open
- Bleed hole row closed
- Alternate holes in row open
- Every third hole in row open

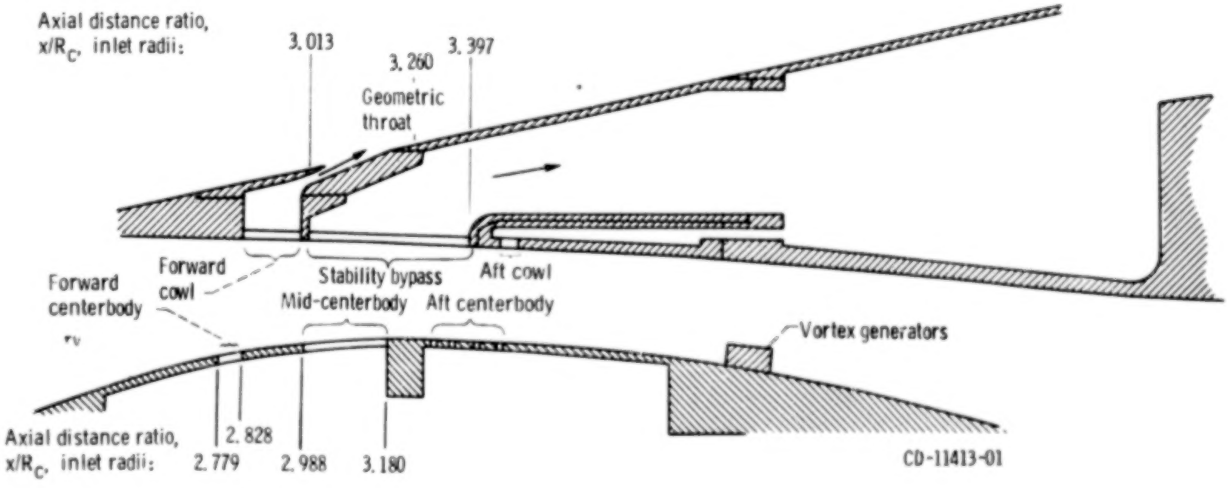

Centerbody bleed configuration

Forward bleed	Midbody bleed	Aft bleed
●●●●	●●●●●●●●●●●●	●●●●

Figure 7. - Sketch of model showing cowl, distributed, porous, stability-bypass-bleed system and centerbody performance-bleed system.

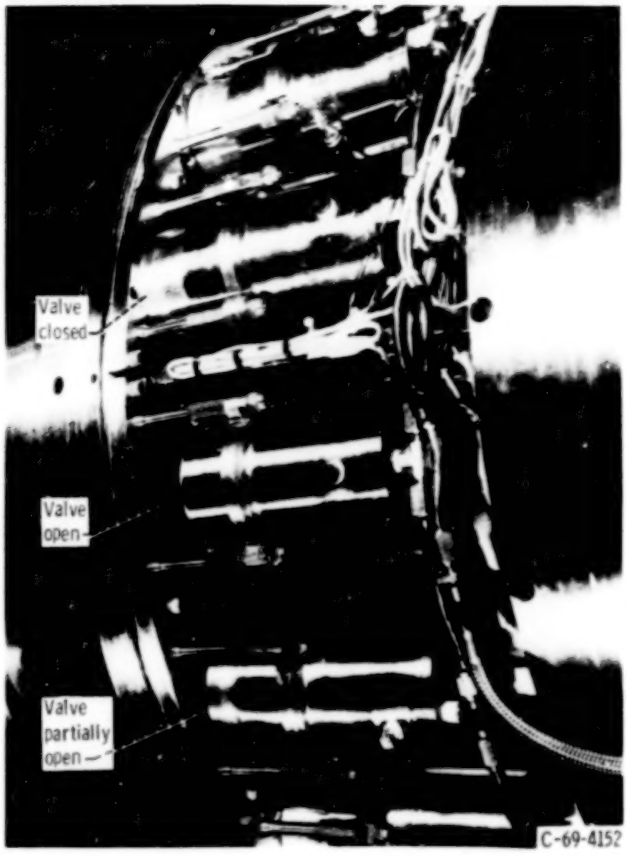

(a) Poppet-valve installation. (Several valve positions shown.)

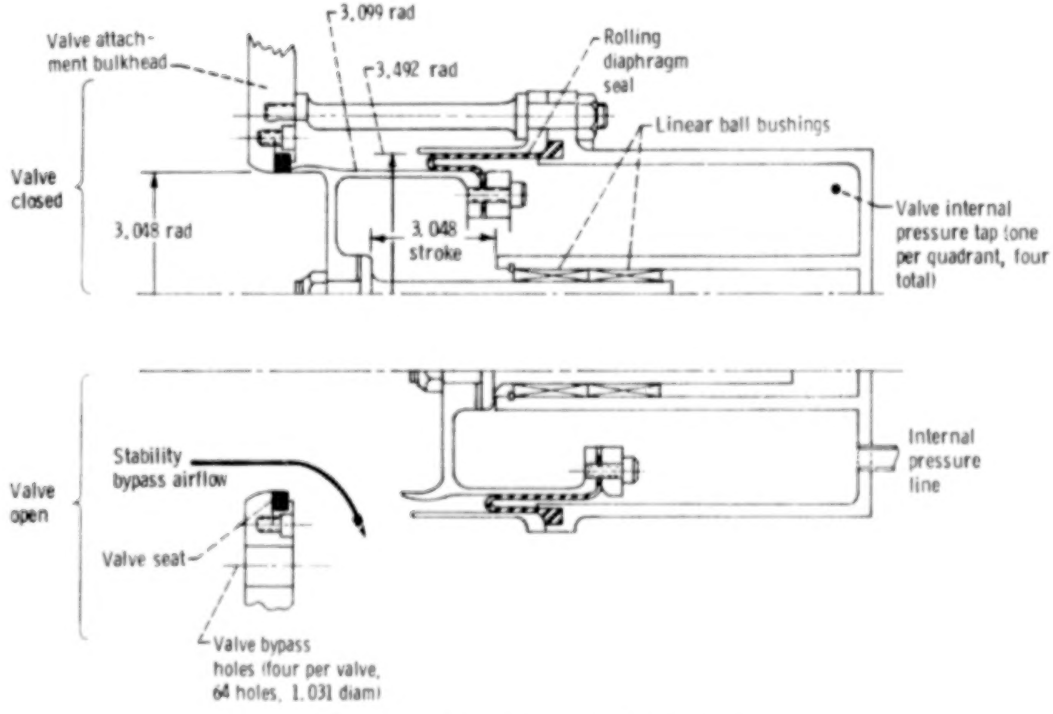

(b) Poppet-valve details. (Dimensions are in cm.)

Figure 8. - Poppet valve.

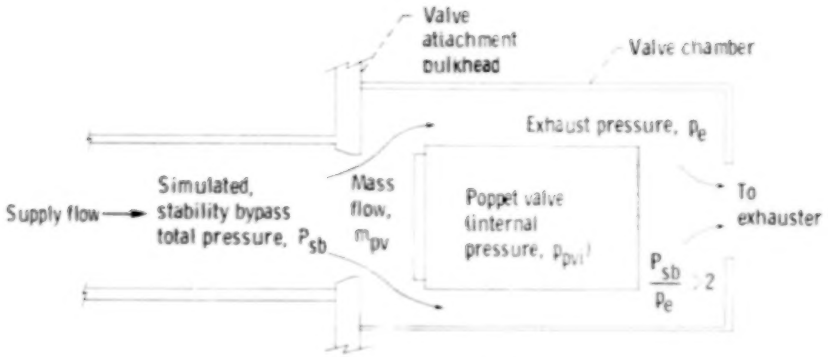

Schematic of bench test

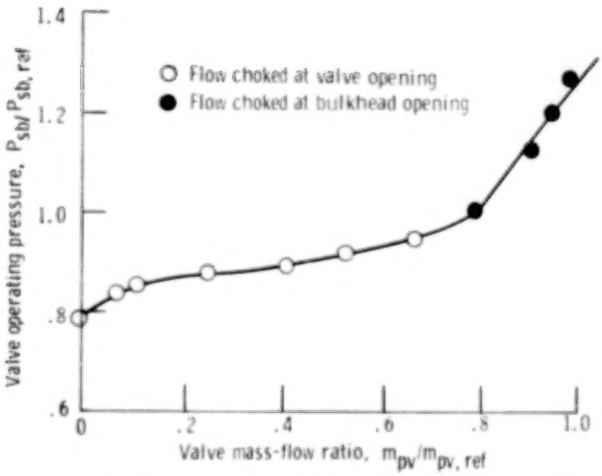

(c) Poppet-valve performance. Initial-stability bypass total pressure, P_{sb}, 3.1 N/cm^2; reference pressure, $P_{sb,ref}$, 3.9 N/cm^2; exhaust pressure, p_e, 0.7 to 1.01 N/cm^2.

Figure 8. - Concluded.

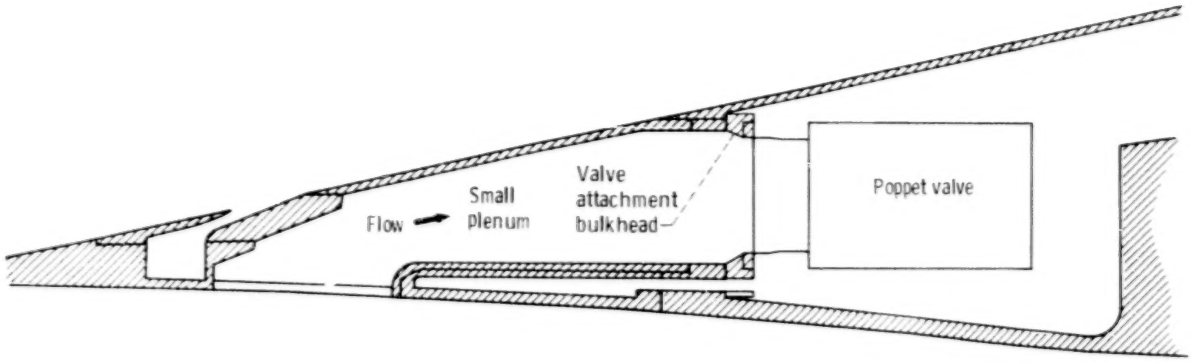

(a-1) Small stability-bypass-plenum volume.

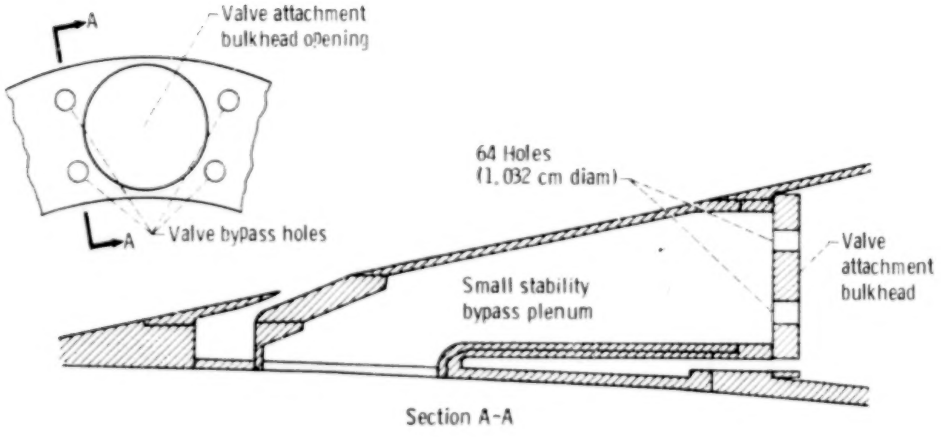

(a-2) Valve bulkhead hole locations for bypassing a mass flow ratio of approximately 0.02.

(a) Poppet valve closed.

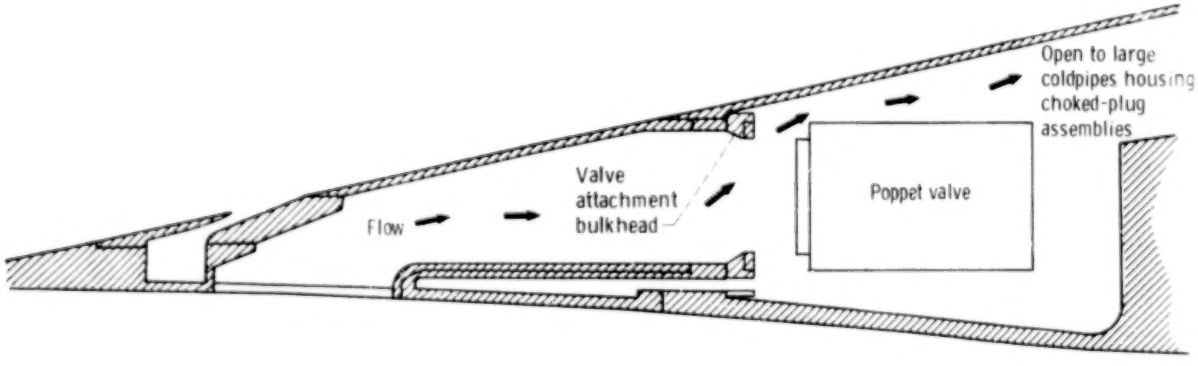

(b) Poppet valve open; large stability-bypass-plenum volume.

Figure 9. - Small and large stability-bypass-plenum volumes.

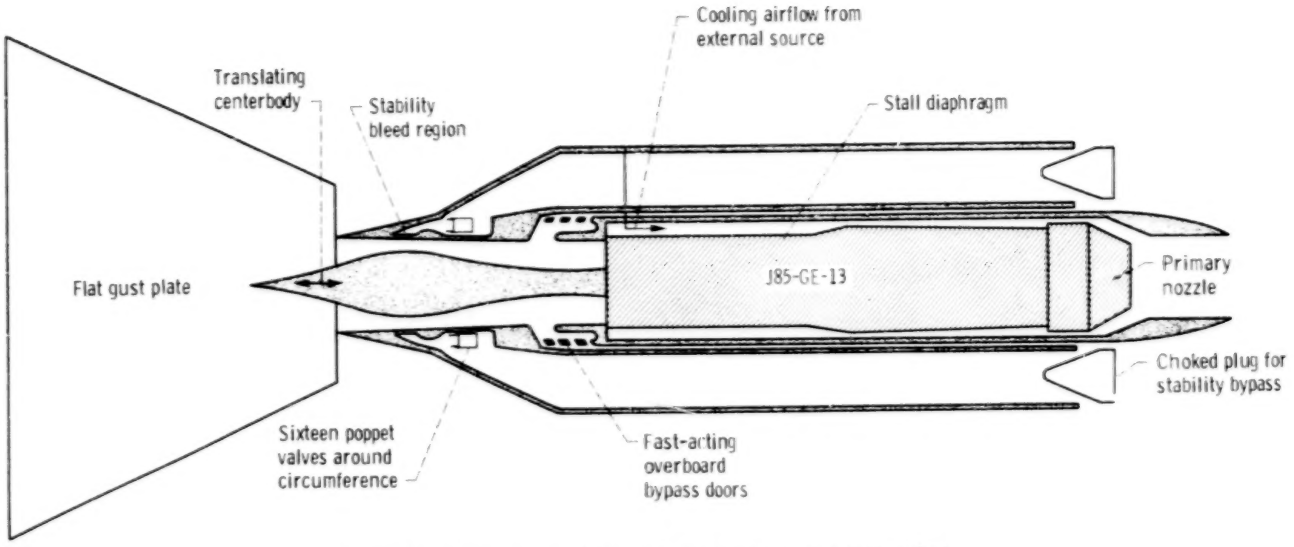

Figure 10. - Sketch of propulsion system and flat gust plate (bottom view).

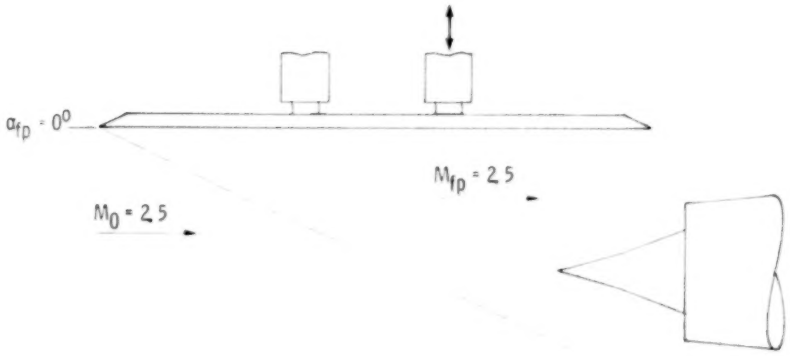

(a) Inlet operating at uniform design conditions: Free-stream Mach number, $M_0 = 2.50$; angle of attack, $\alpha = 0^0$.

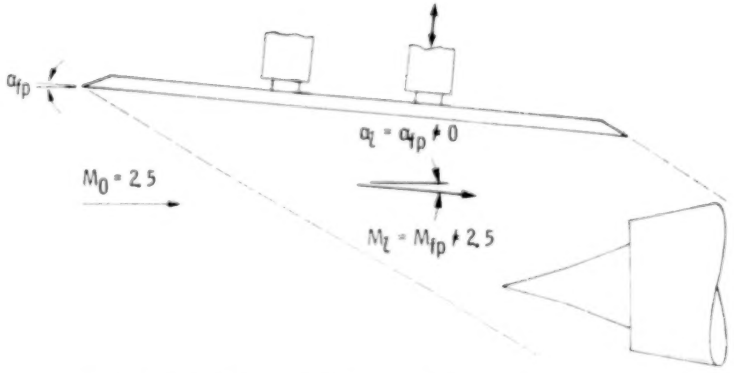

(b) Inlet operating at off-design conditions: Local Mach number, $M_l \neq 2.5$; local angle of attack, $\alpha_l \neq 0^0$.

Figure 11. - Typical installation of Mach 2.5 inlet with flat plate, where local inlet Mach number is a function of flat-plate angle.

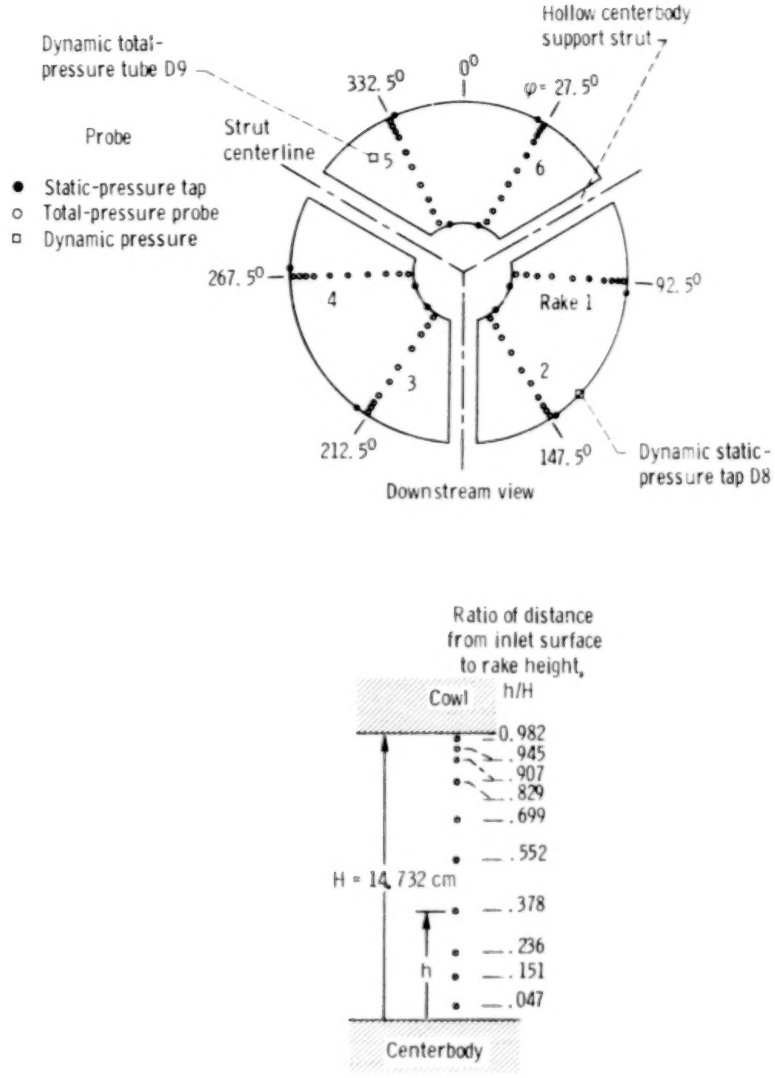

Figure 12. - Subsonic diffuser pressure instrumentation, showing typical exit rake and rake position at inlet station 2.

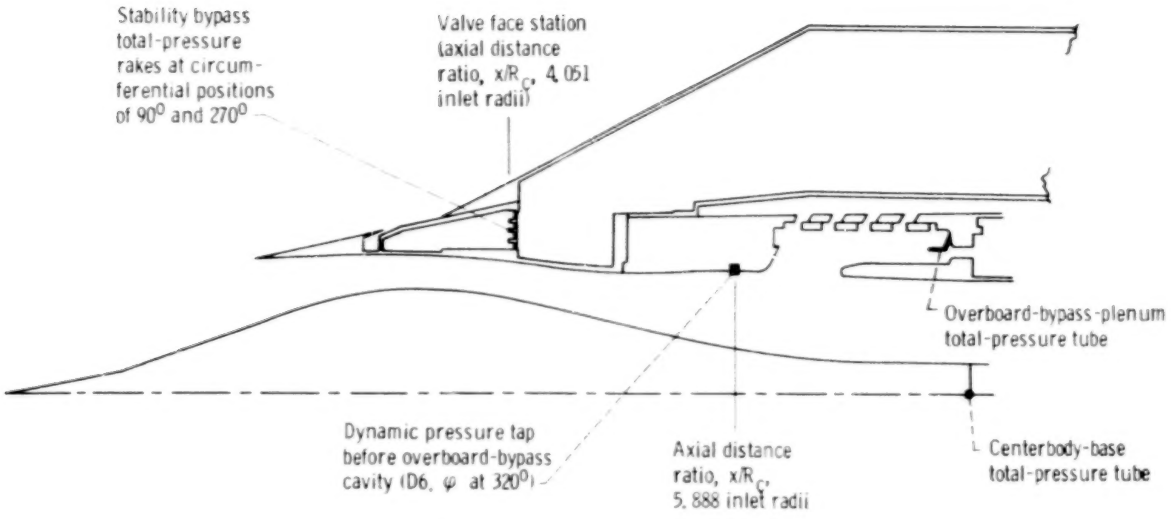

Figure 13. - Bleed and bypass pressure instrumentation.

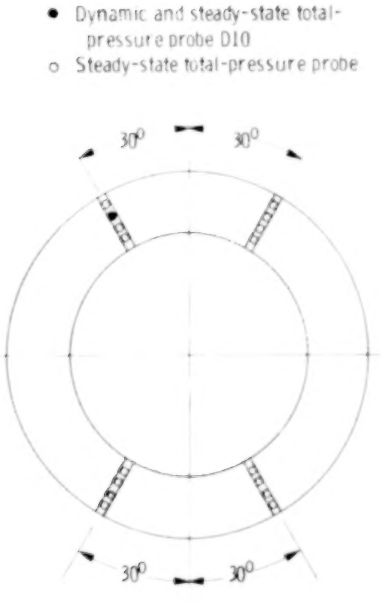

Figure 14. - Compressor discharge pressure instrumentation (downstream view).

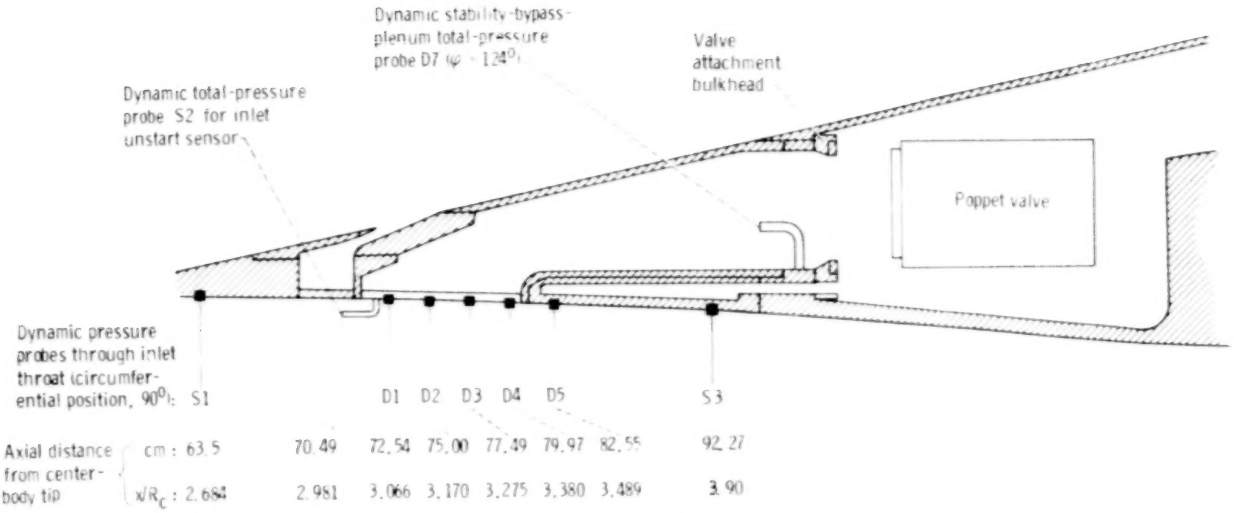

Figure 15. - Inlet-throat-region dynamic pressure instrumentation.

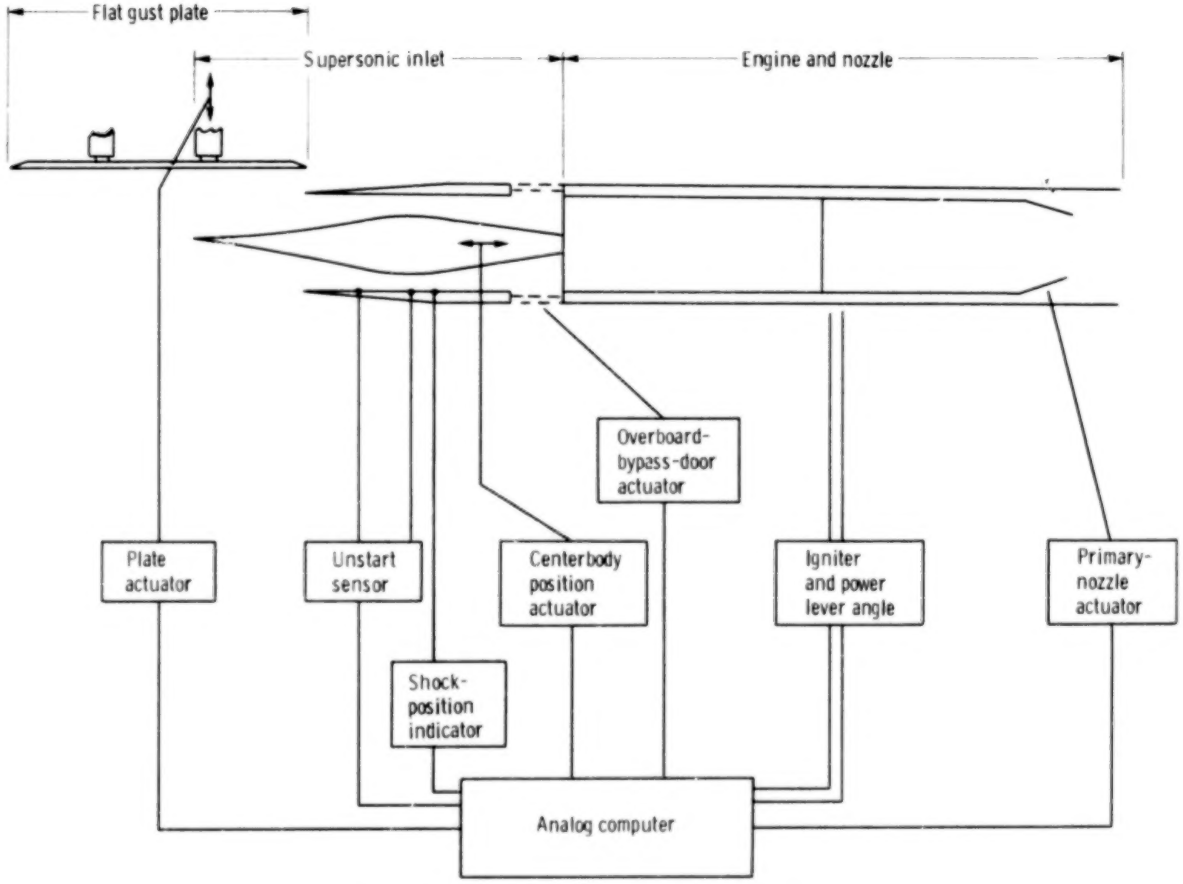

Figure 16. - Block diagram of propulsion system control.

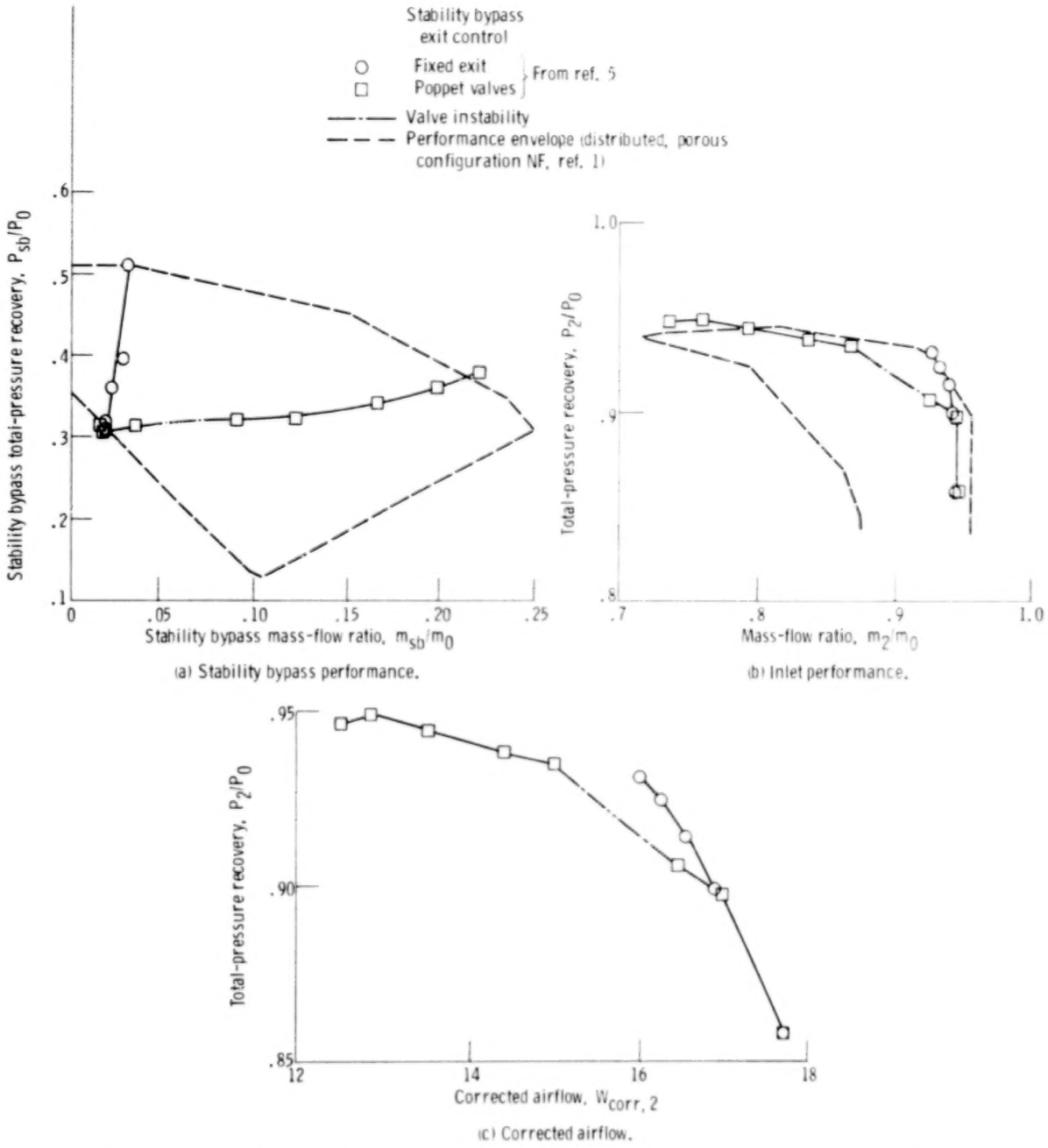

Figure 17. - Steady-state performance of inlet configuration as determined from previous coldpipe studies with fixed and poppet-valve stability bypass exit controls. Free-stream Mach number, M_0, 2.5.

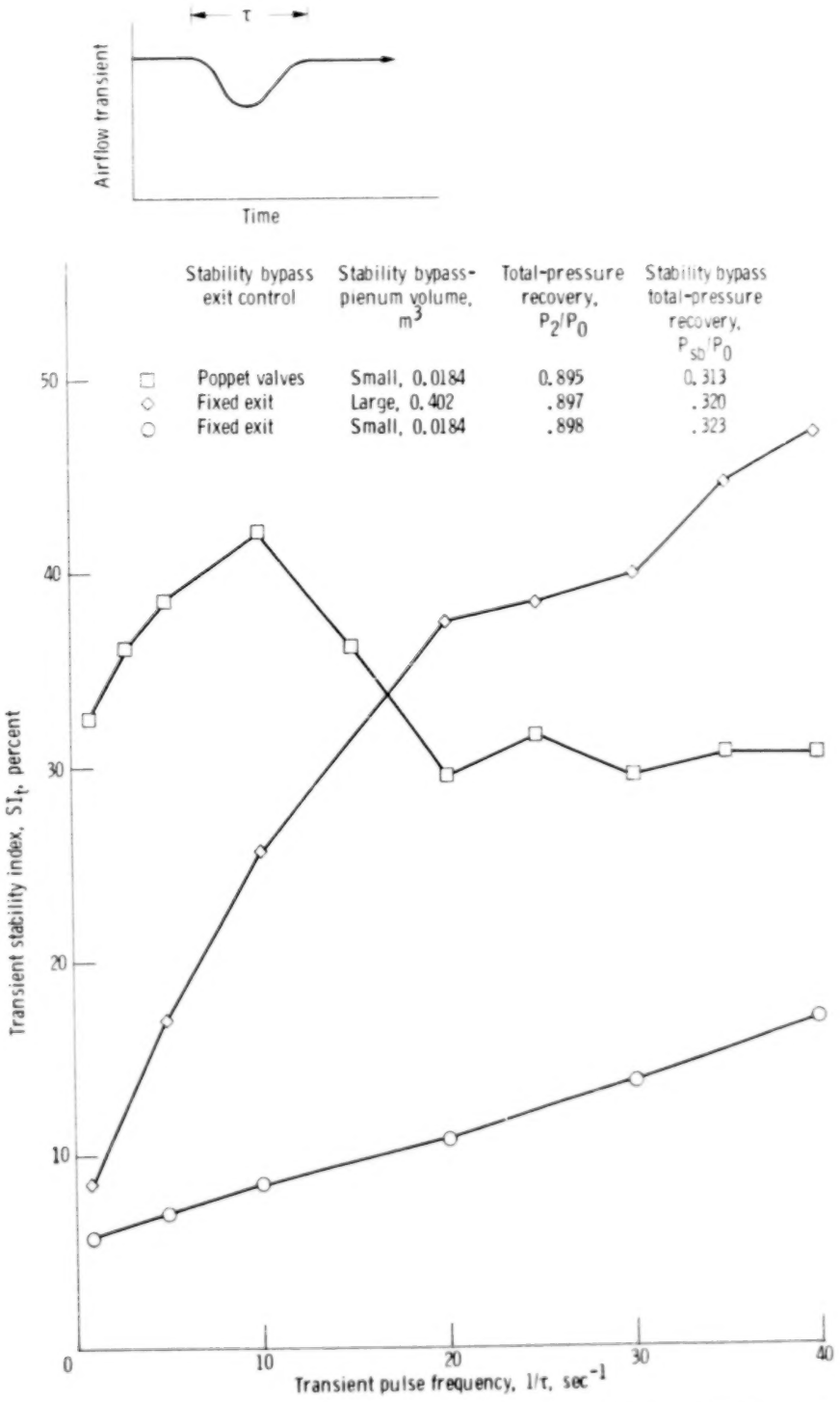

Figure 18. - Unstart limits of inlet configuration with several different stability bypass exit controls when subjected to transient internal airflow disturbances. Free-stream Mach number, M_0, 2.5.

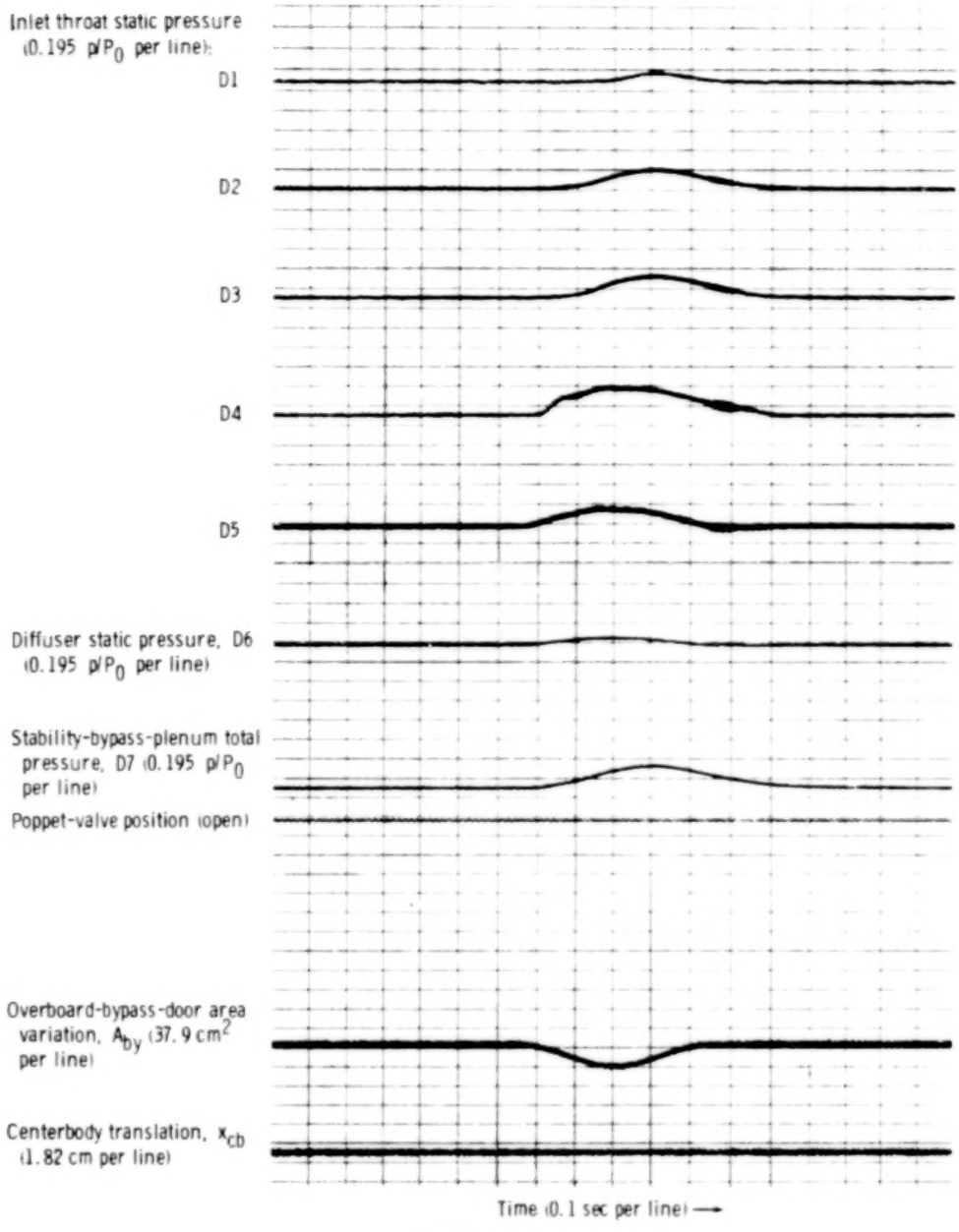

(a) Inlet response.

Figure 19. - Transient reduction in overboard bypass area with small, fixed exit as stability-bypass-bleed control and large stability bypass plenum - for transient overboard bypass flow area $A_{by,t}$ of 43.4 square centimeters. Free-stream Mach number, M_0, 2.5; transient pulse frequency, $1/\tau$, 2 seconds^{-1}; corrected engine speed, $N/N^* \sqrt{\theta}$, 0.848; total-pressure recovery, P_2/P_0, 0.907; mass-flow ratio, m_2/m_0, 0.844; primary-nozzle area, A_8, 0.0677 square meter.

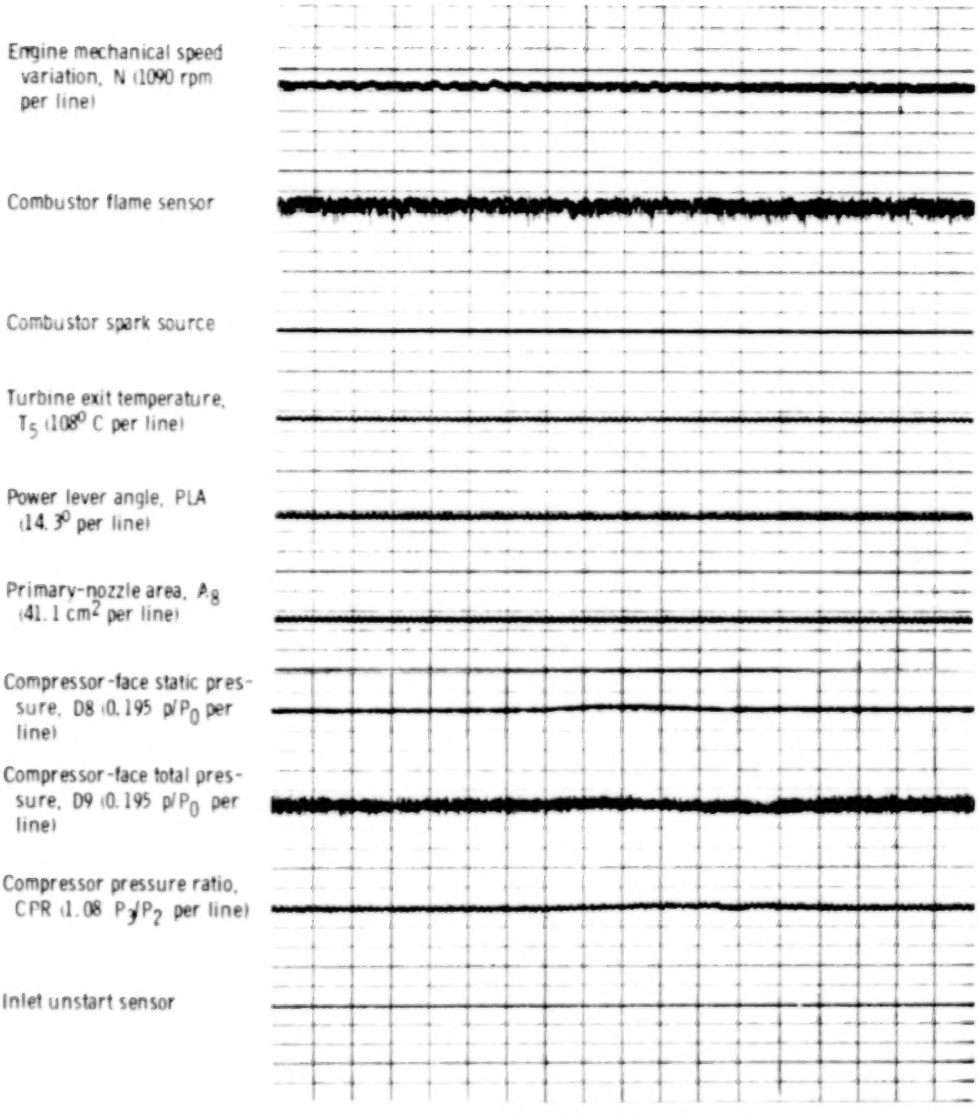

(b) Engine response.

Figure 19. - Concluded.

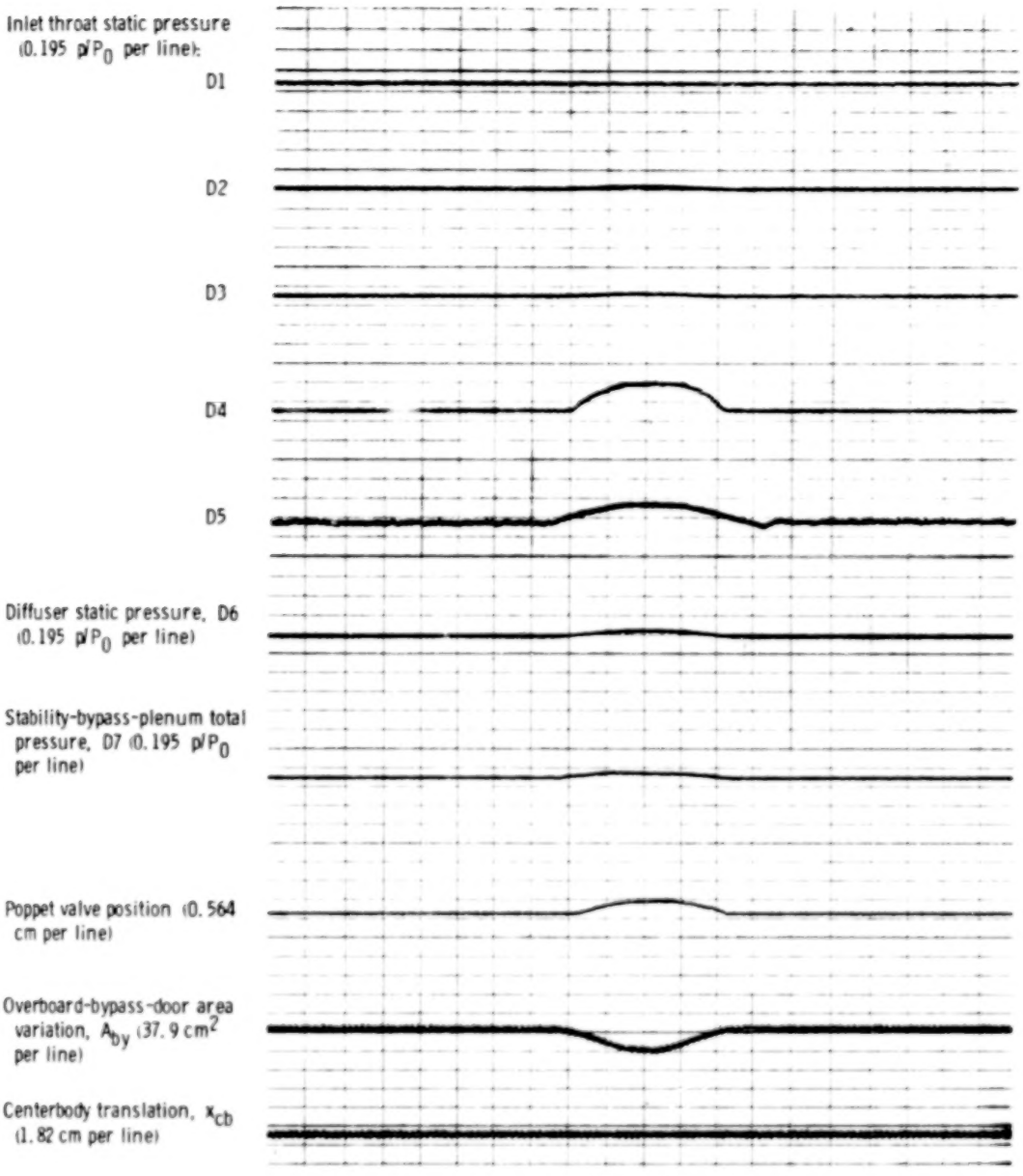

(a) Inlet response.

Figure 20. - Transient reduction in overboard bypass area with poppet valves as the stability-bypass-bleed control - for transient, overboard bypass flow area $A_{by,t}$ of 43.4 square centimeters. Free-stream Mach number, M_0, 2.5; transient pulse frequency, $1/\tau$, 2 seconds^{-1}; corrected engine speed, $N/N^\circ \sqrt{\theta}$, 0.853; total-pressure recovery, P_2/P_0, 0.905; mass flow ratio, m_2/m_0, 0.848; primary-nozzle area, A_8, 0.0647 square meter.

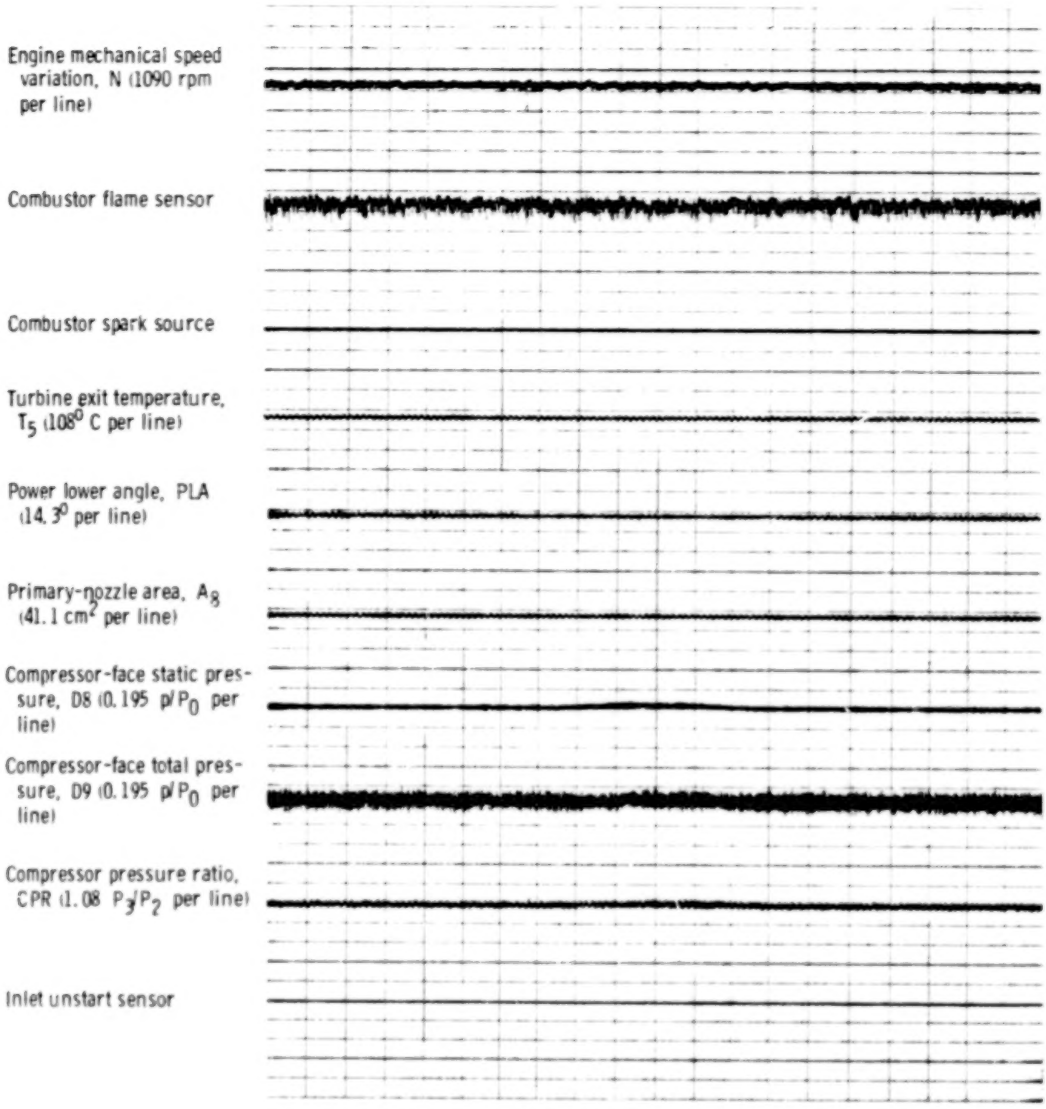

(b) Engine response.

Figure 20. - Concluded.

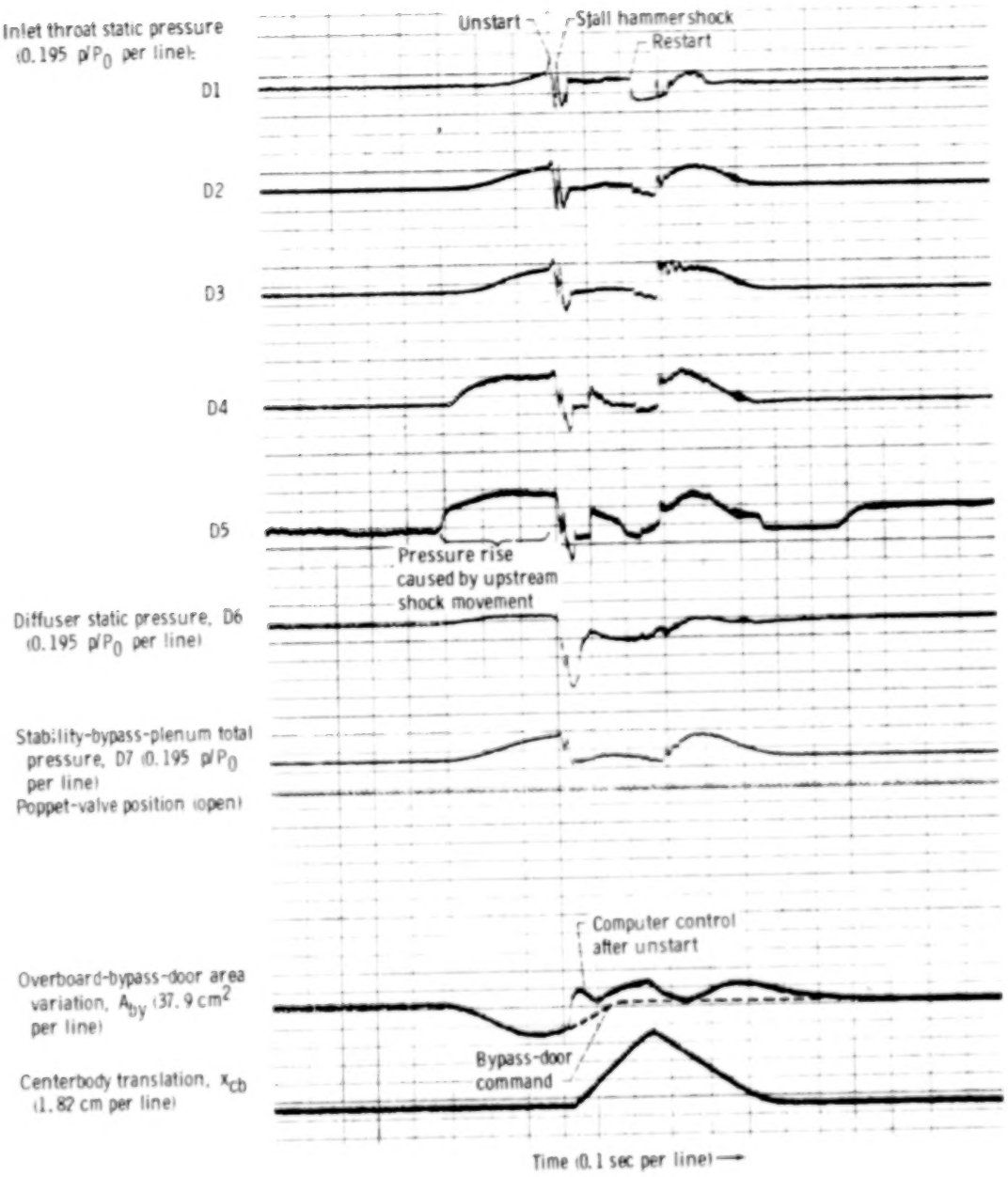

(a) Inlet response.

Figure 21. - Transient reduction in overboard bypass area with small, fixed exit as stability-bypass-bleed control and large stability bypass plenum - for transient overboard bypass flow area $A_{by,t}$ of 75.9 square centimeters. Free-stream Mach number, M_0, 2.5; transient pulse frequency, $1/\tau$, 2 seconds^{-1}; corrected engine speed, $N/N^* \sqrt{\theta}$, 0.848, total-pressure recovery, P_2/P_0, 0.907; mass-flow ratio, m_2/m_0, 0.844; primary-nozzle area, A_8, 0.0647 square meter.

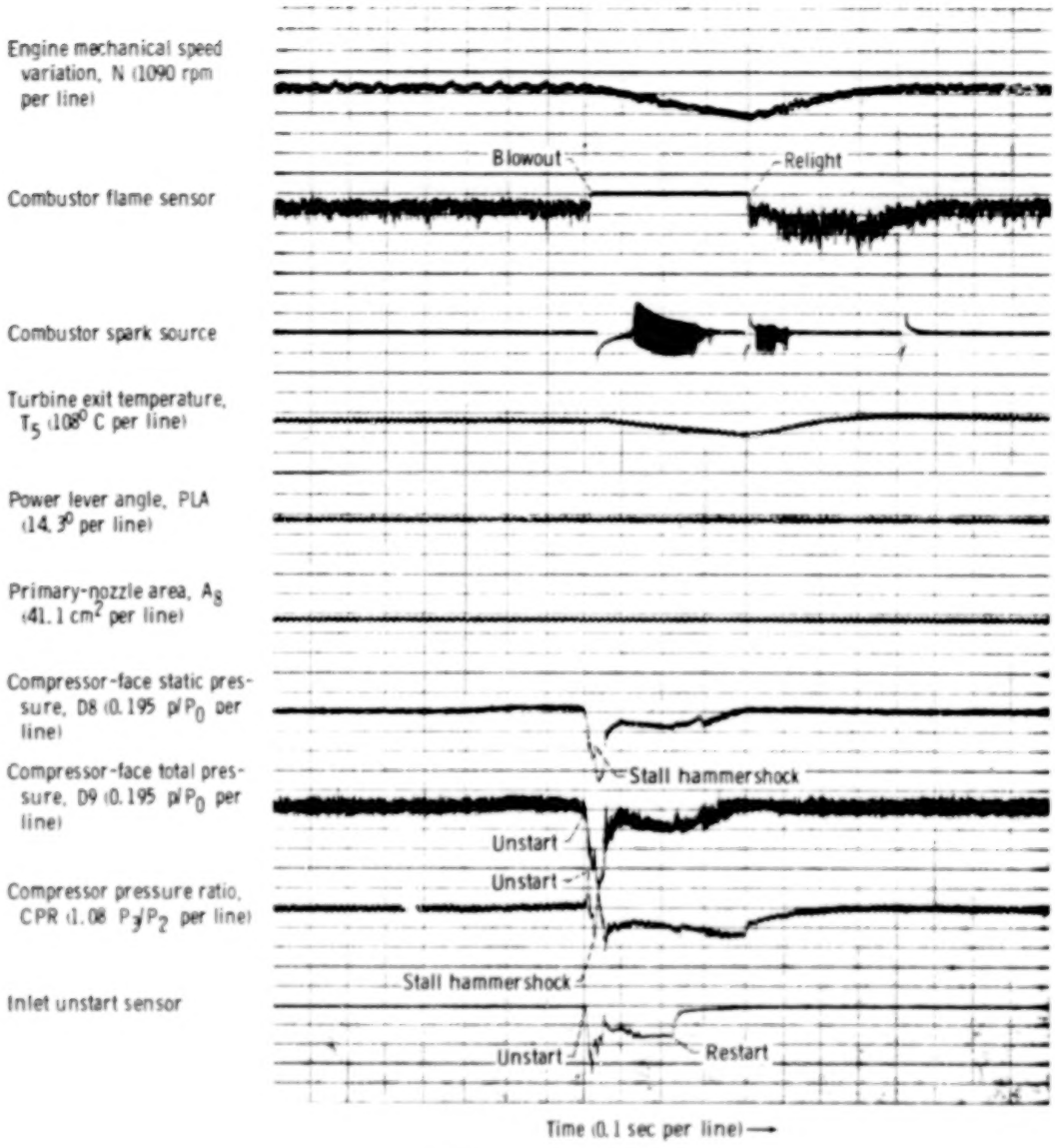

(b) Engine response.

Figure 21. - Concluded.

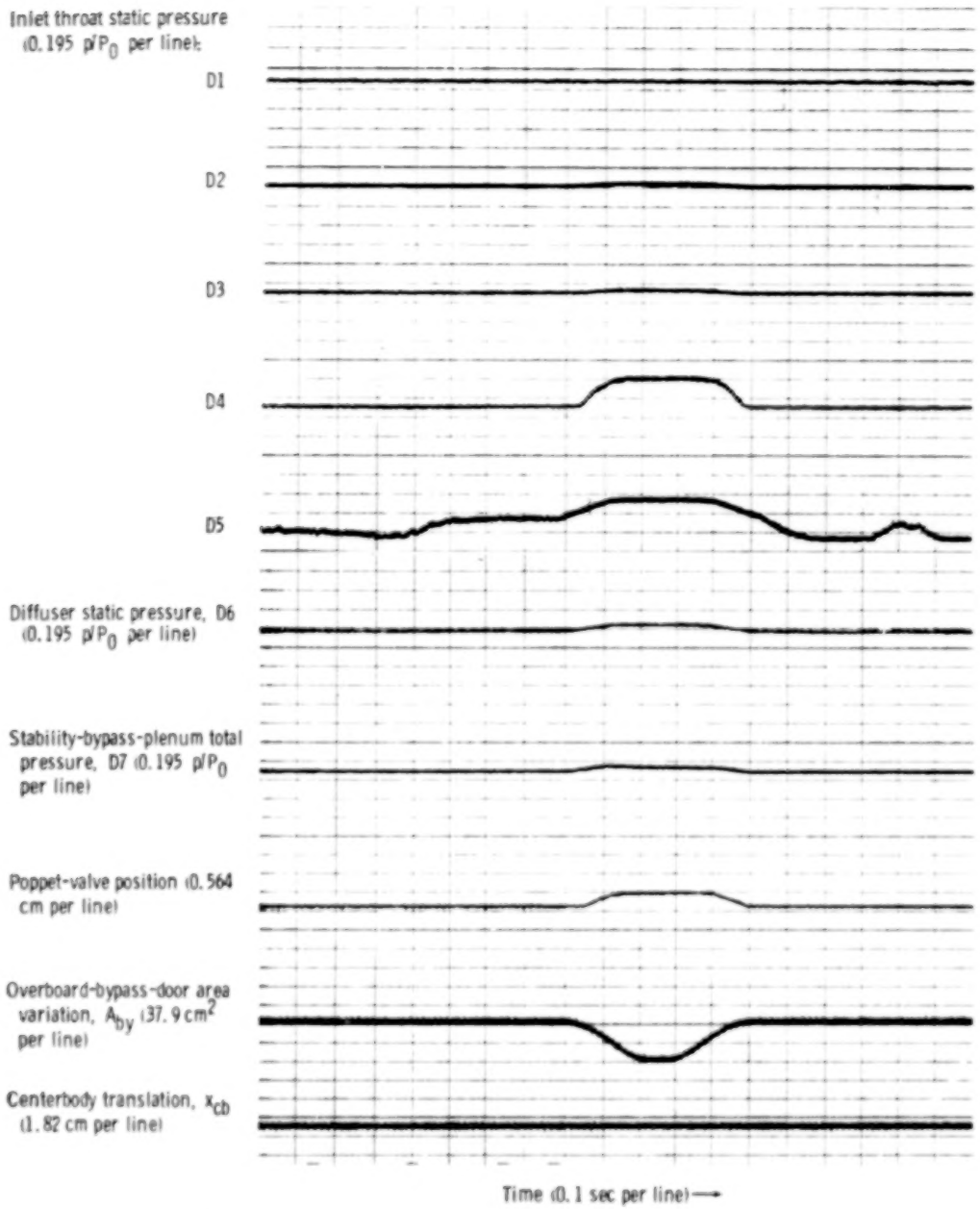

(a) Transient overboard bypass flow area, $A_{by,t}$, 81.3 square centimeters.

Figure 22. - Transient reduction in overboard bypass area with poppet valves as stability-bypass-bleed control. Free-stream Mach number, M_0, 2.5; transient pulse frequency, $1/\tau$, 2 seconds^{-1}; corrected engine speed, $N/N^\circ\sqrt{\theta}$ 0.853; total-pressure recovery, P_2/P_0, 0.905; mass-flow ratio, m_2/m_0, 0.848; primary-nozzle area, A_8, 0.0647 square meter.

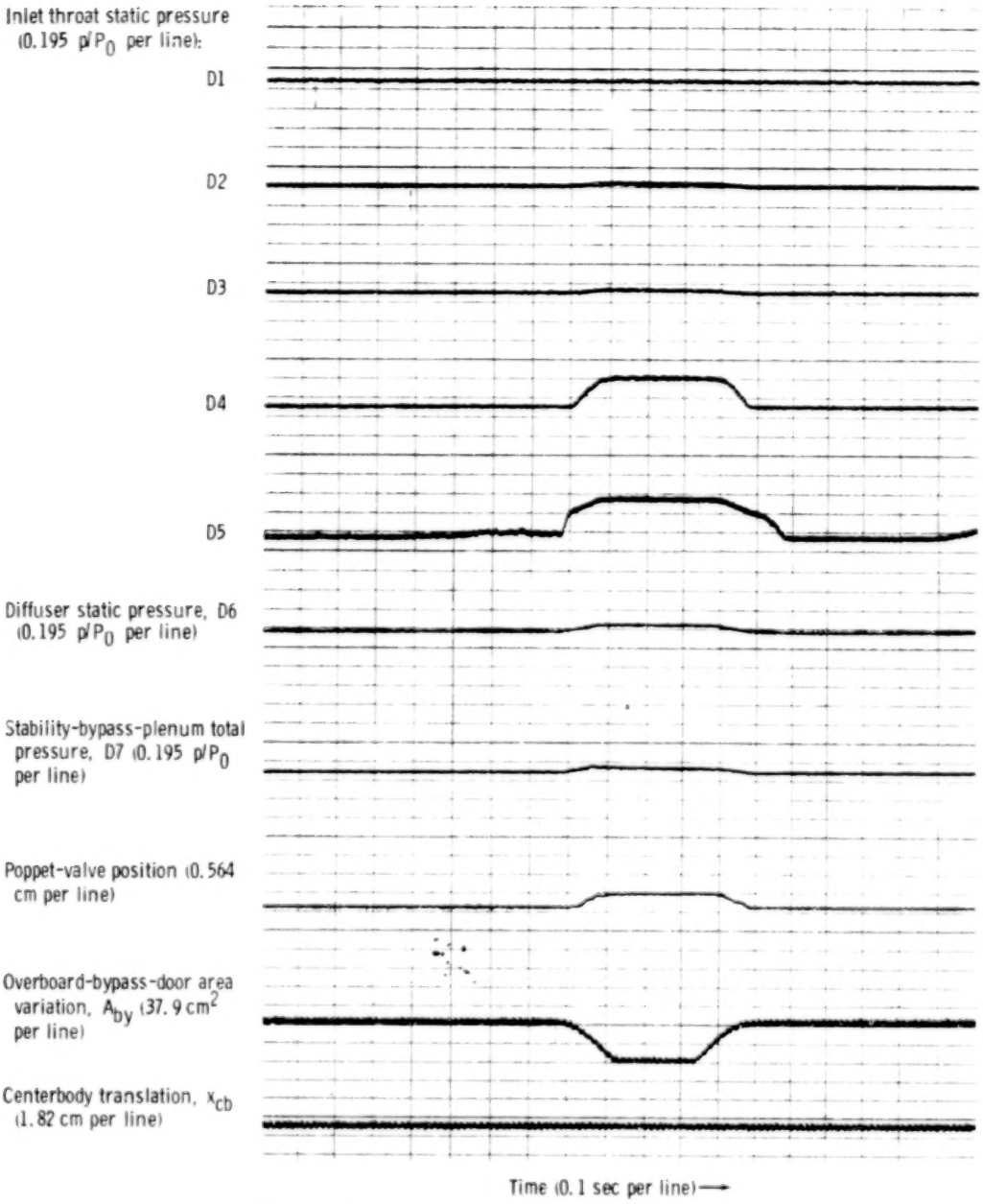

(b) Transient overboard bypass flow area, $A_{by,t}$, 86.7 square centimeters.

Figure 22. - Concluded.

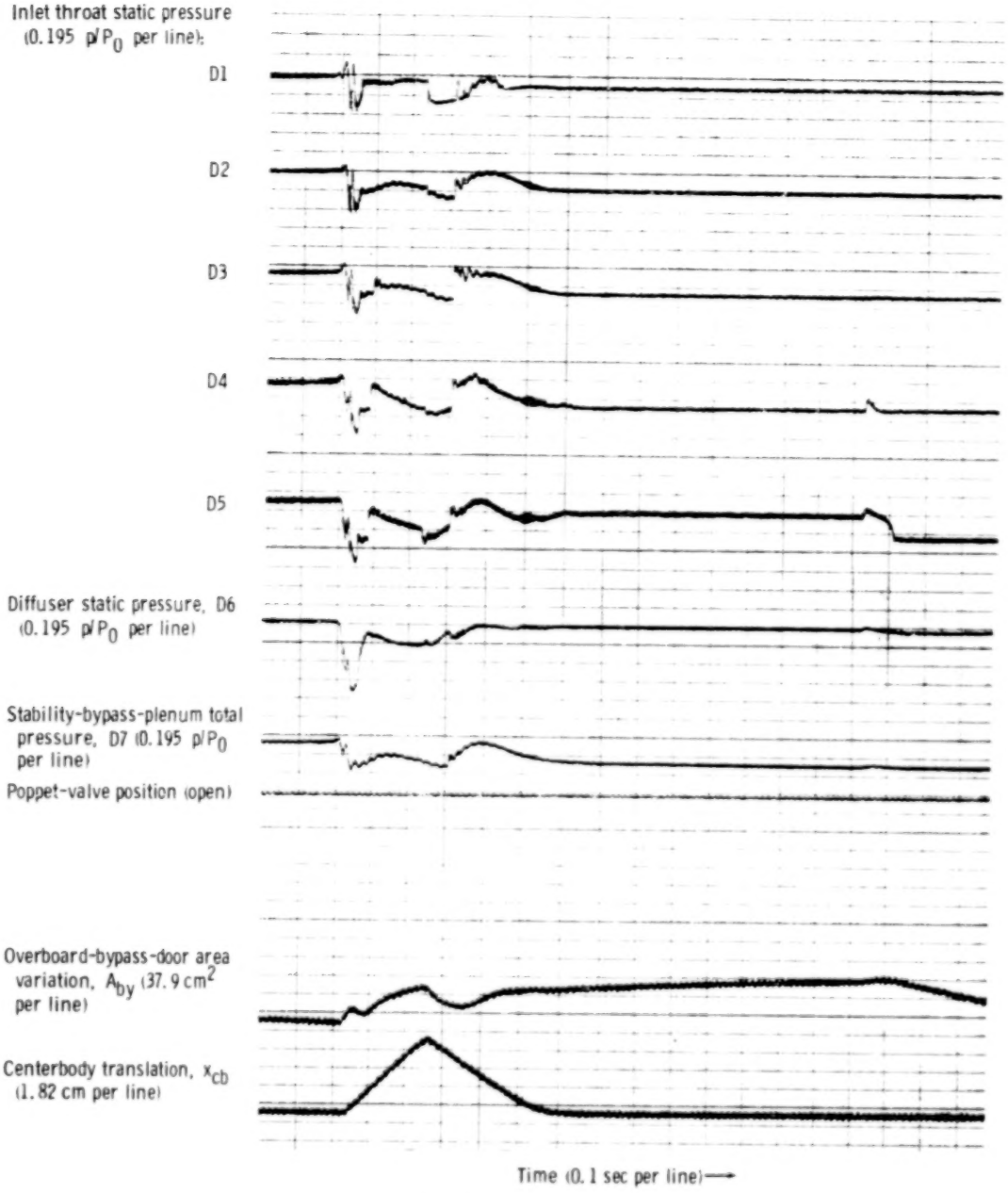

(a) Inlet response.

Figure 23. - Slow, manual reduction in overboard bypass area to inlet unstart with small, fixed exit as stability-bypass-bleed control and large stability bypass plenum. Free-stream Mach number, M_0, 2.5; corrected engine speed, $N/N^* \sqrt{\theta}$, 0.848; total-pressure recovery, P_2/P_0, 0.907; mass-flow ratio, m_2/m_0, 0.844; primary-nozzle area, A_8, 0.0647 square meter.

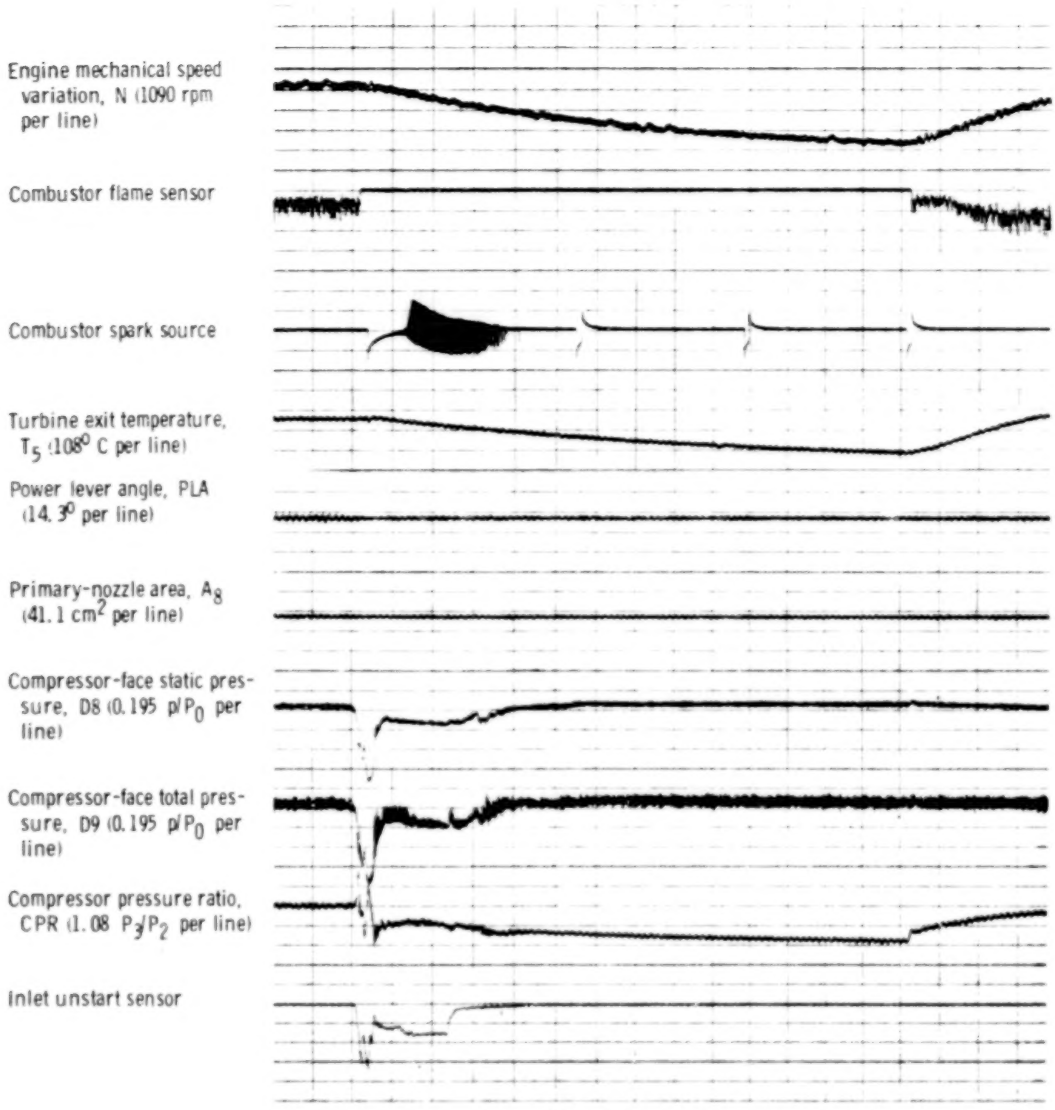

(b) Engine response.

Figure 23. - Concluded.

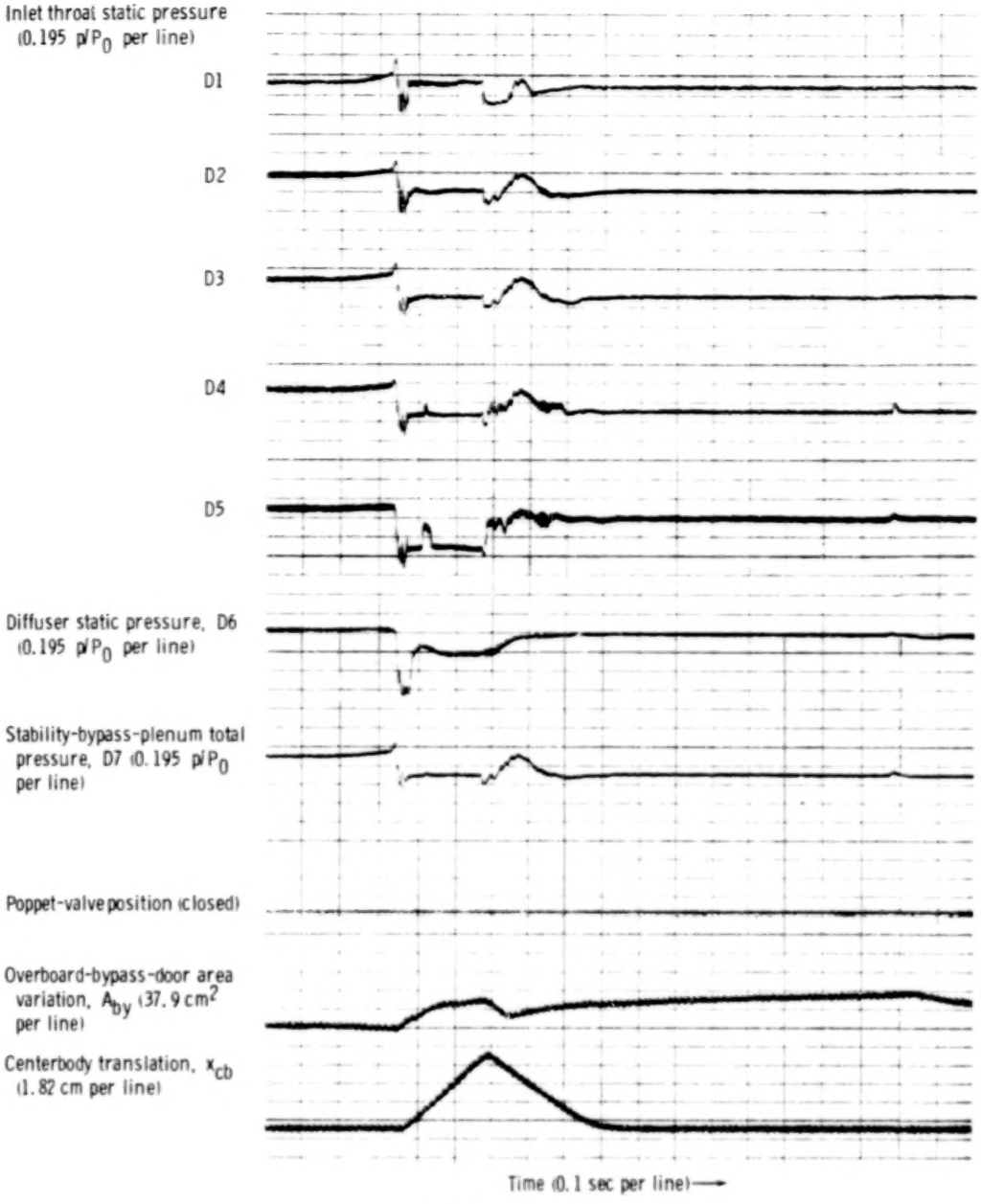

(a) Inlet response.

Figure 24. - Slow, manual reduction in overboard bypass area to inlet unstart with small, fixed exit as stability-bypass-bleed control and small stability bypass plenum - for corrected engine speed $N/N^{\circ}\sqrt{\theta}$ of 0.822 and primary-nozzle area A_8 of 0.0674 square meter. Free-stream Mach number, M_0, 2.5; total-pressure recovery, P_2/P_0, 0.907; mass-flow ratio, m_2/m_0, 0.836.

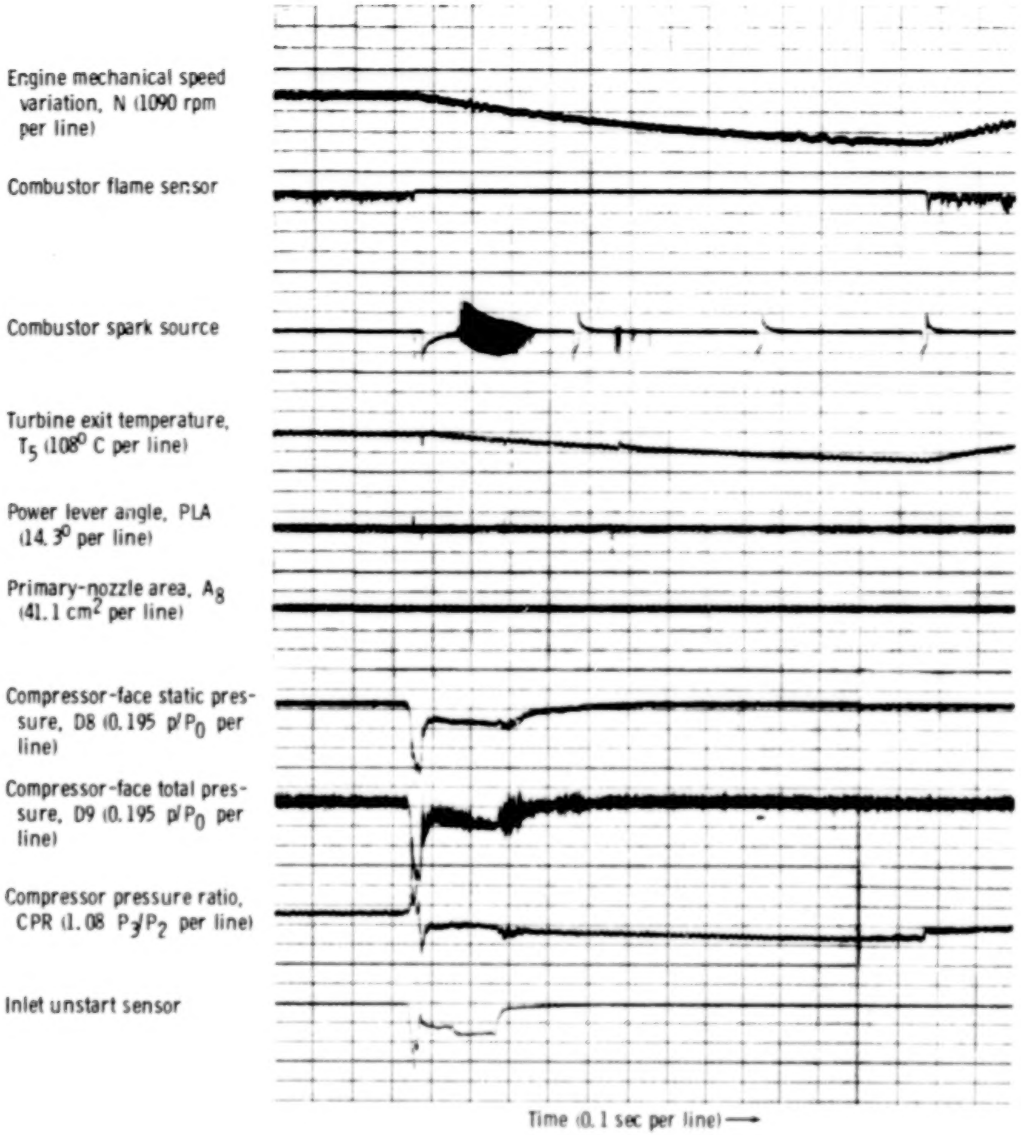

(b) Engine response.

Figure 24. - Concluded.

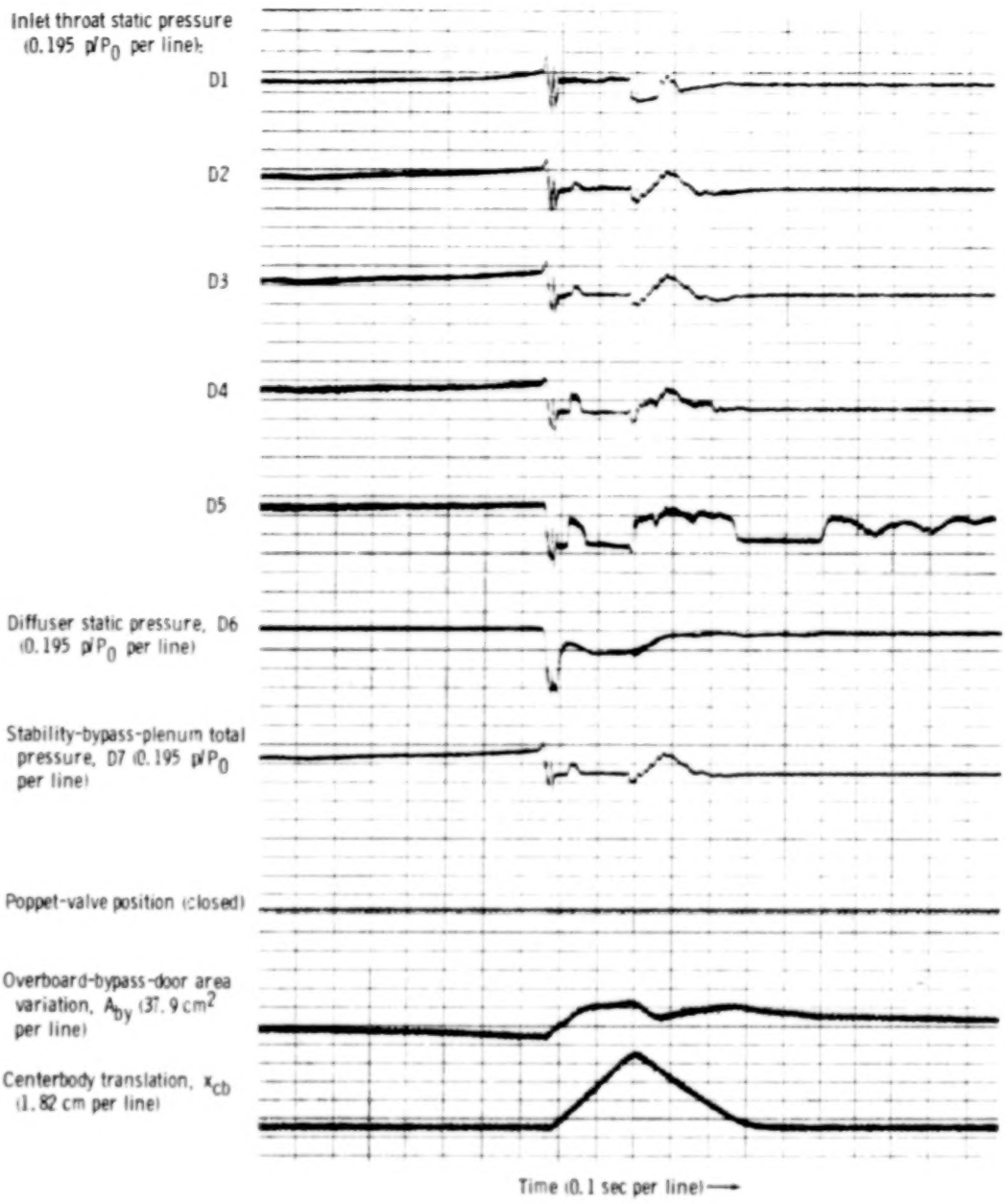

(a) Inlet response.

Figure 25. - Slow, manual reduction in overboard bypass area to inlet unstart with small, fixed exit as stability-bypass-bleed control and small stability bypass plenum - for corrected engine speed $N/N^* \sqrt{\theta}$ of 0.844 and primary-nozzle area A_8 of 0.0727 square meter. Free-stream Mach number, M_0, 2.5; total-pressure recovery, P_2/P_0, 0.904; mass-flow ratio, m_2/m_0, 0.836.

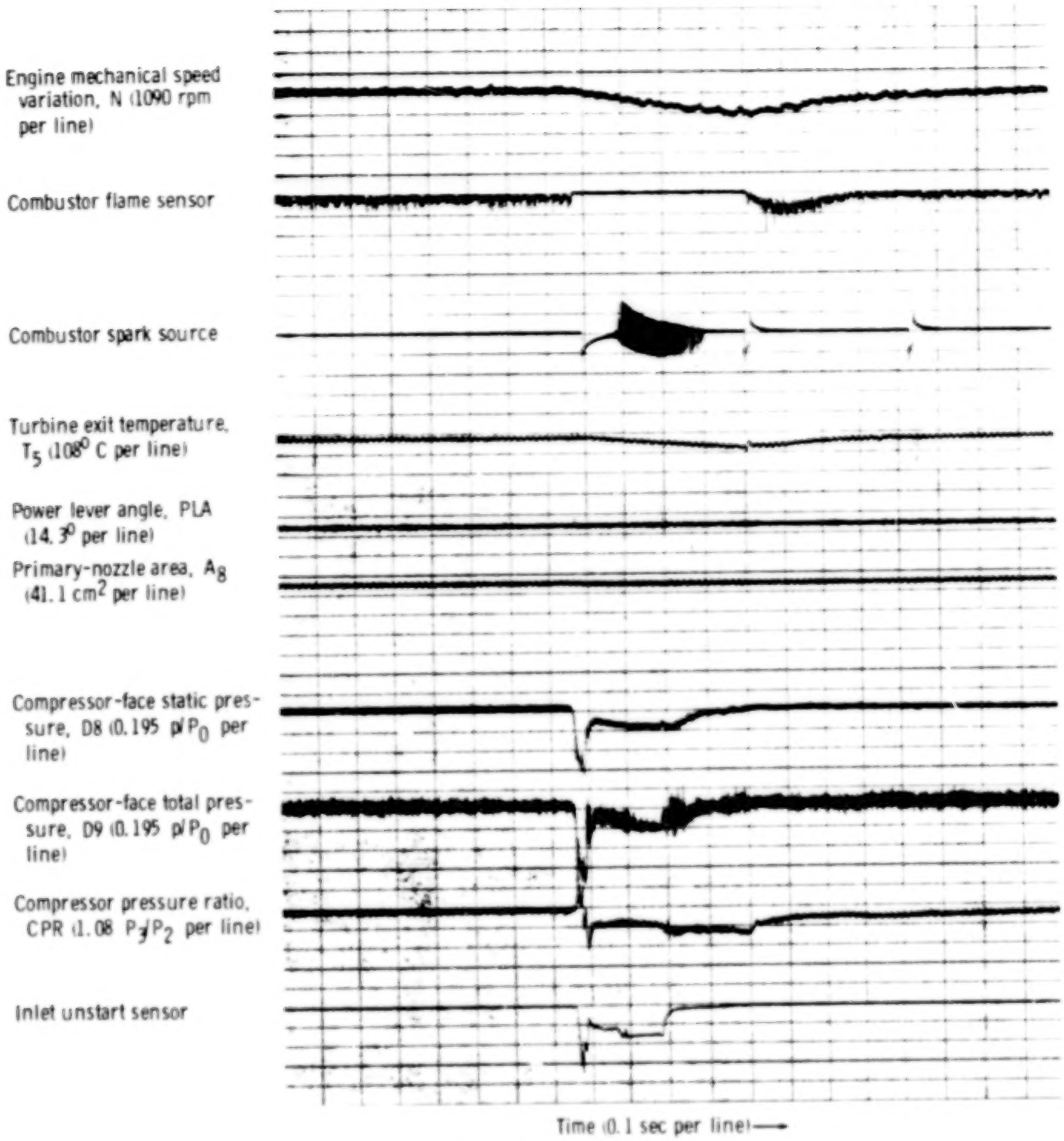

(b) Engine response.

Figure 25. - Concluded.

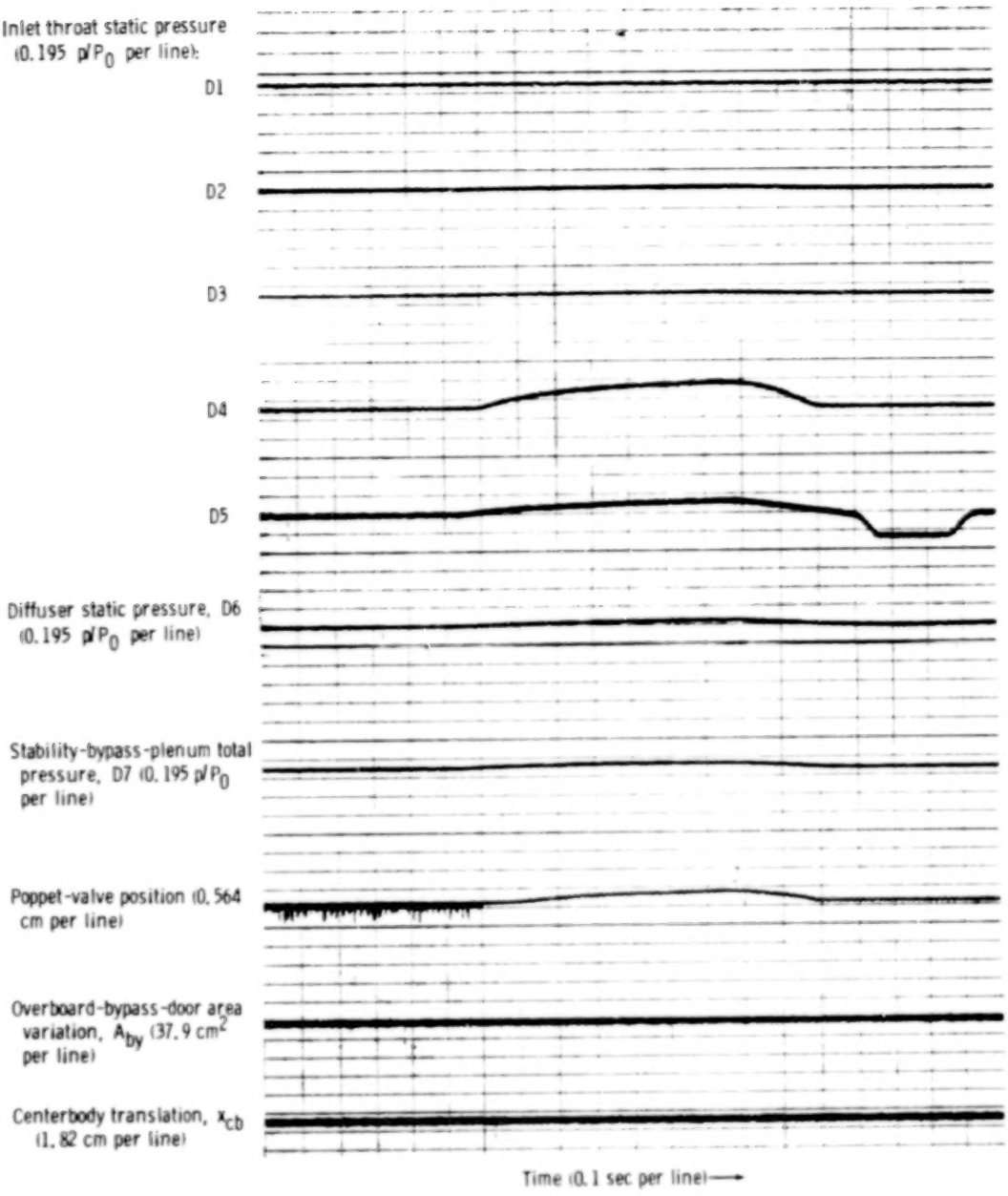

(a) Inlet response.

Figure 26. - Transient 10^0 reduction in power lever angle with poppet valves as stability-bypass-bleed control. Free-stream Mach number, M_0, 2.5; transient pulse frequency, $1/\tau$, 1 $second^{-1}$; corrected engine speed, $N/N^\circ\sqrt{\theta}$, 0.872; total-pressure recovery, P_2/P_0, 0.905; mass-flow ratio, m_2/m_0, 0.877; primary-nozzle area, A_8, 0.0636 square meter.

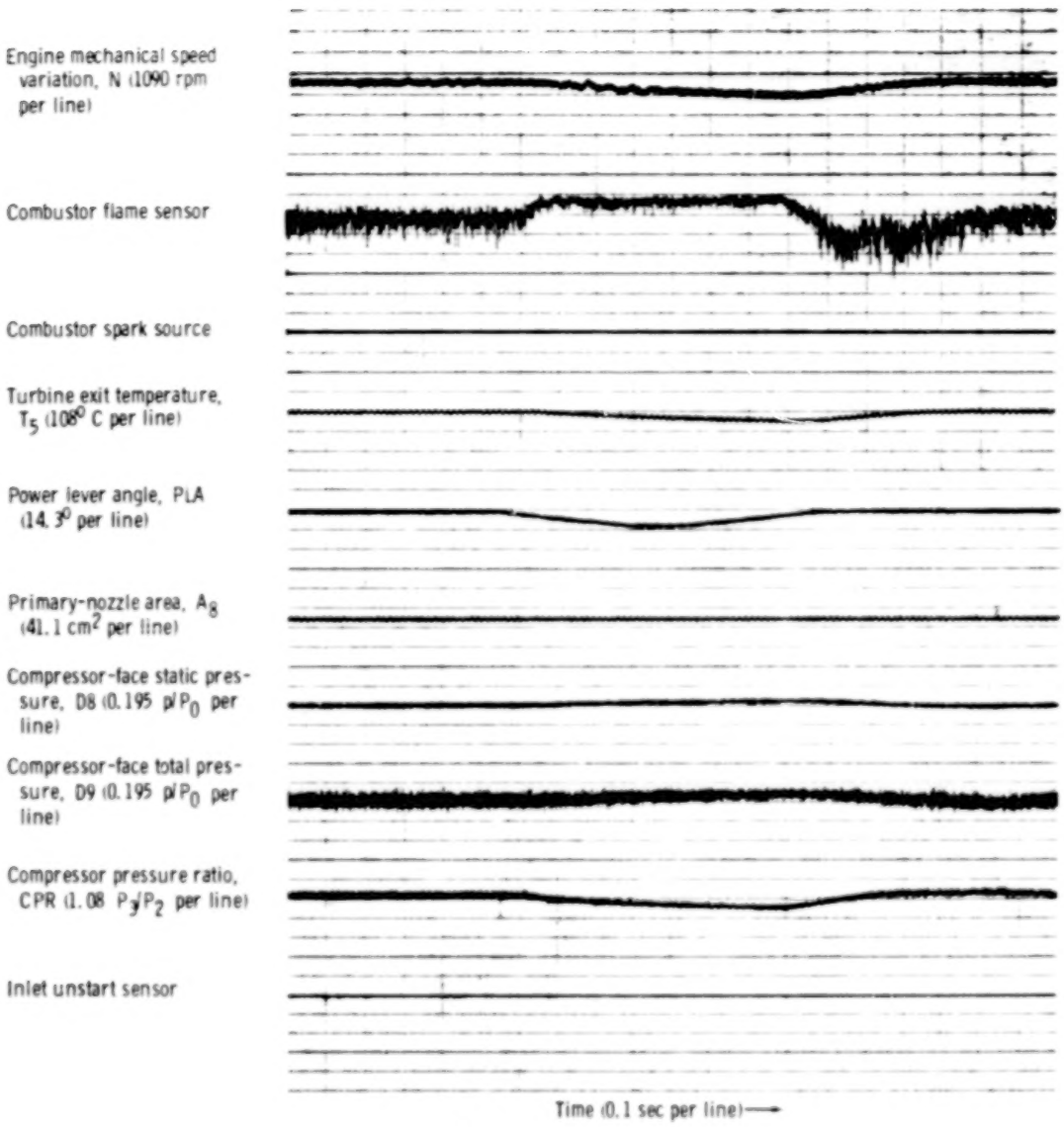

(b) Engine response.

Figure 26. - Concluded.

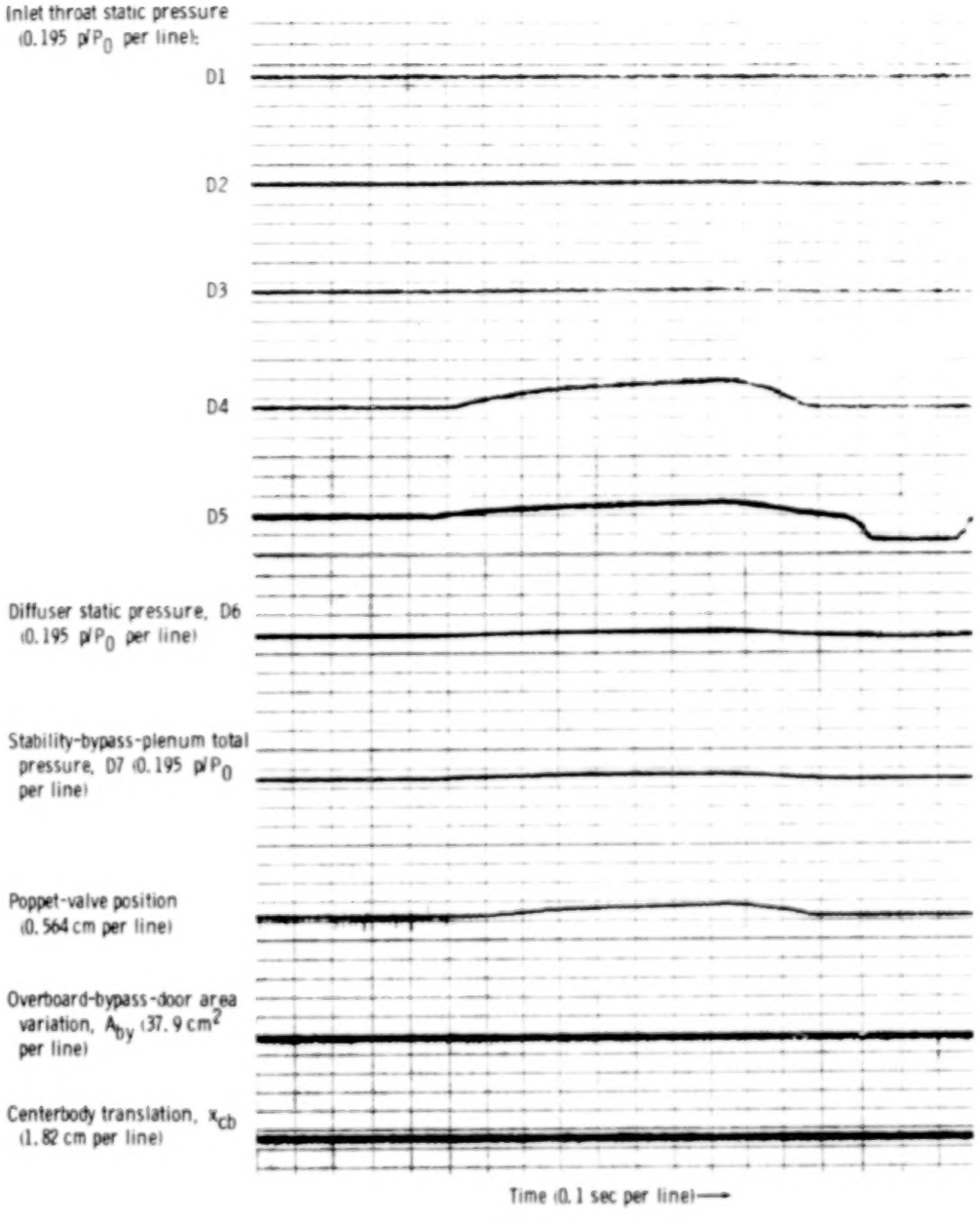

(a) Inlet response.

Figure 27. - Transient 20° reduction in power lever angle with poppet valves as stability-bypass-bleed control. Free-stream Mach number, M_0, 2.5; transient pulse frequency, $1/\tau$, 1 $second^{-1}$; corrected engine speed, $N/N^* \sqrt{\theta}$, 0.871; total-pressure recovery, P_2/P_0, 0.905; mass-flow ratio, m_2/m_0, 0.877; primary-nozzle area, A_8, 0.0636 square meter.

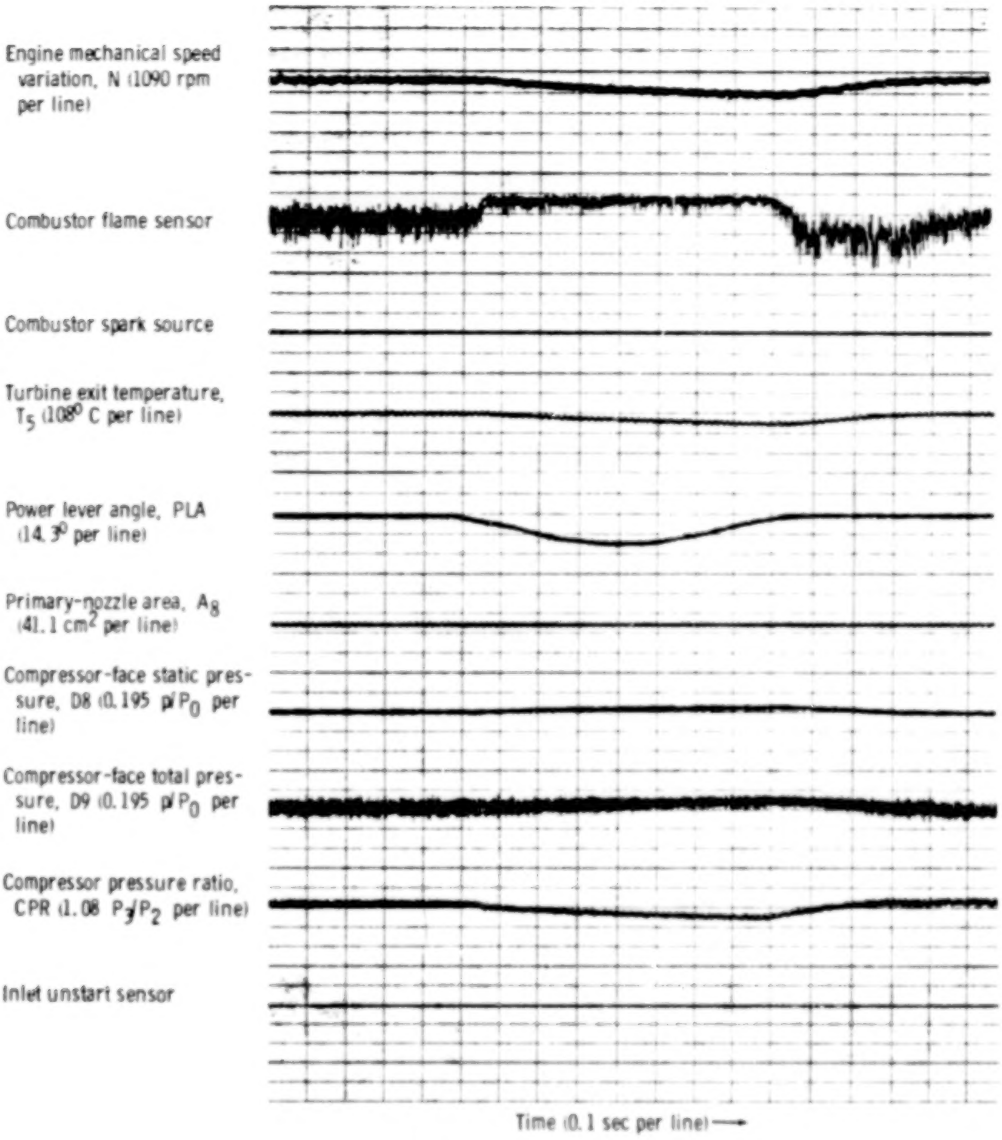

(b) Engine response.

Figure 27. - Concluded.

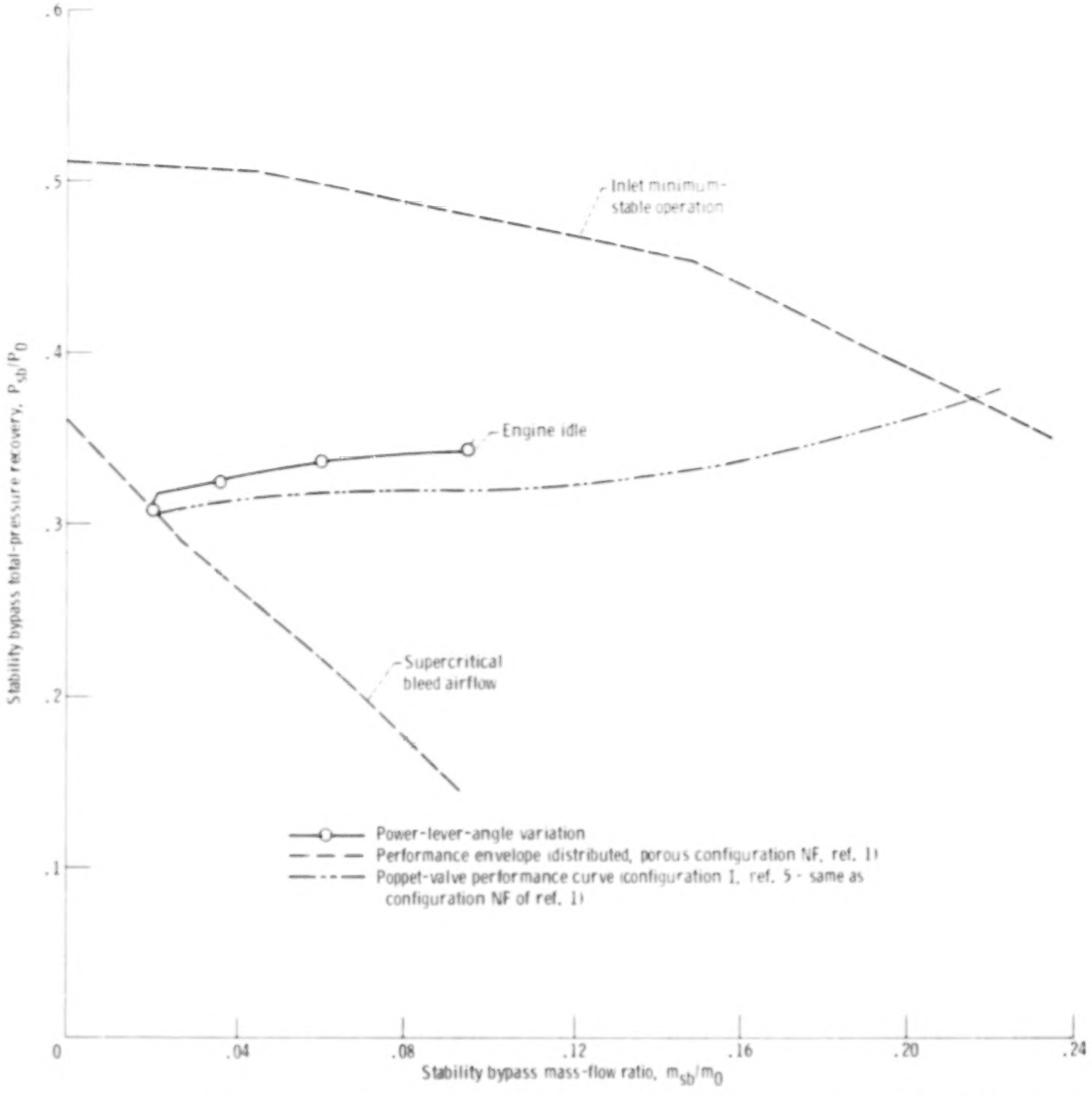

Figure 28. - Stability-bypass-bleed performance with poppet-valve exit control for a reduction in power lever angle from match to engine idle. Free-stream Mach number, M_0, 2.5.

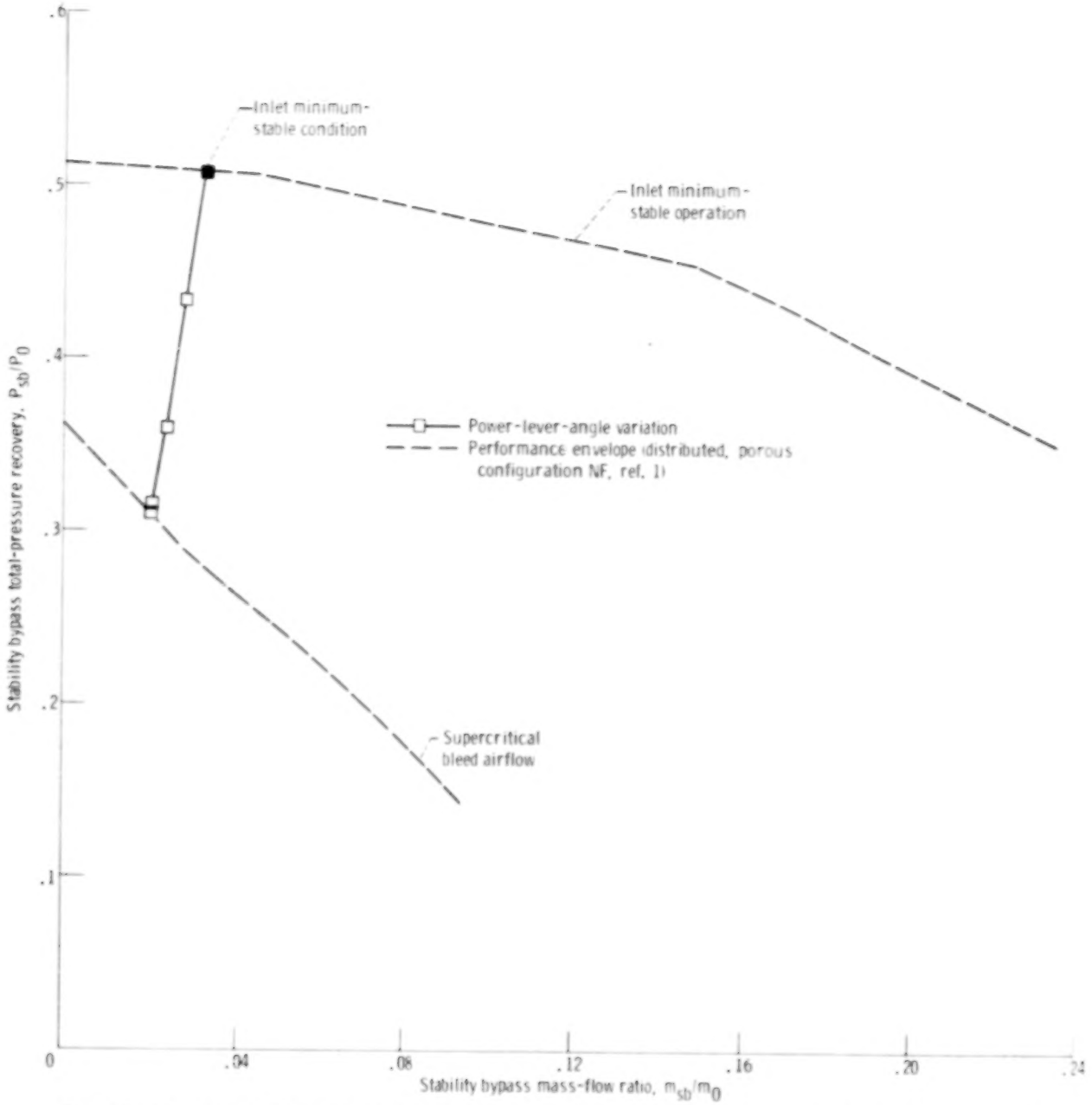

Figure 29. - Stability-bypass-bleed performance with small, fixed exit area for a reduction in power lever angle to inlet unstart. Free-stream Mach number, M_0, 2.5.

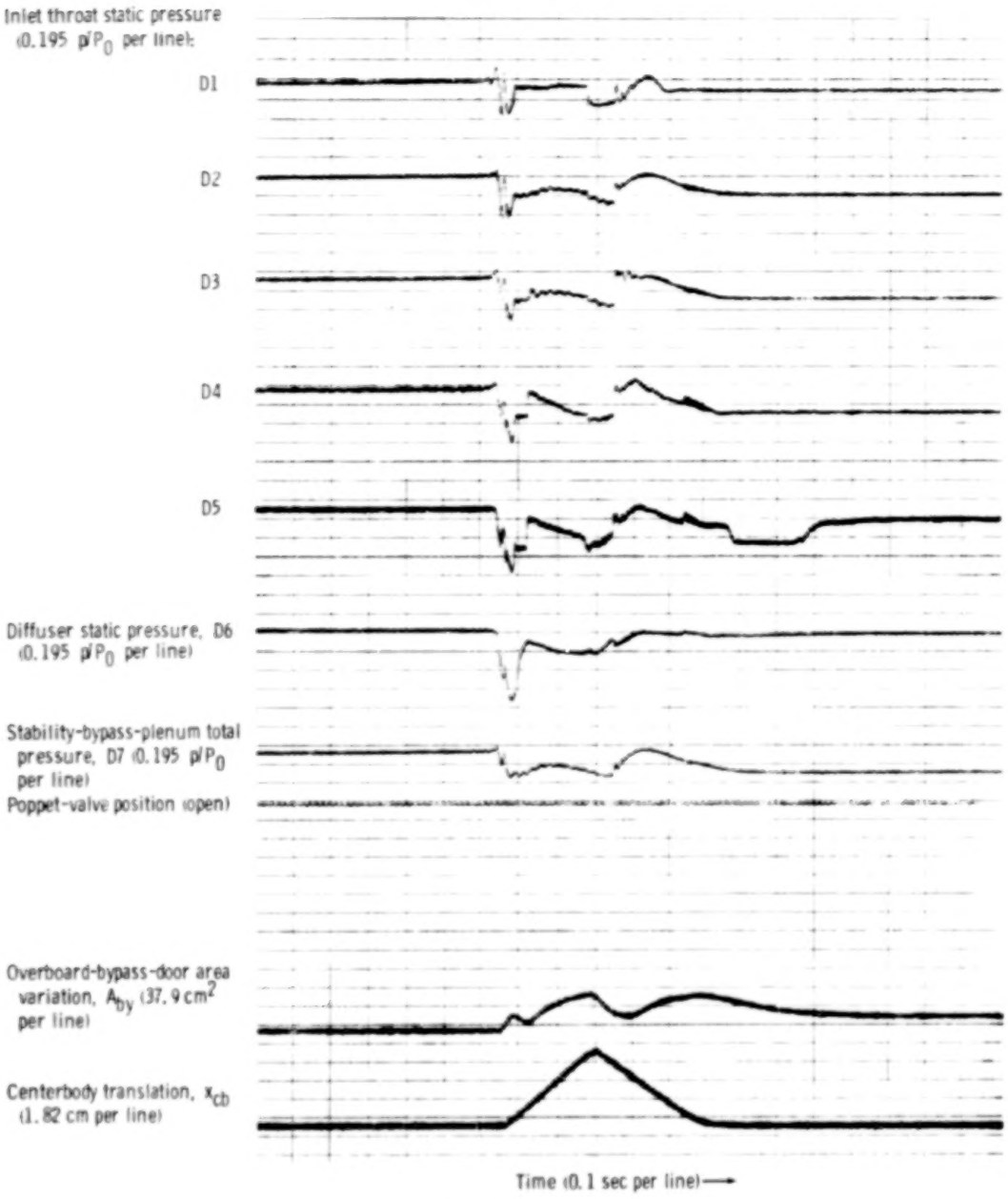

(a) Inlet response.

Figure 30. - Slow, manual reduction in power lever angle to inlet unstart from inlet minimum stable condition, with small, fixed exit as stability-bypass-bleed control and large stability bypass plenum. Free-stream Mach number, M_0, 2.5; stability bypass total-pressure recovery, P_{sb}/P_0, 0.507; stability bypass mass-flow ratio, m_{sb}/m_0, 0.032; corrected engine speed, $N/N^* \sqrt{\theta}$, 0.8403; total-pressure recovery, P_2/P_0, 0.938; mass-flow ratio, m_2/m_0, 0.902; primary-nozzle area, A_8, 0.0645 square meter.

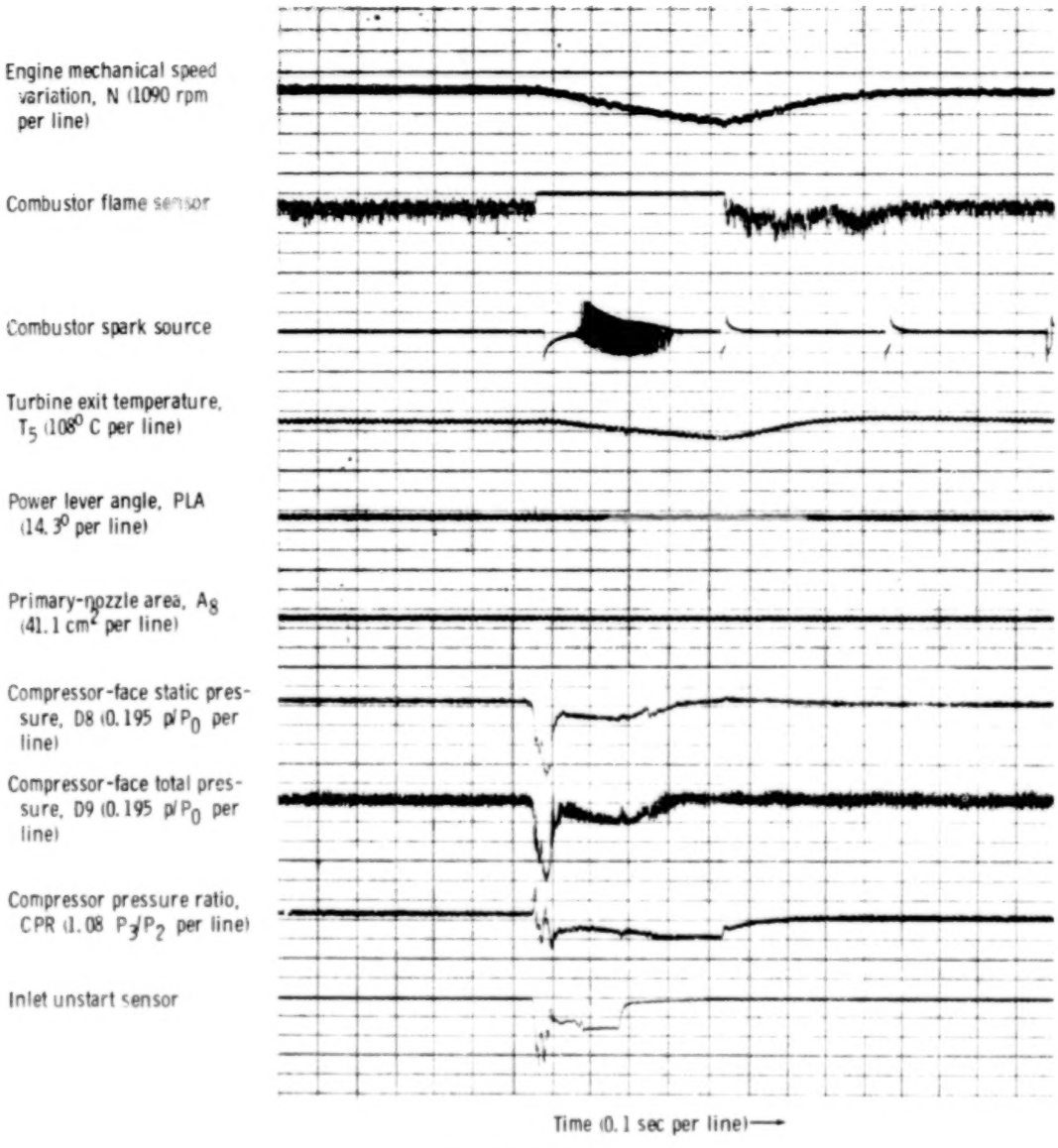

(b) Engine response.

Figure 30. - Concluded.

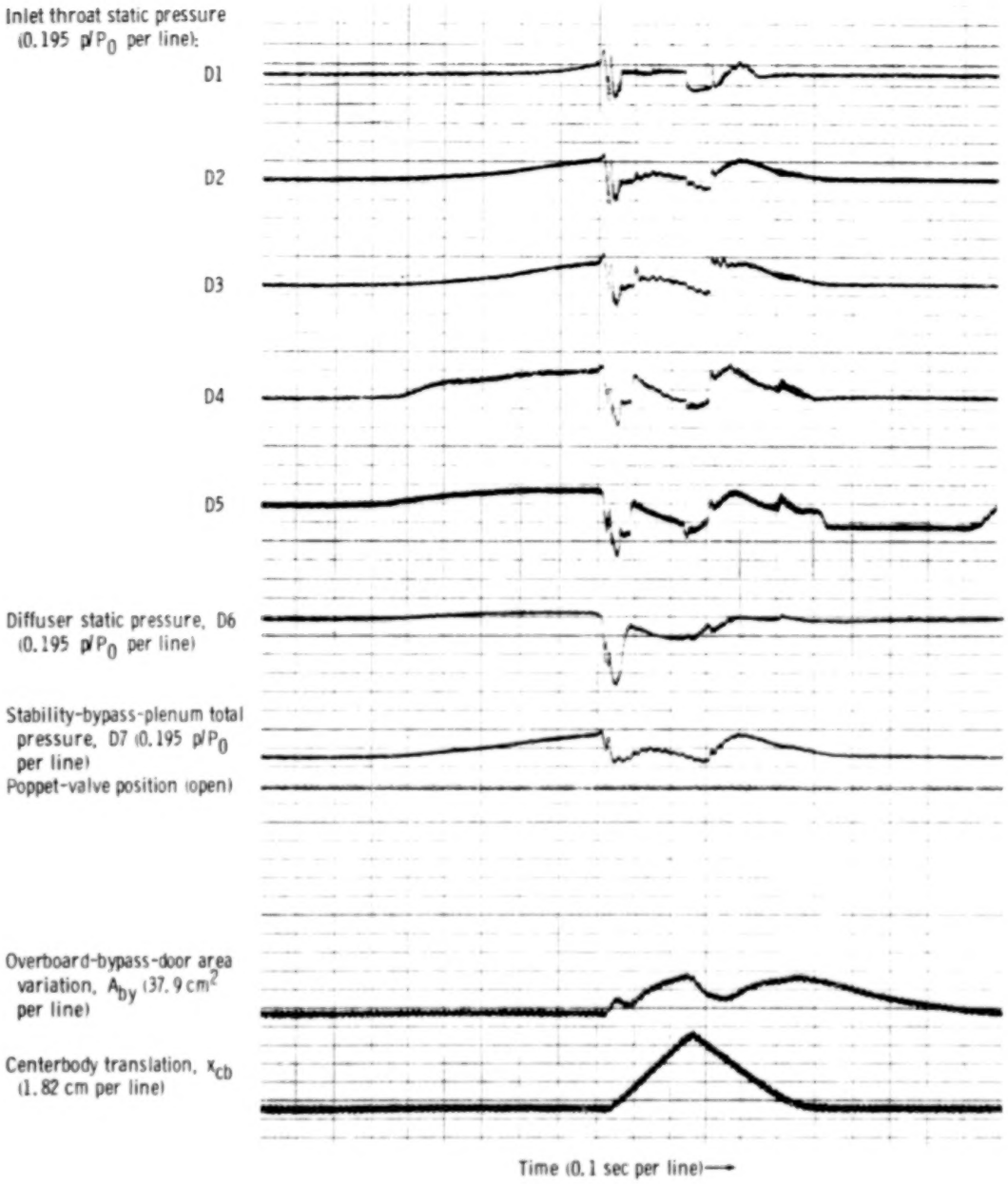

(a) Inlet response.

Figure 31. - Transient 10^0 reduction in power lever angle with small, fixed exit as stability-bypass-bleed control and large stability bypass plenum. Free-stream Mach number, M_0, 2.5; transient pulse frequency, $1/\tau$, 1 $second^{-1}$; corrected engine speed, $\sqrt{\theta}/N^{\circ}\sqrt{\theta}$, 0.872; total-pressure recovery, P_2/P_0, 0.901; mass-flow ratio, m_2/m_0, 0.904; primary-nozzle area, A_8, 0.9635 square meter.

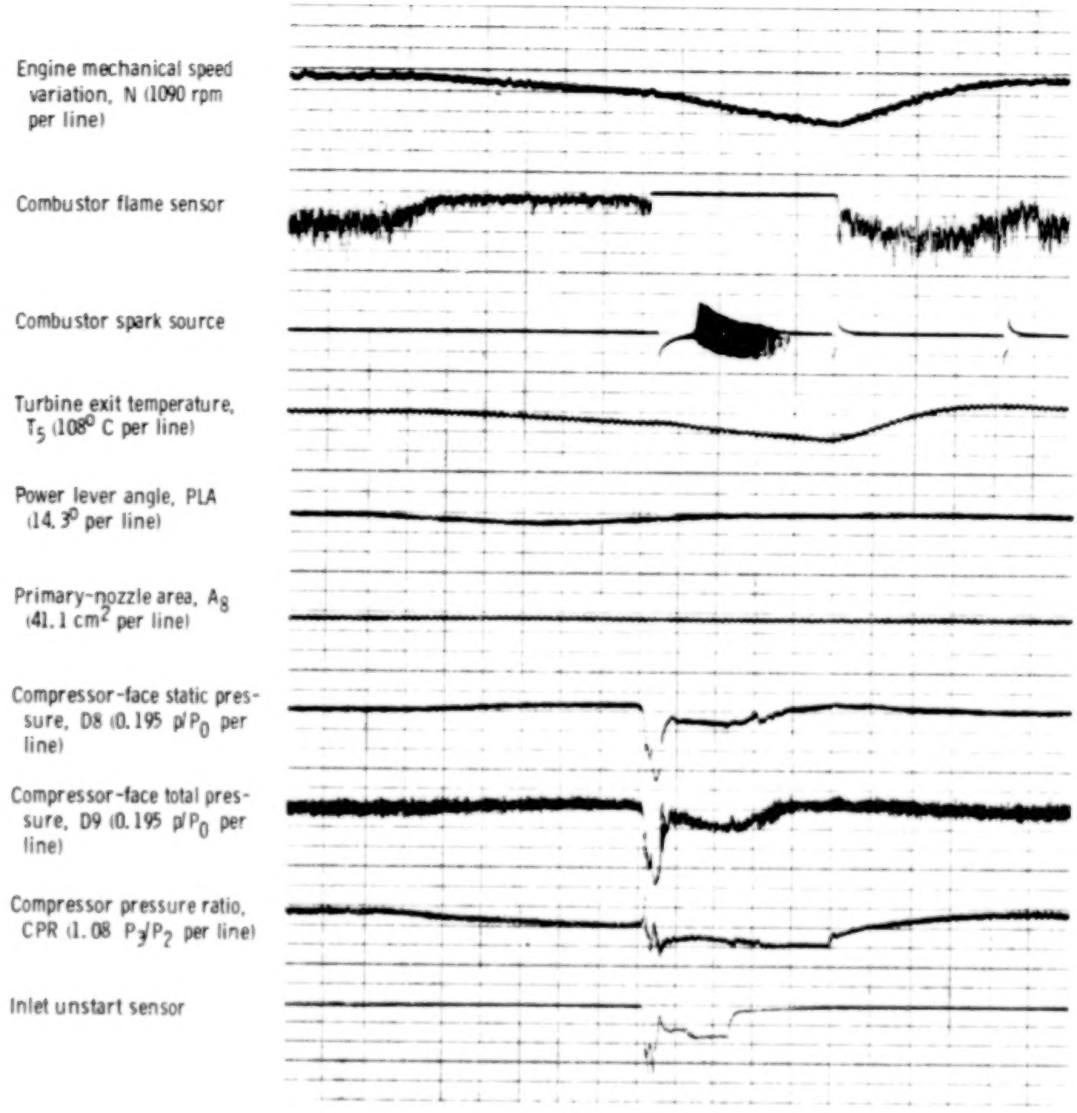

(b) Engine response.

Figure 31. - Concluded.

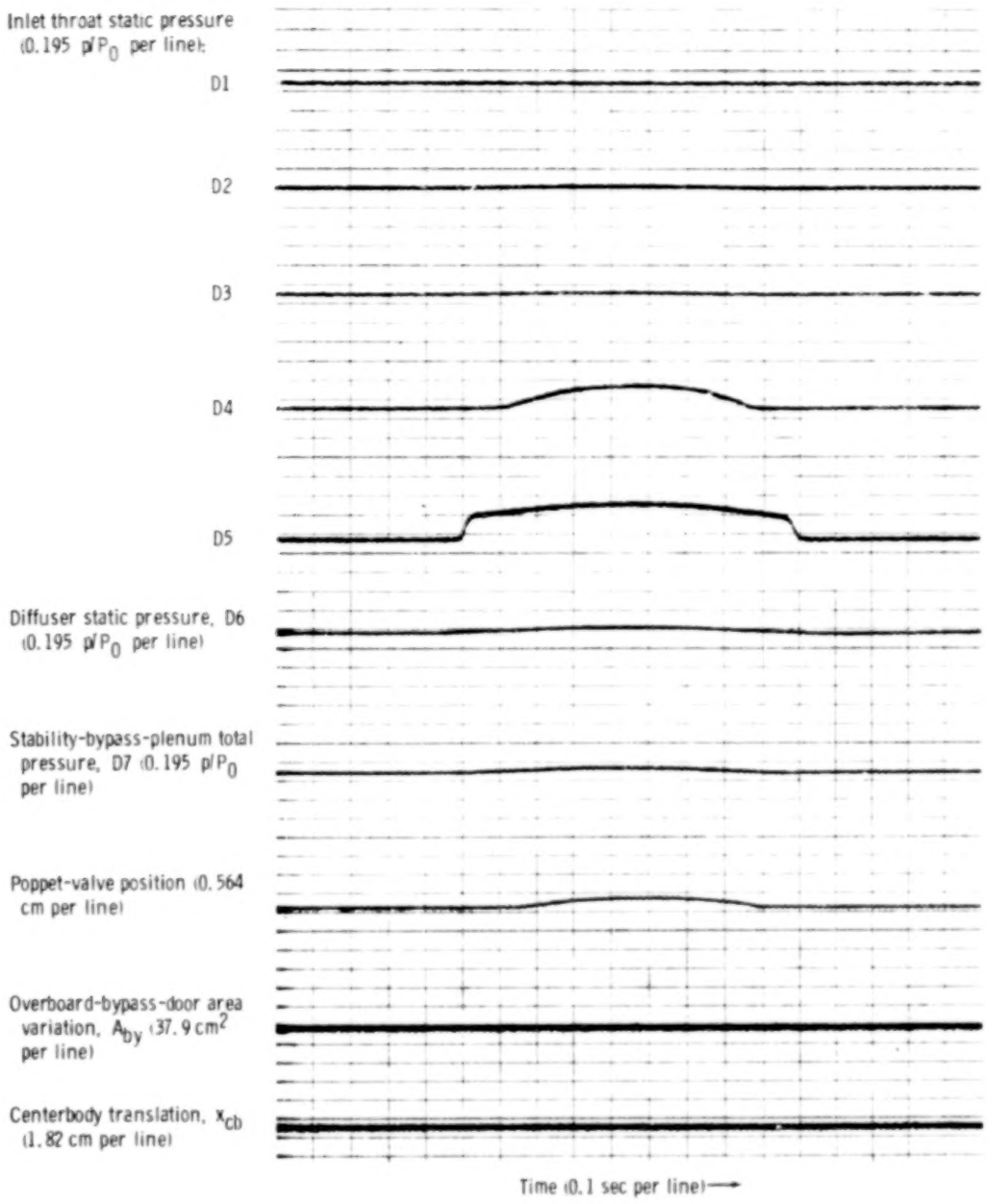

(a) Inlet response.

Figure 32. - Transient reduction in primary-nozzle area with poppet valves at stability-bypass-bleed control. Free-stream Mach number, M_0, 2.5; transient primary-nozzle area, $A_{8,t}$, 129 square centimeters; transient pulse frequency, $1/\tau$, 1 second^{-1}; corrected engine speed, $N/N^{\circ}\sqrt{\theta}$, 0.874; total-pressure recovery, P_2/P_0, 0.903; mass-flow ratio, m_2/m_0, 0.879; primary-nozzle area, A_8, 0.0637 square meter.

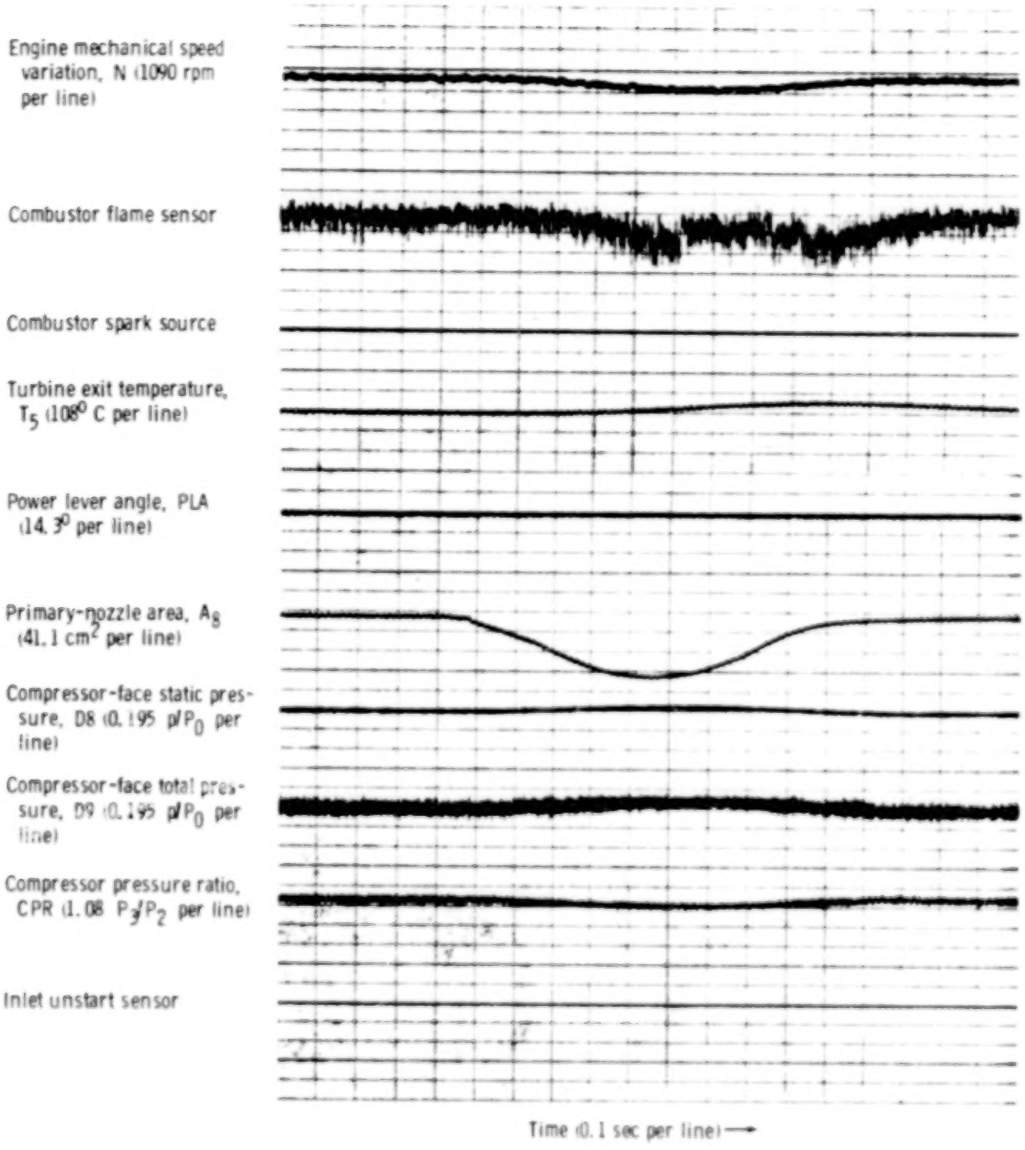

(b) Engine response.

Figure 32. - Concluded.

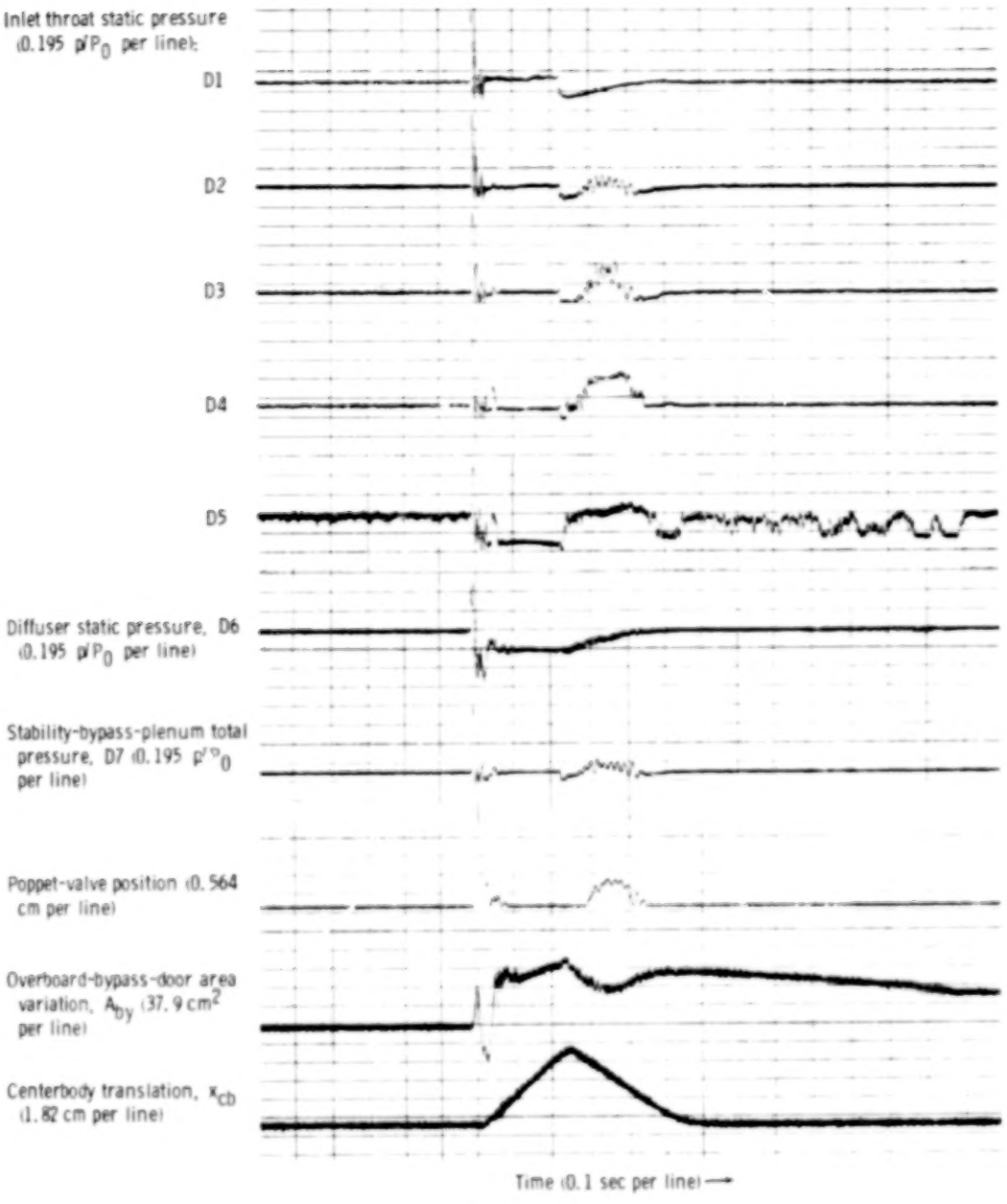

(a) Inlet response.

Figure 33. - Compressor stall induced by slow, manual reduction in primary-nozzle area, with poppet valves as stability-bypass-bleed control. Free-stream Mach number, M_0, 2.5; corrected engine speed, $N/N^* \sqrt{\theta}$, 0.901; total-pressure recovery, P_2/P_0, 0.901; mass-flow ratio, m_2/m_0, 0.896; primary-nozzle area, A_8, 0.0553 square meter.

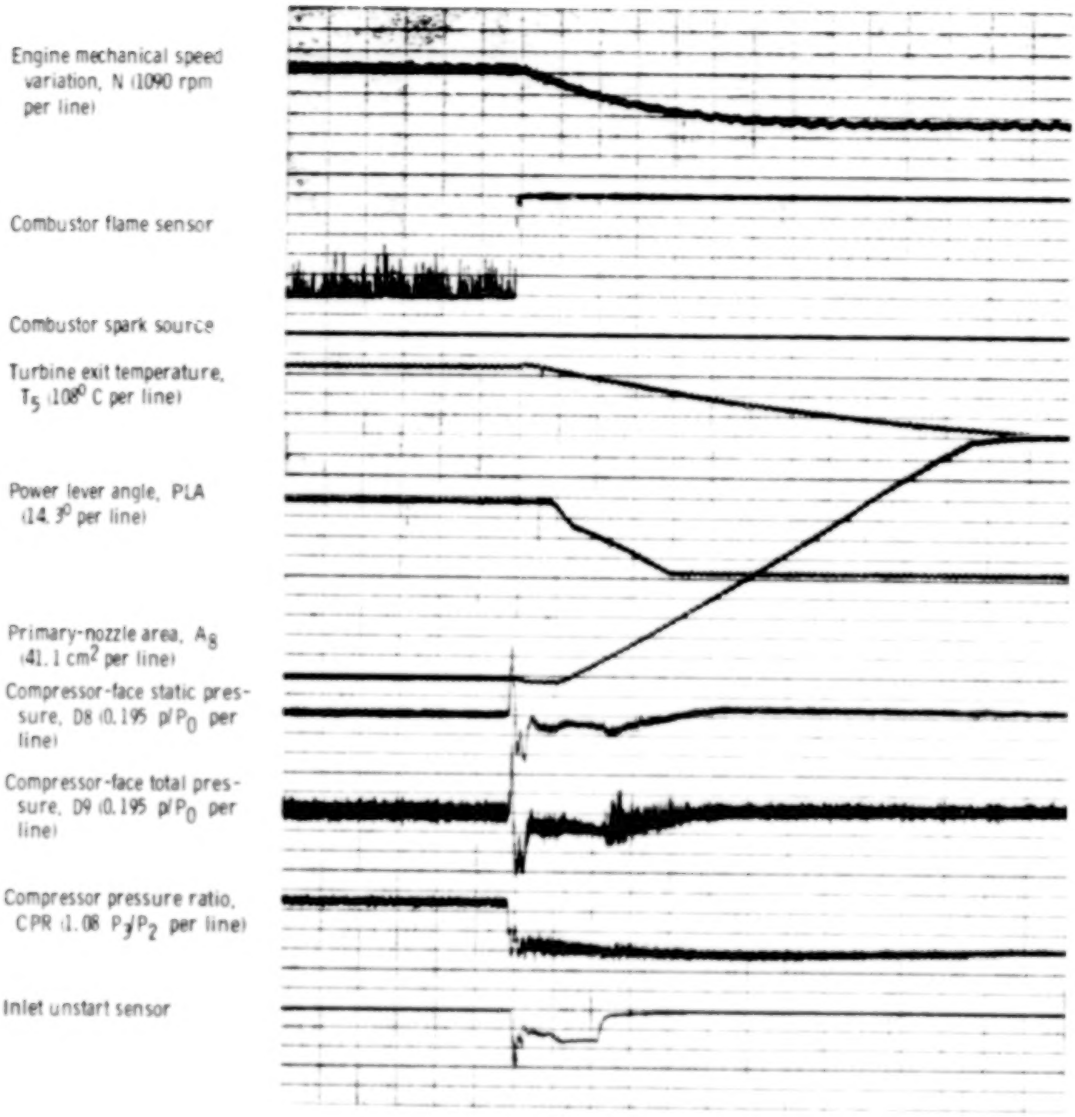

(b) Engine response.

Figure 33. - Concluded.

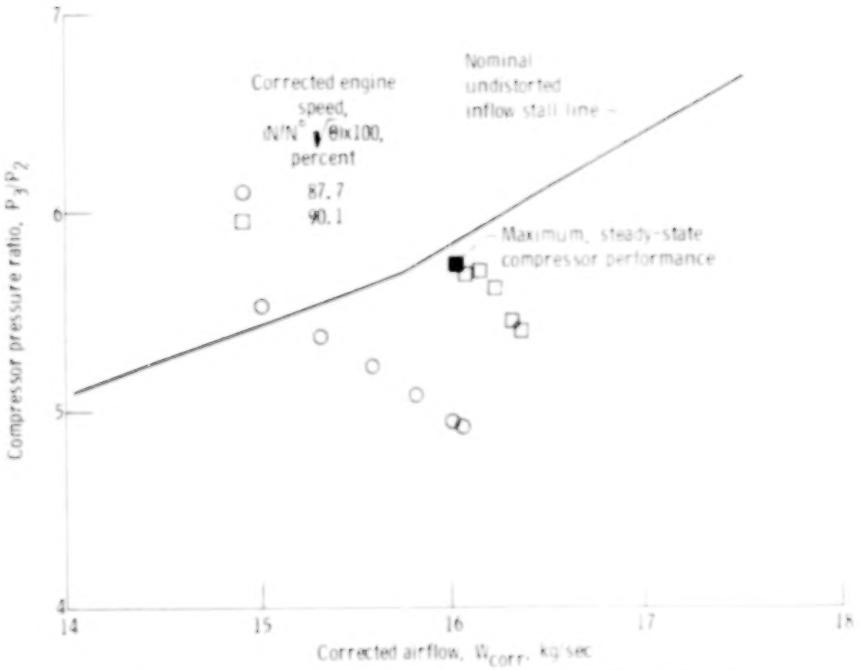

Figure 34. - Compressor performance with poppet valves as stability-bypass-bleed control. Free-stream Mach number, M_0, 2.5.

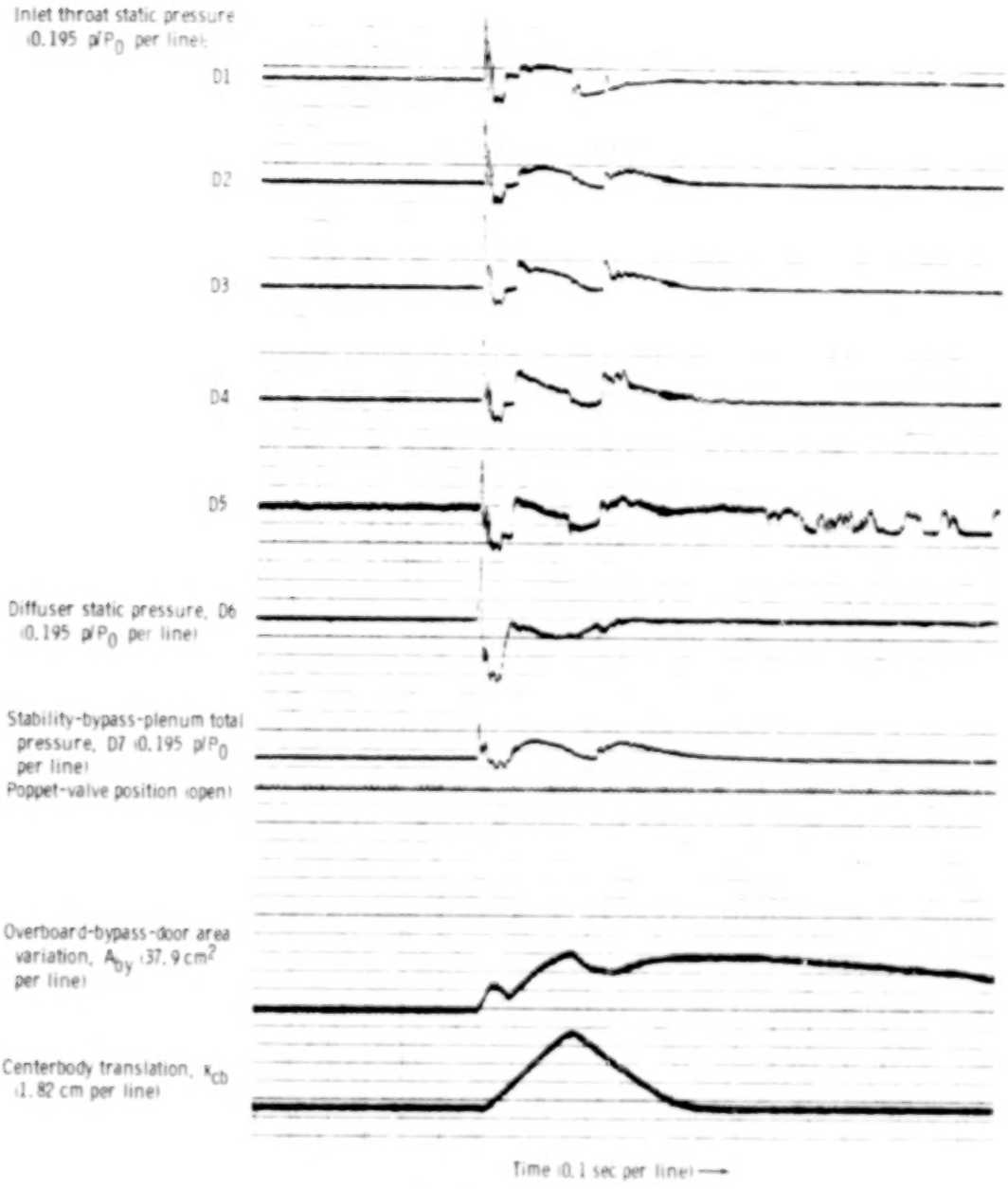

(a) Inlet response.

Figure 35. - Compressor stall induced by slow, manual reduction in primary-nozzle area, with small, fixed exit as stability-bypass-bleed control and large stability bypass plenum. Free-stream Mach number, M_0, 2.5; corrected engine speed, $N/N^\circ\sqrt{\theta}$, 0.896; total-pressure recovery, P_2/P_0, 0.904; mass-flow ratio, m_2/m_0, 0.891; primary-nozzle area, A_8, 0.0544 square meter.

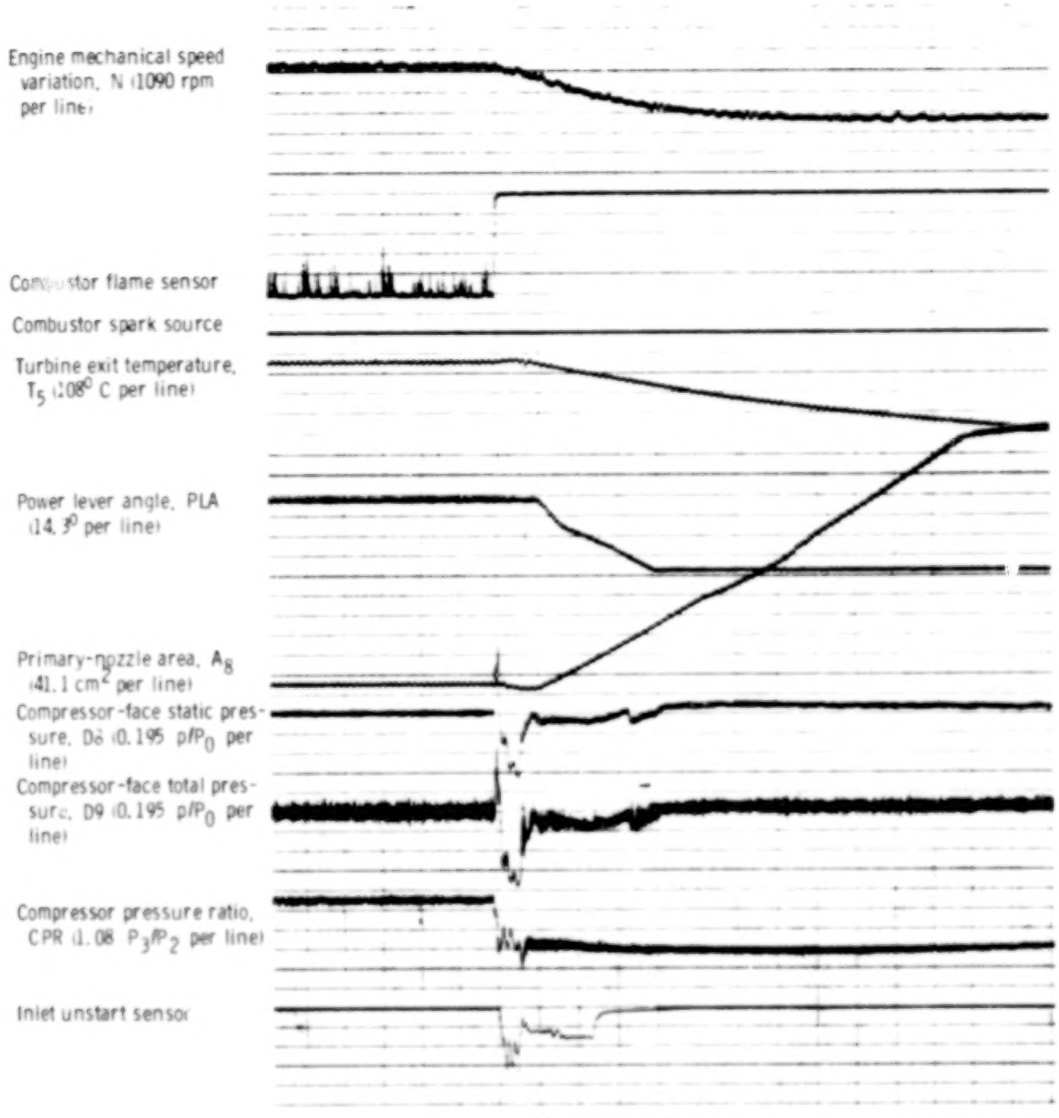

(b) Engine response.

Figure 35. - Concluded.

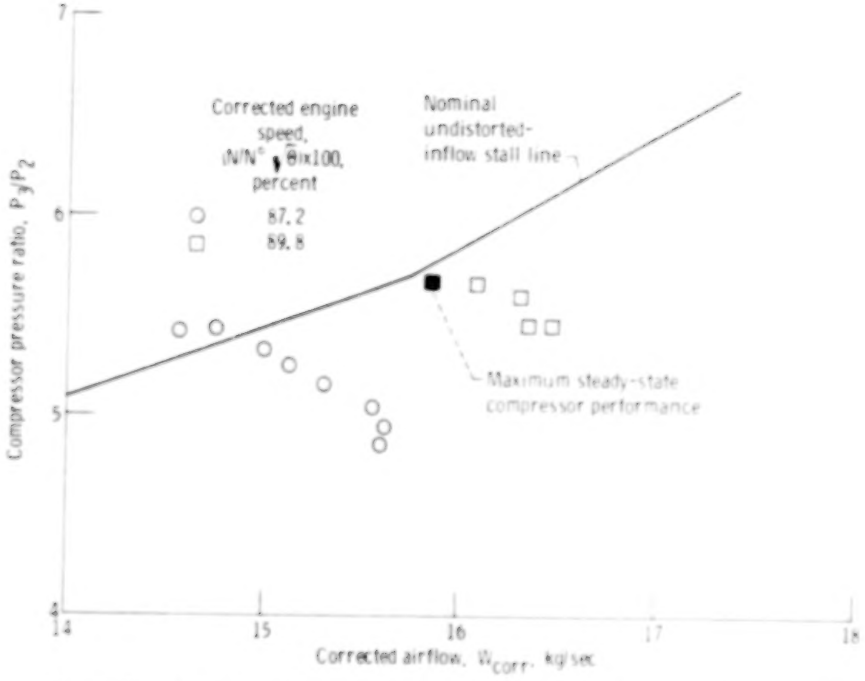

Figure 36. - Compressor performance with small, fixed exit as stability-bypass-bleed control and large stability bypass plenum. Free-stream Mach number, M_0, 2.5.

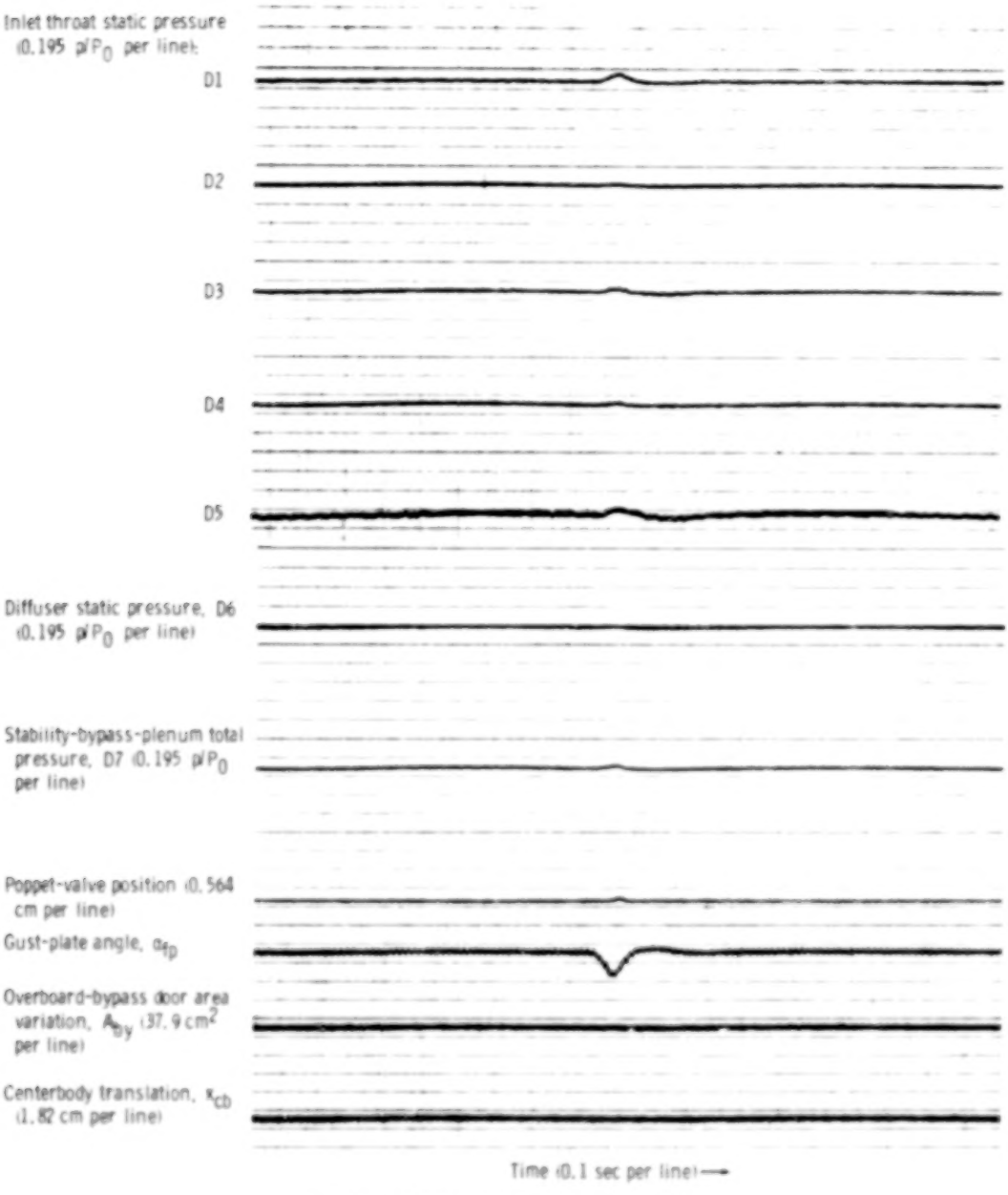

(a) Transient flat gust-plate angle, $\alpha_{fp,t}$, 1.0°.

Figure 37. - External airflow transients induced by flat gust plate, with poppet valves as stability-bypass-bleed control. Free-stream Mach number, M_0, 2.5; transient pulse frequency, $1/\tau$, 10 seconds^{-1}; corrected engine speed, $N/N^* \sqrt{\theta}$, 0.873; total-pressure recovery, P_2/P_0, 0.901; mass-flow ratio, m_2/m_0, 0.903; primary-nozzle area, A_8, 0.0639 square meter.

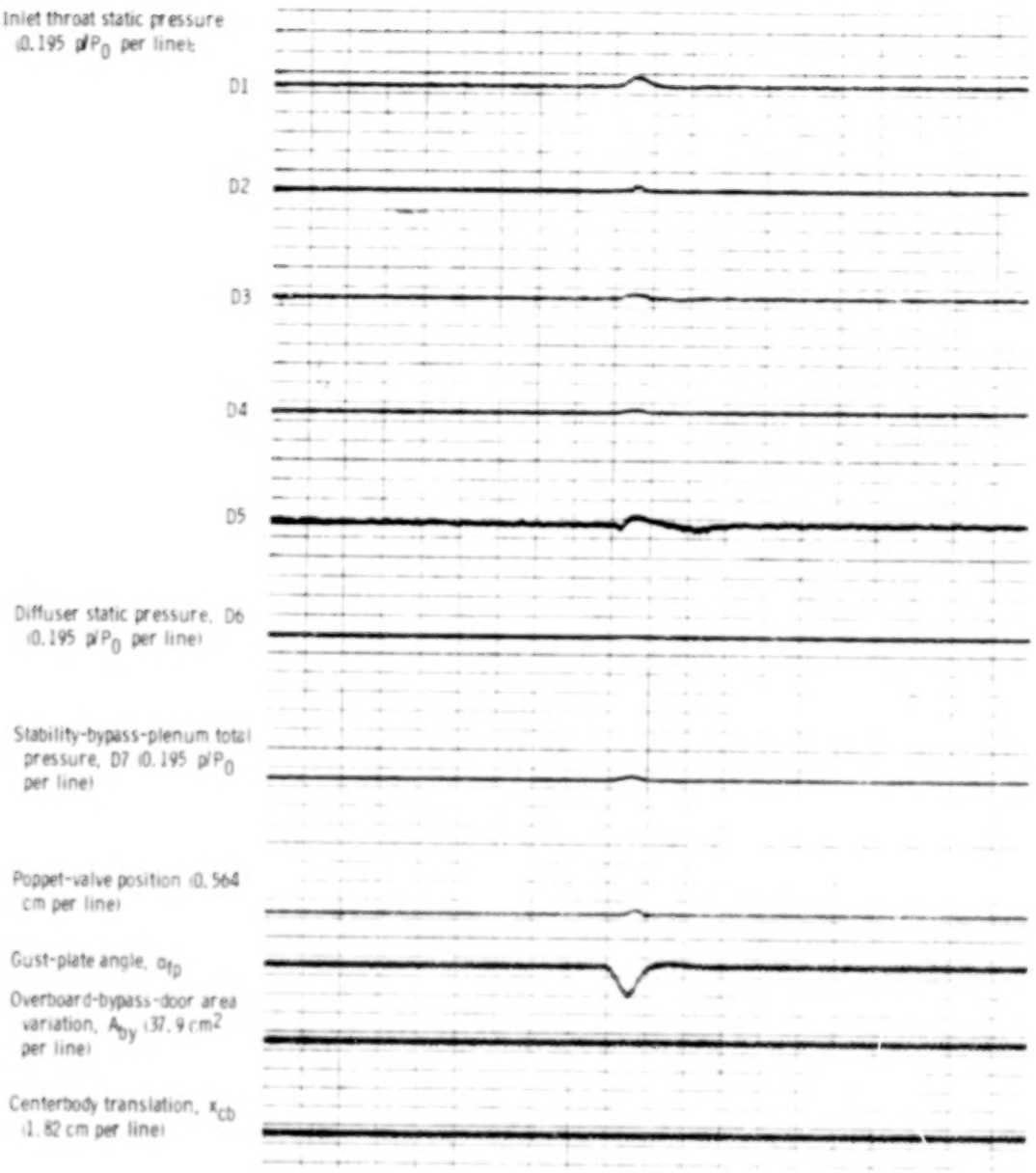

(b) Transient flat gust-plate angle, $\alpha_{fp,t}$, 1.2°.

Figure 37. - Concluded.

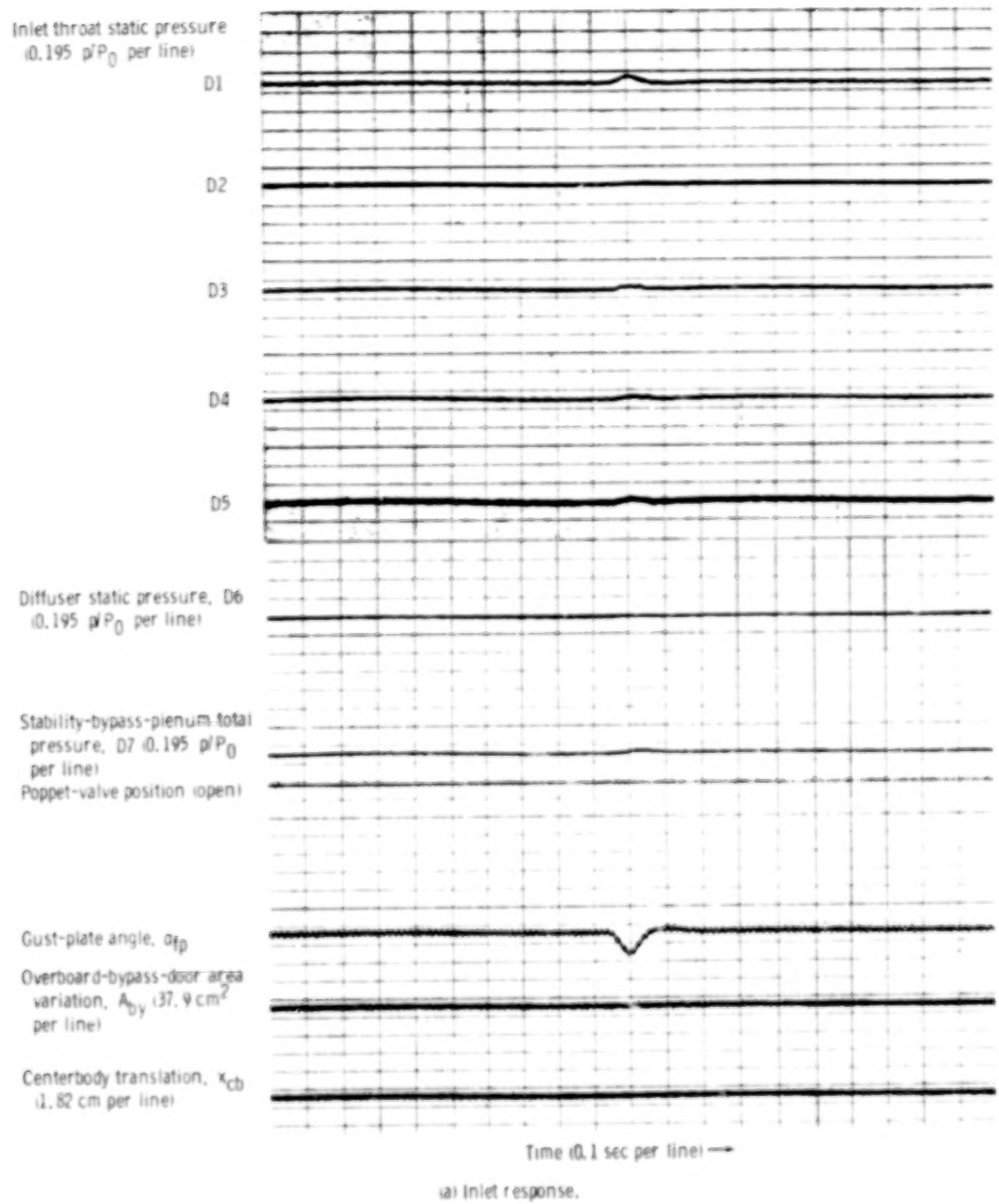

(a) Inlet response.

Figure 38. - External airflow transient induced by flat gust plate, with small, fixed exit as stability-bypass-bleed control and large stability bypass plenum - transient flat-gust plate angle, $\alpha_{fp,t}$, 1.0°; Free-stream Mach number, M_0, 2.5; transient pulse frequency, $1/\tau$, 10 seconds^{-1}; corrected engine speed, $N/N^* \sqrt{\theta}$, 0.871; total-pressure recovery P_2/P_0, 0.903; mass-flow ratio, m_2/m_0, 0.90; primary-nozzle area, A_8, 0.0639 square meter.

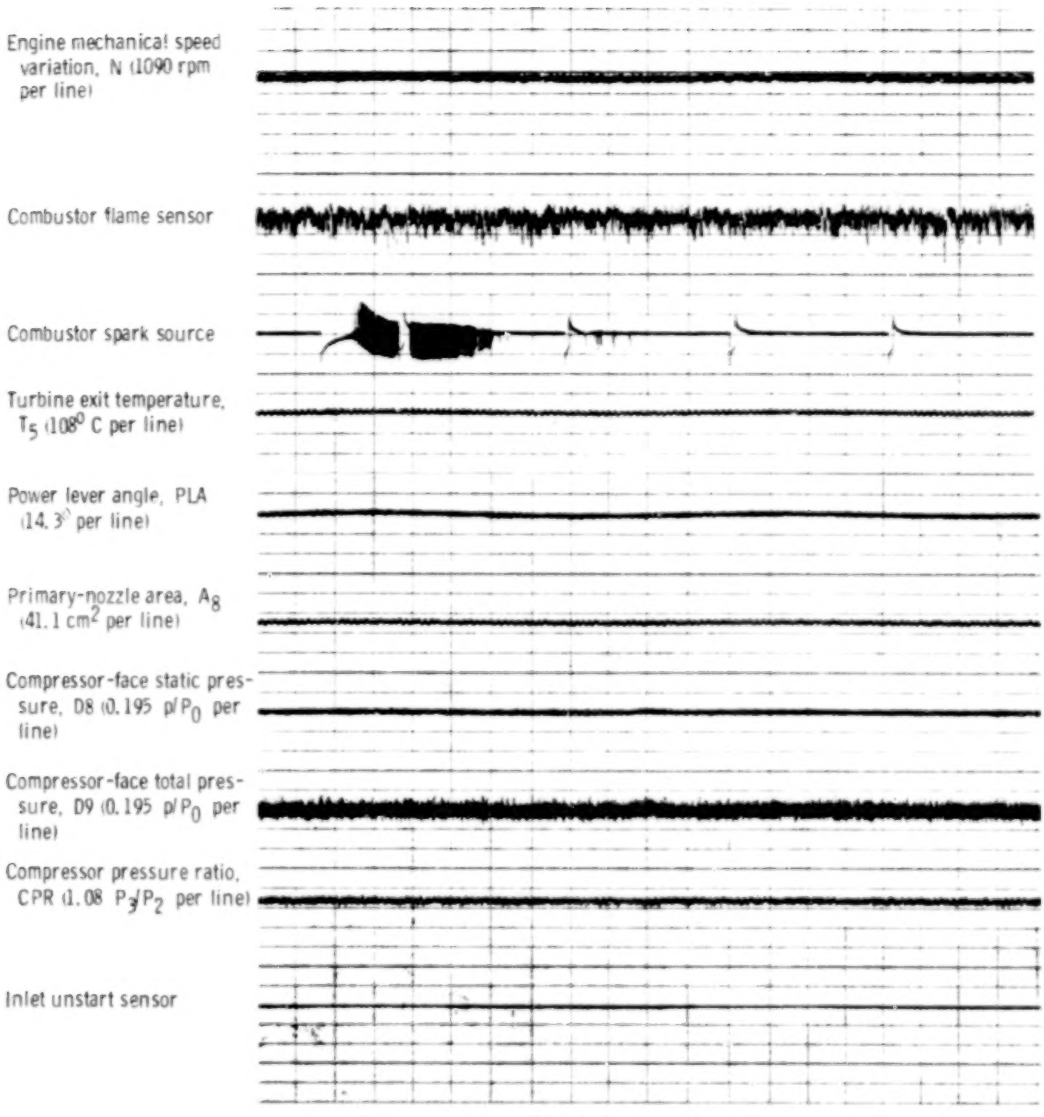

(b) Engine response.

Figure 38. - Concluded.

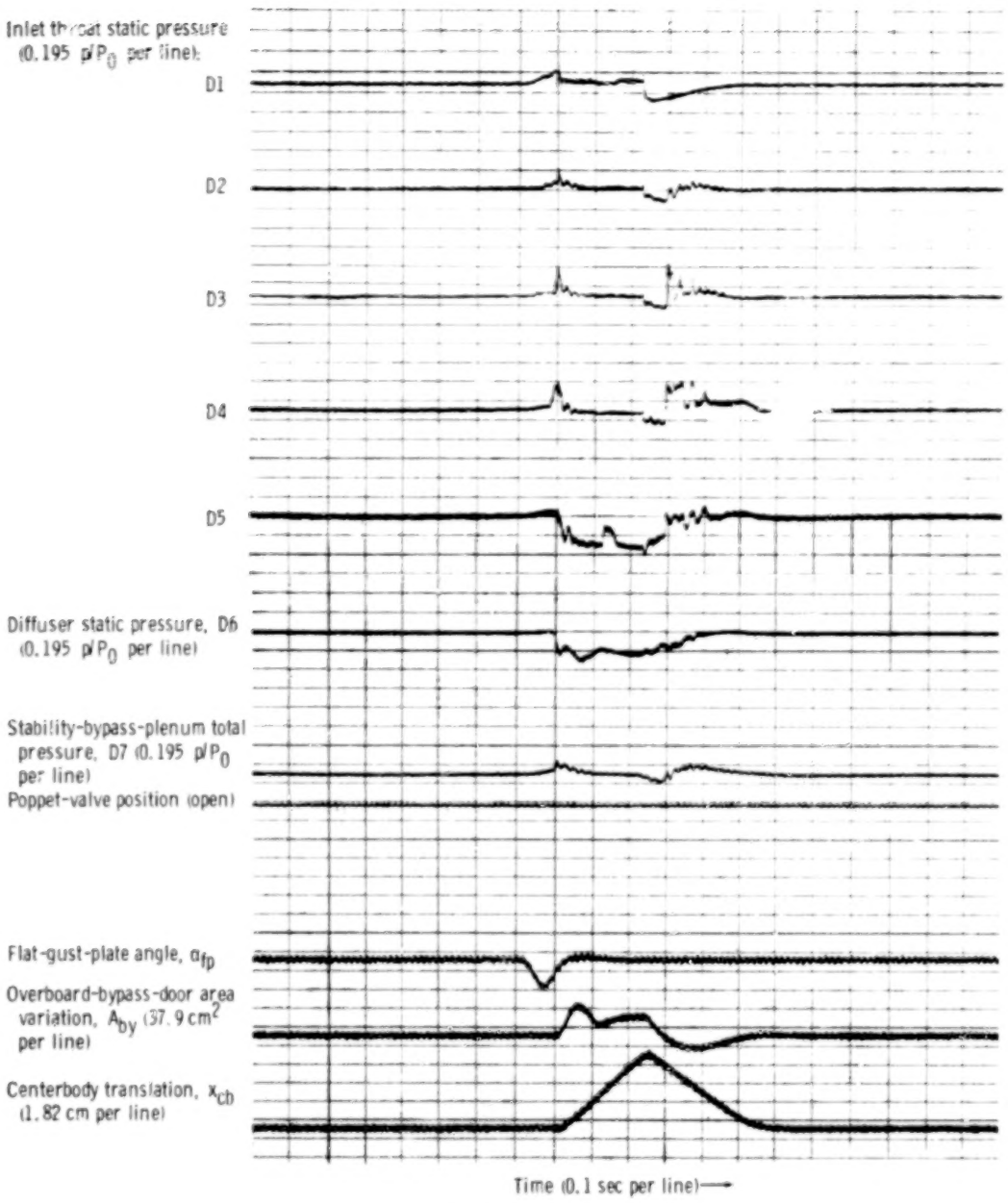

(a) Inlet response.

Figure 39. - External airflow transient induced by flat gust plate, with small, fixed exit as stability-bypass-bleed control and large stability bypass plenum - transient flat-gust-plate angle, $\alpha_{fp,t}$, 1.2^{0}. Free-stream Mach number, M_0, 2.5; transient pulse frequency, $1/\tau$, 10 seconds^{-1}; corrected engine speed, $N/N^{*}\sqrt{\theta}$, 0.871; total-pressure recovery, P_2/P_0, 0.903; mass-flow ratio, m_2/m_0, 0.90; primary-nozzle area, A_8, 0.0639 square meter.

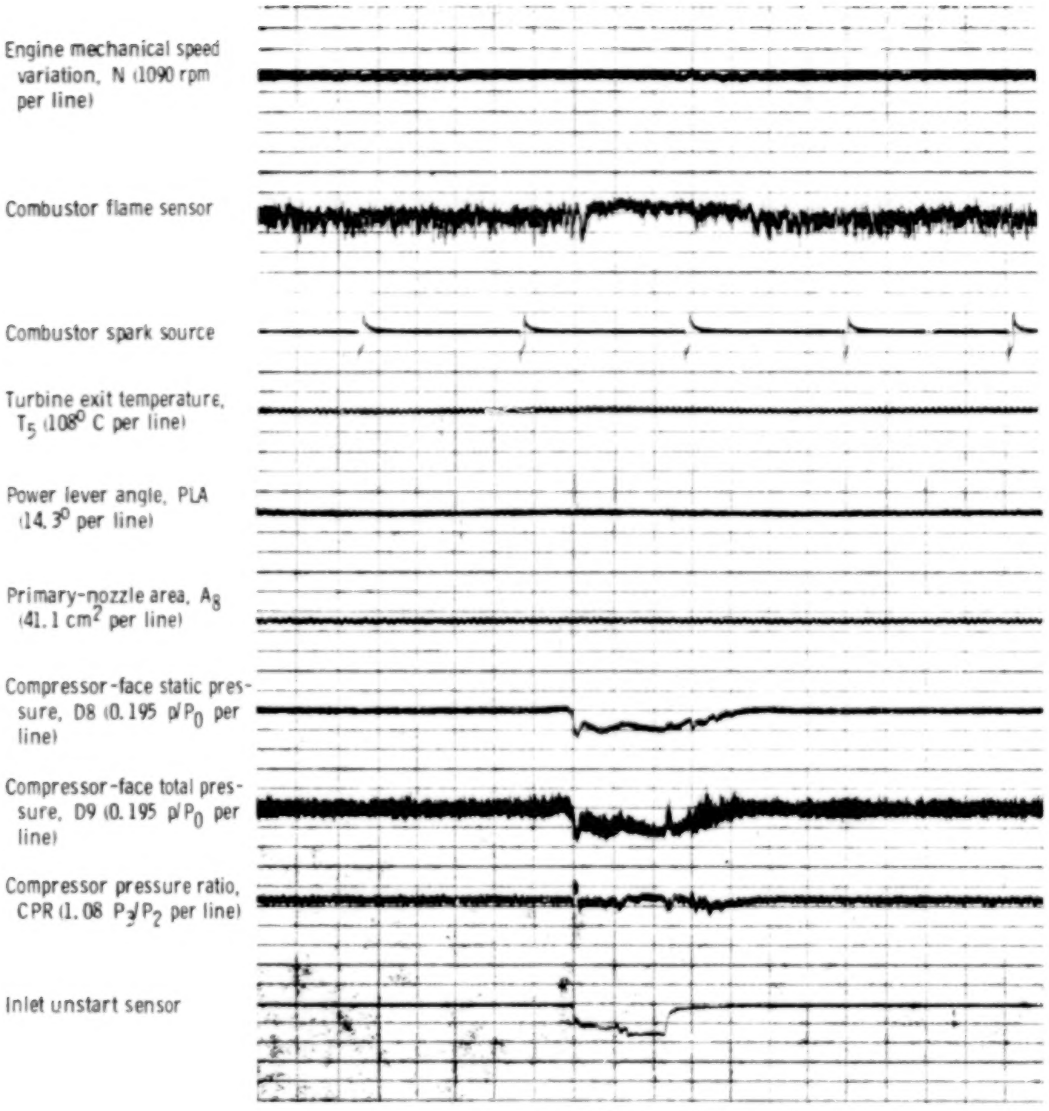

(b) Engine response.

Figure 39. - Concluded.

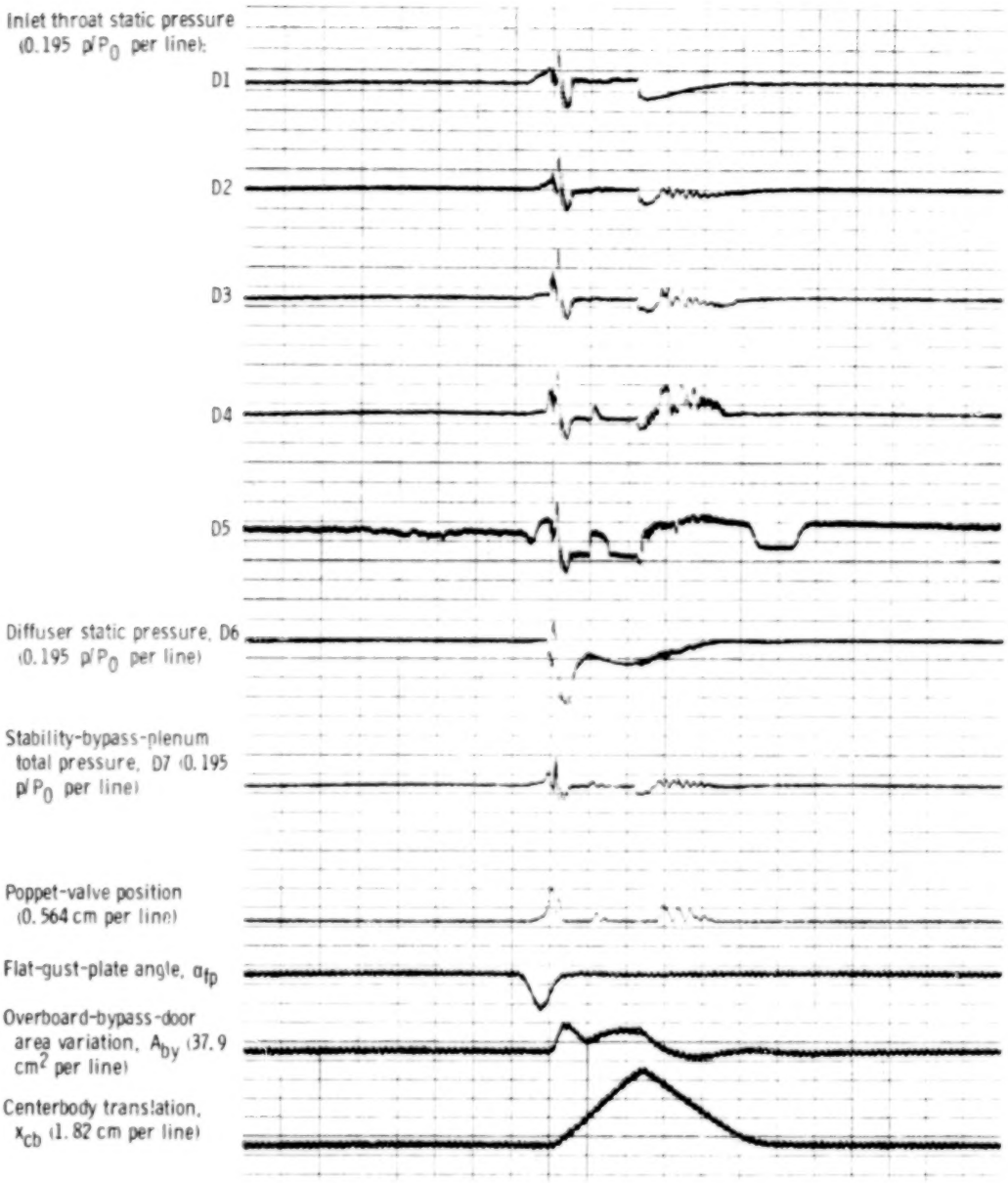

(a) Inlet response.

Figure 40. - External airflow transient induced by flat gust plate, with poppet valves as stability-bypass-bleed-control - transient flat-gust-plate angle, $\alpha_{fp,t}$, 1.4°. Free-stream Mach number, M_0, 2.5; transient pulse frequency, $1/\tau$, 10 seconds^{-1}; corrected engine speed, $N/N^* \sqrt{\theta}$, 0.873; total-pressure recovery, P_2/P_0, 0.901; mass-flow ratio, m_2/m_0, 0.903; primary-nozzle area, A_8, 0.0639 square meter.

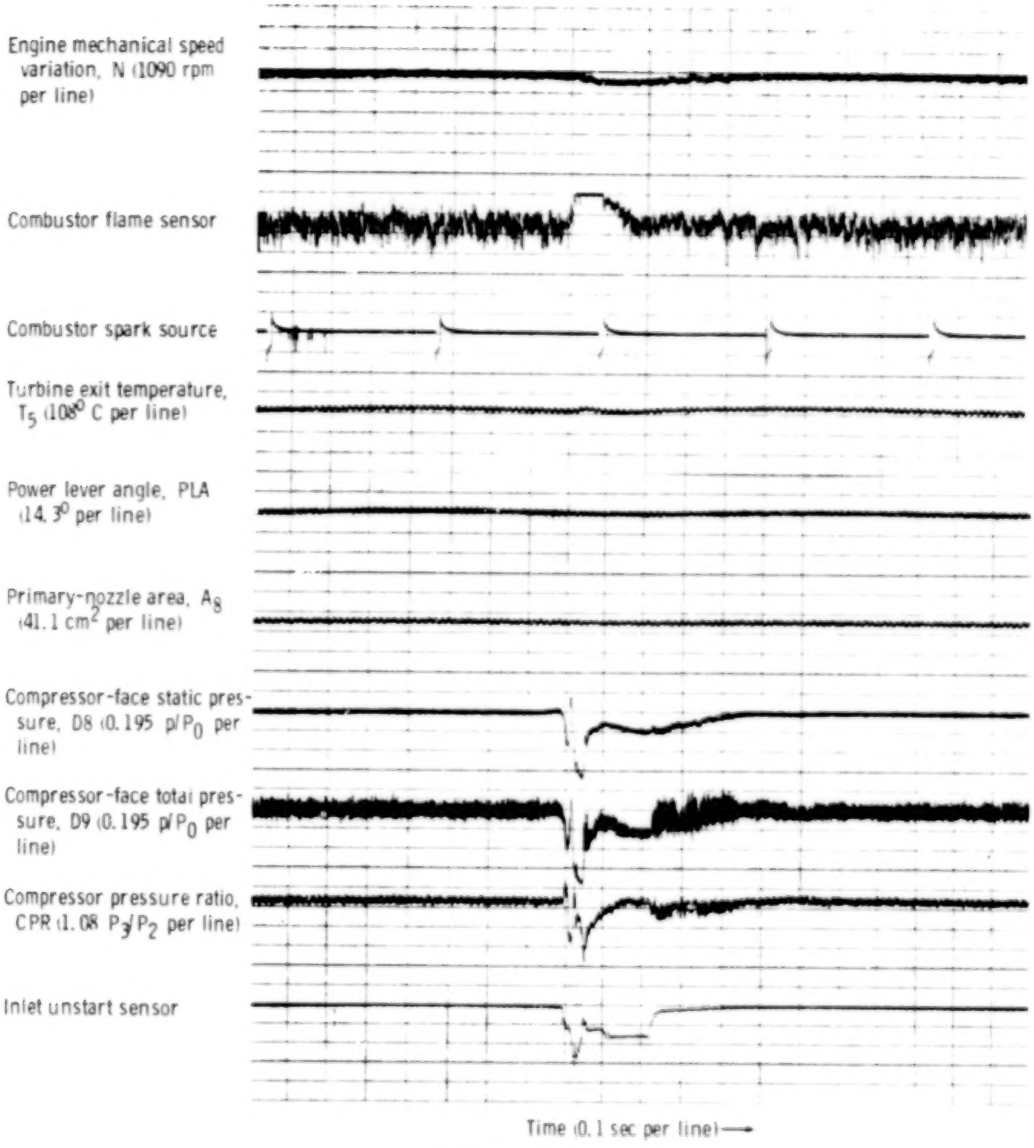

(b) Engine response.

Figure 40. - Concluded.

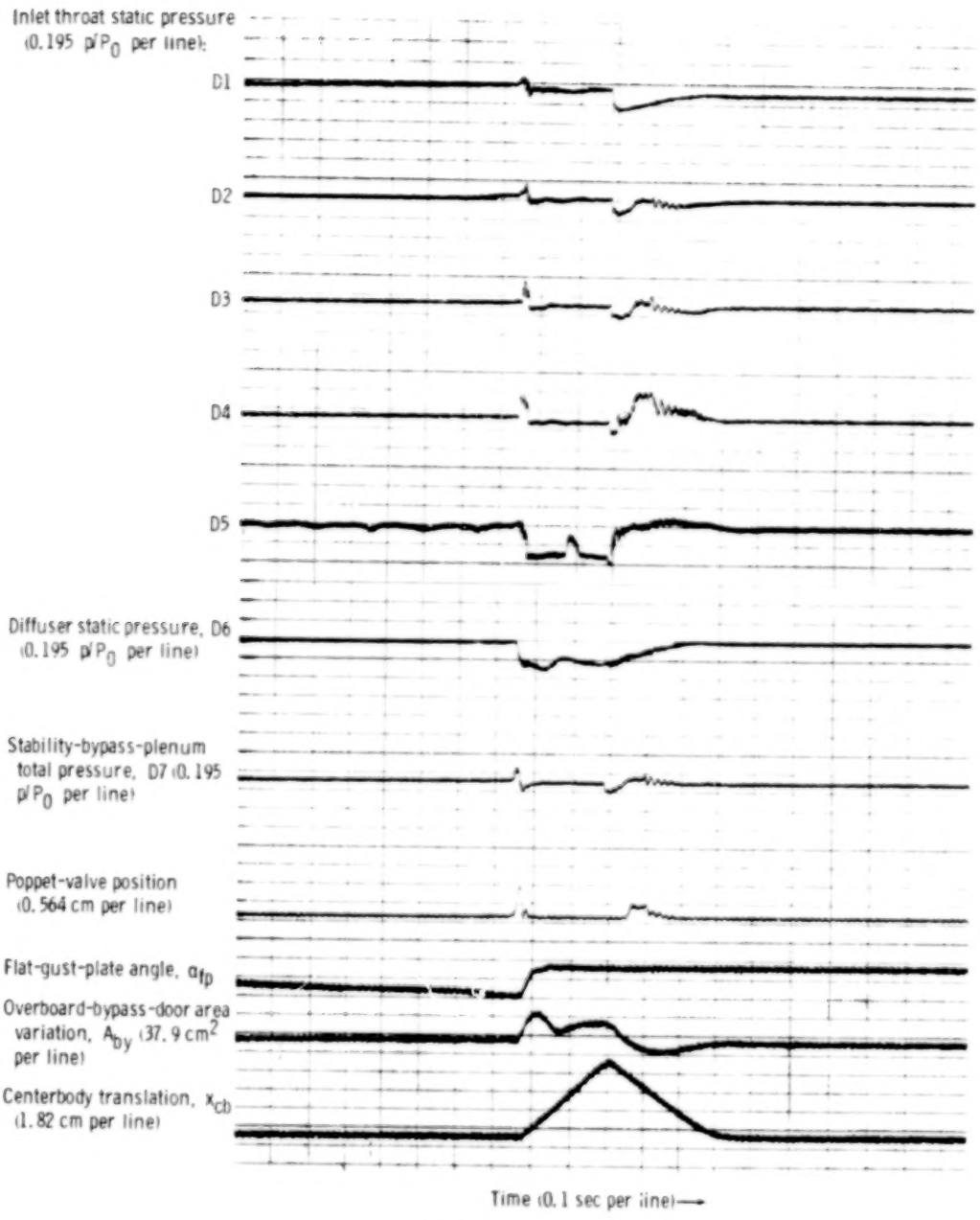

(a) Inlet response.

Figure 41. - Slow, manual change in flat-gust-plate angle of attack to inlet unstart, with poppet valves as stability-bypass-bleed control. Free-stream Mach number, M_0, 2.5; corrected engine speed, $N/N^{\circ}\sqrt{\theta}$, 0.873; total-pressure recovery, P_2/P_0, 0.901; mass-flow ratio, m_2/m_0, 0.913; primary-nozzle area, A_8, 0.0805 square meter.

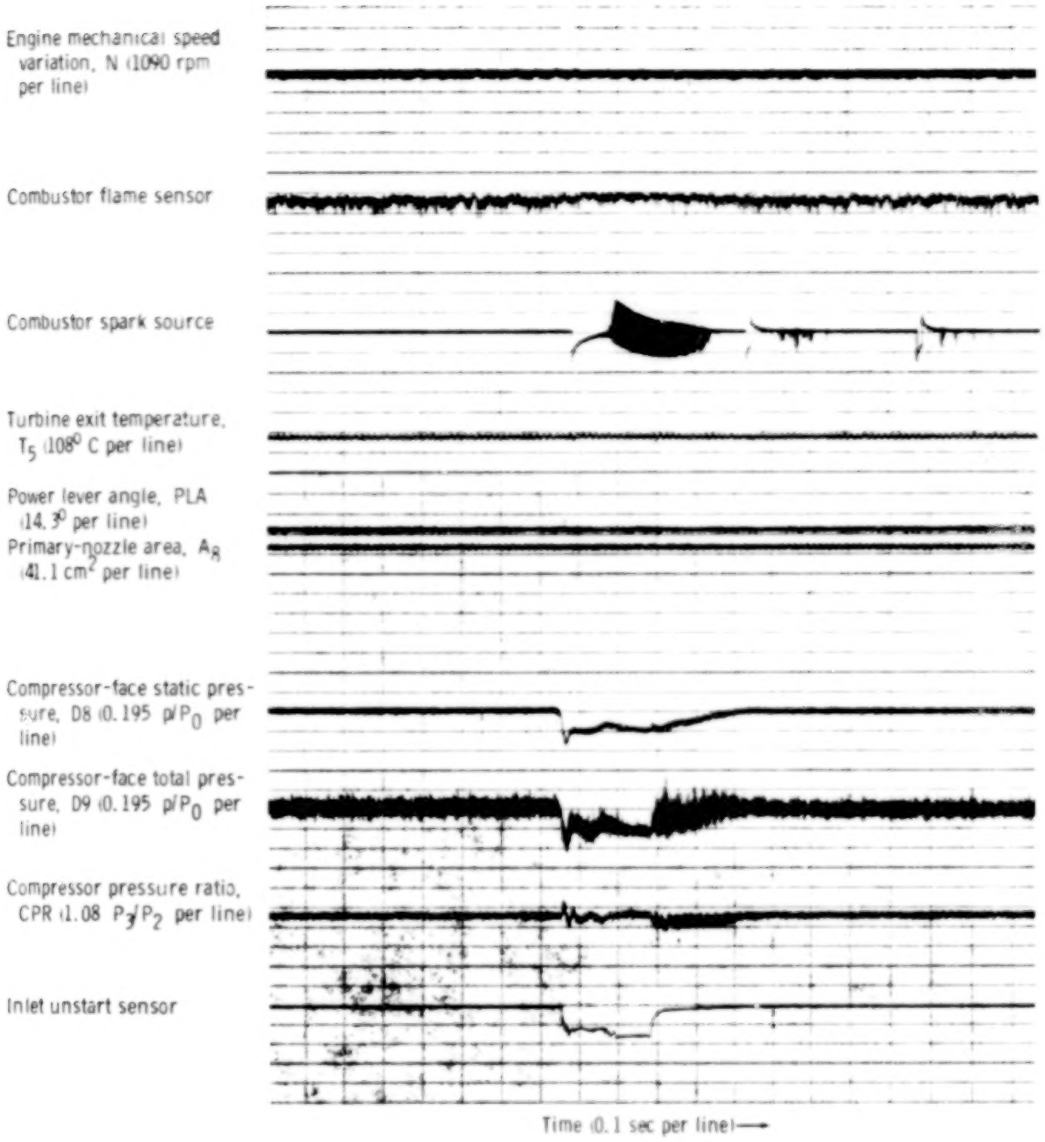

(b) Engine response.

Figure 41. - Concluded.

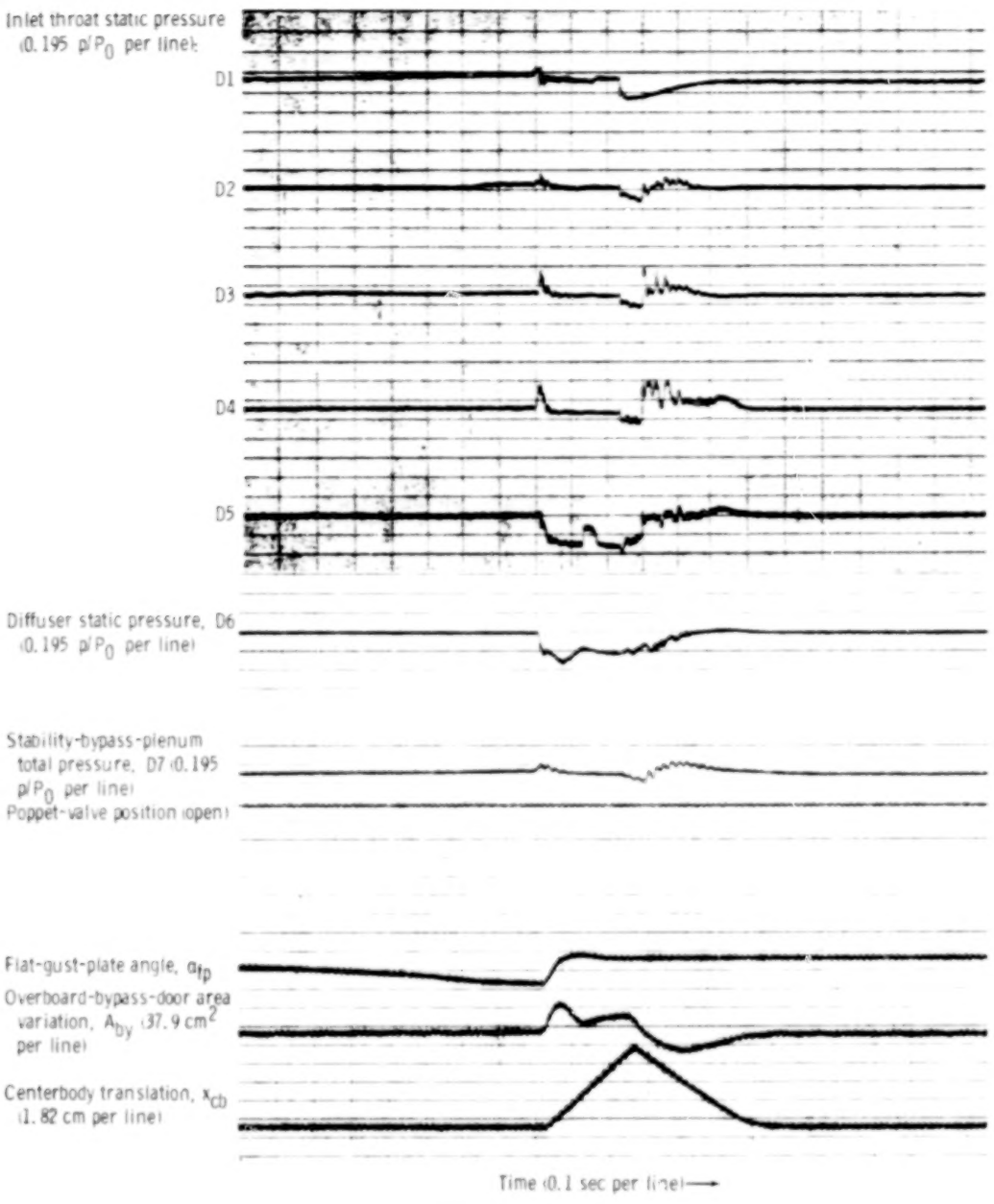

(a) Inlet response.

Figure 42. - Slow, manual change in flat-gust-plate angle of attack to inlet unstart with small, fixed exit as stability-bypass-bleed control and large stability bypass plenum. Free-stream Mach number, M_0, 2.5; corrected engine speed, $N/N^* \sqrt{\theta}$, 0.872; total-pressure recovery, P_2/P_0, 0.901; mass-flow ratio, m_2/m_0, 0.901; primary-nozzle area, A_8, 0.0656 square meter.

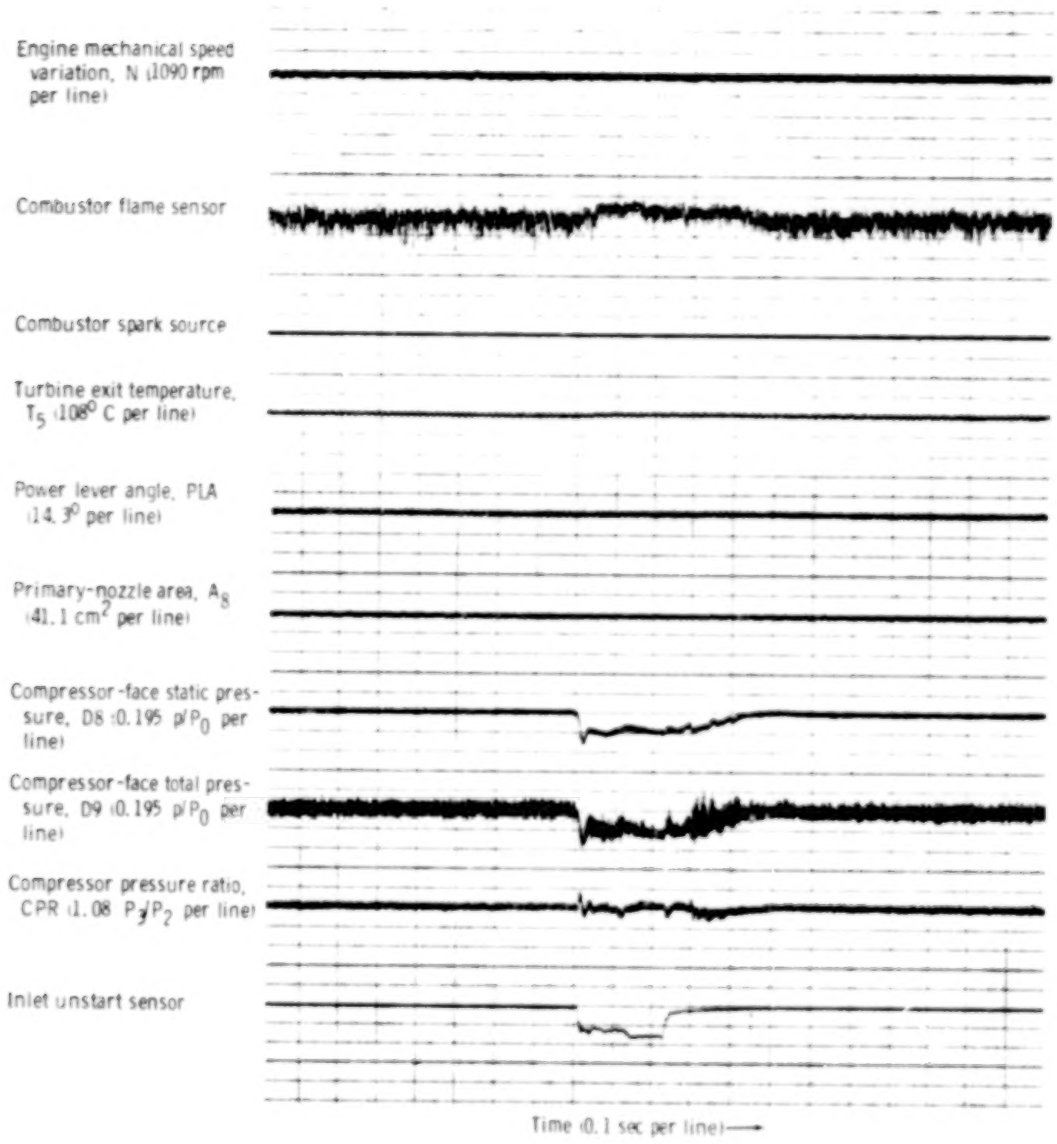

(b) Engine response.

Figure 42. - Concluded.

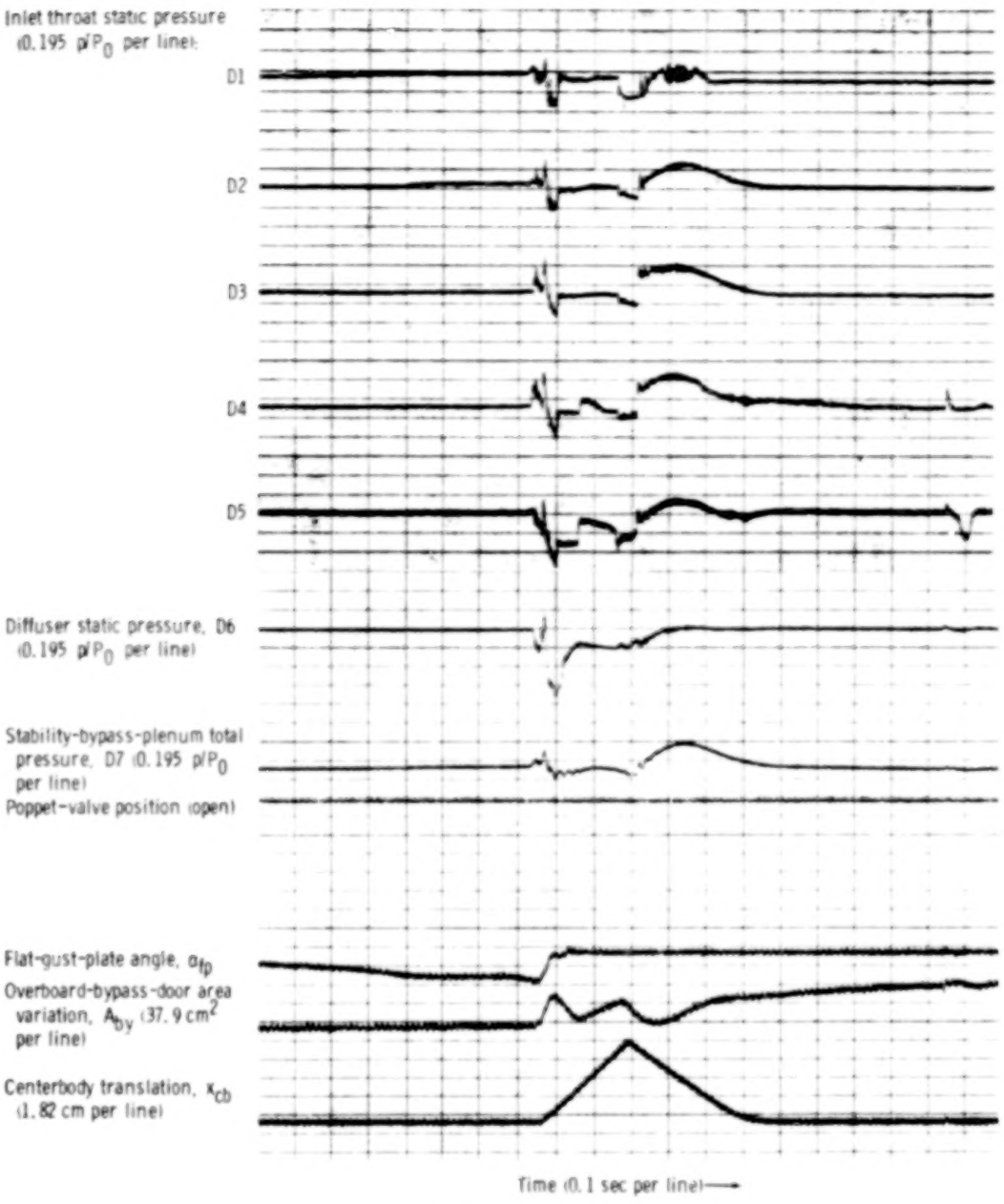

(a) Inlet response.

Figure 43. - Compressor stall and combustor blowout caused by slow, manual change in flat-gust-plate angle of attack to inlet unstart, with small, fixed exit as stability-bypass-bleed control and large stability bypass plenum. Free-stream Mach number, M_0, 2.5; corrected engine speed, $N/N^* \sqrt{\theta}$, 0.871; total-pressure recovery, P_2/P_0, 0.903; mass-flow ratio, m_2/m_0, 0.904; primary-nozzle area, A_8, 0.0643 square meter.

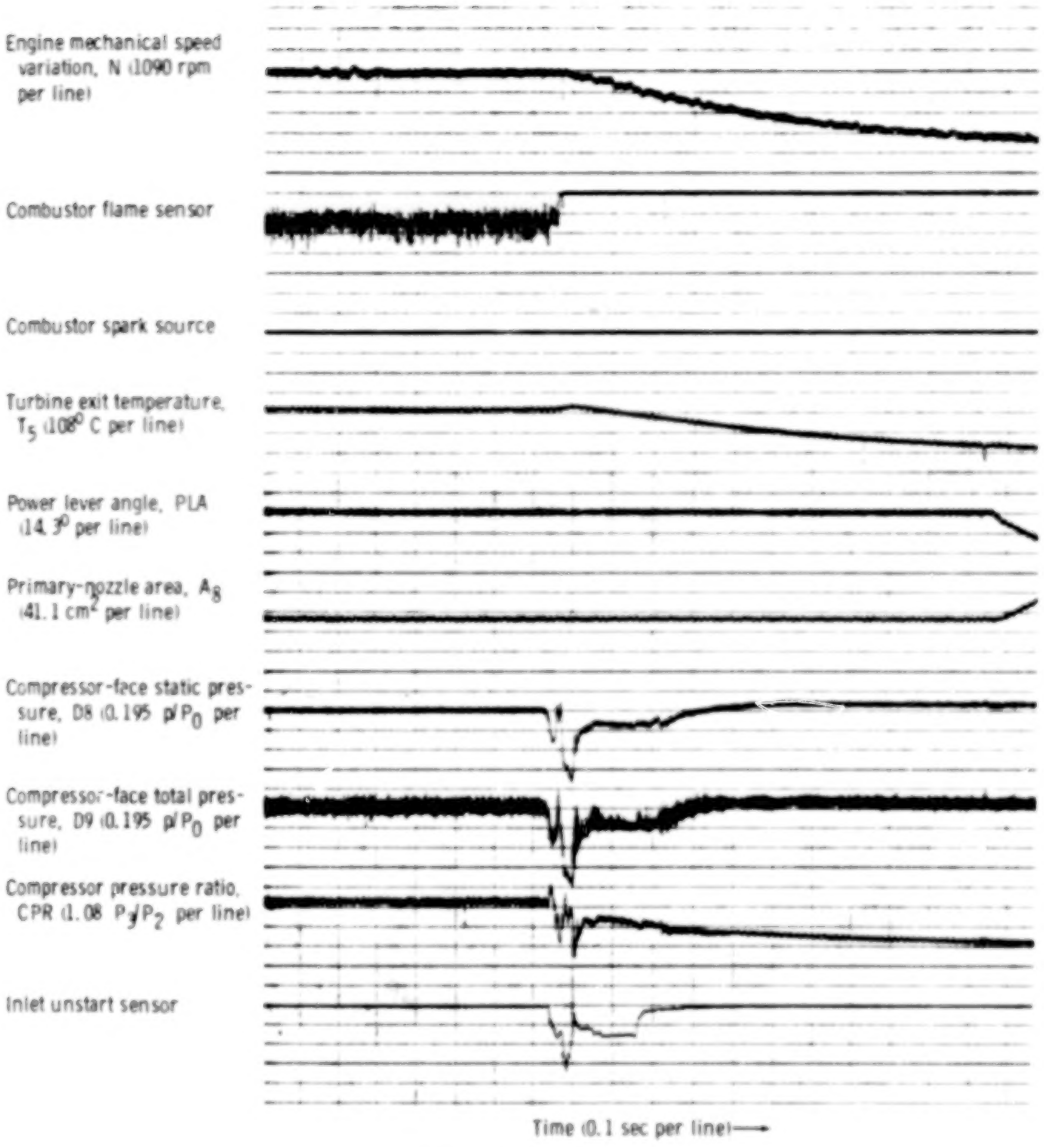

(b) Engine response.

Figure 43. - Concluded.

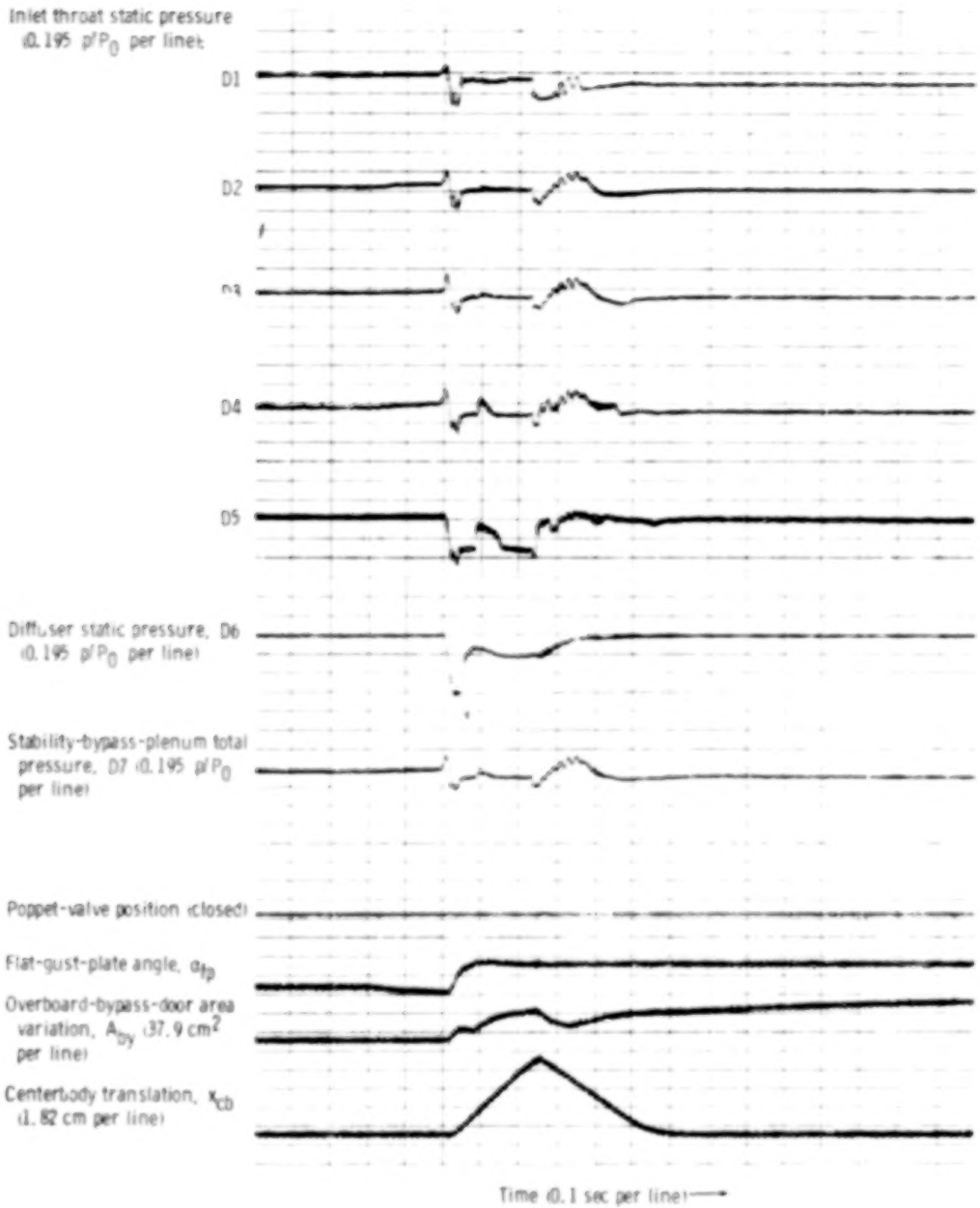

(a) Inlet response.

Figure 44. - Slow, manual change in flat-gust-plate angle of attack to inlet unstart, with small, fixed exit as stability-bypass-bleed control and small stability bypass plenum. Free-stream Mach number, M_0, 2.5; corrected engine speed, $N/N^\circ\sqrt{\theta}$, 0.873; total-pressure recovery, P_2/P_0, 0.900; mass-flow ratio, $\dot{m}_2/\dot{m}_0$, 0.910; primary-nozzle area, A_8, 0.0812 square meter.

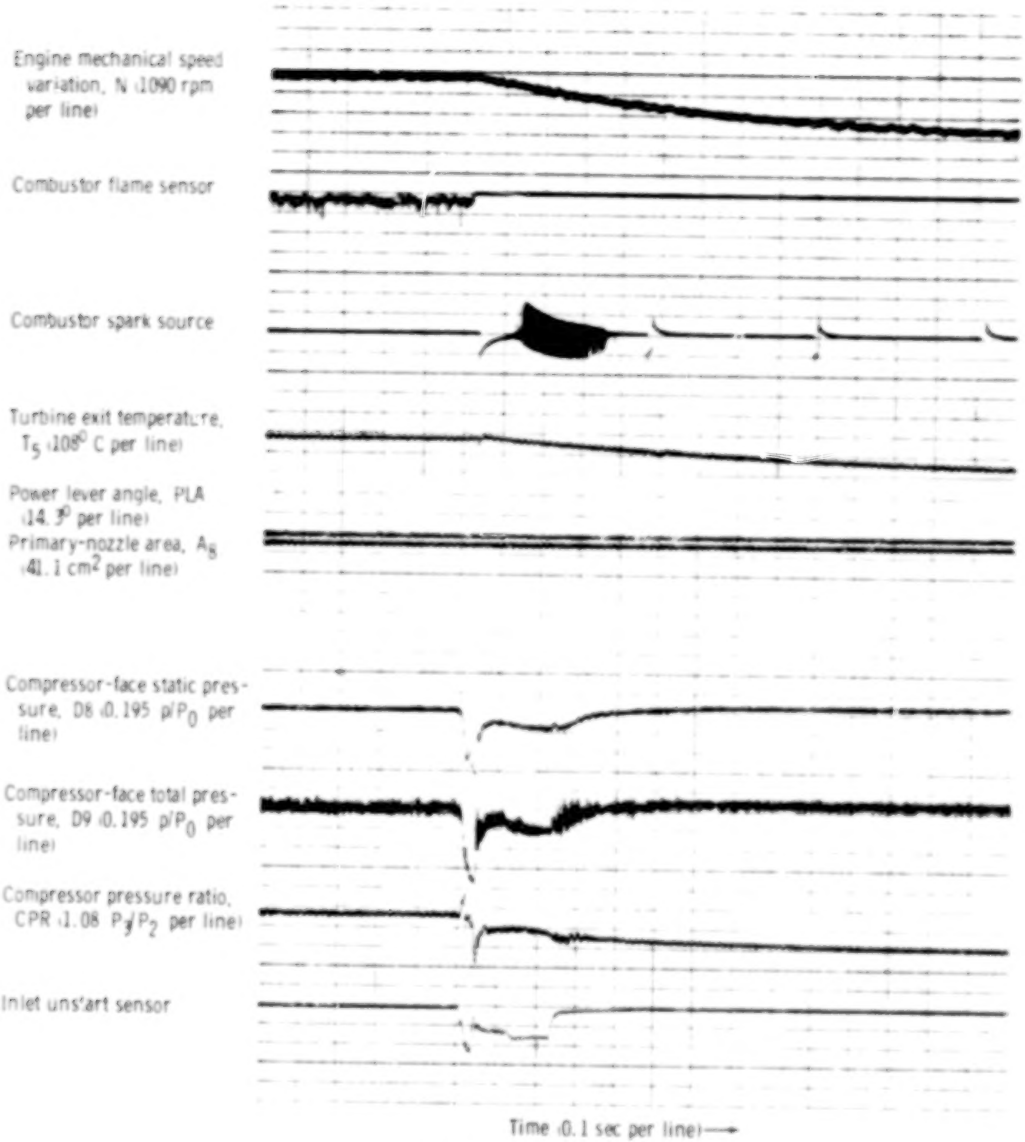

(b) Engine response.

Figure 44. - Concluded.

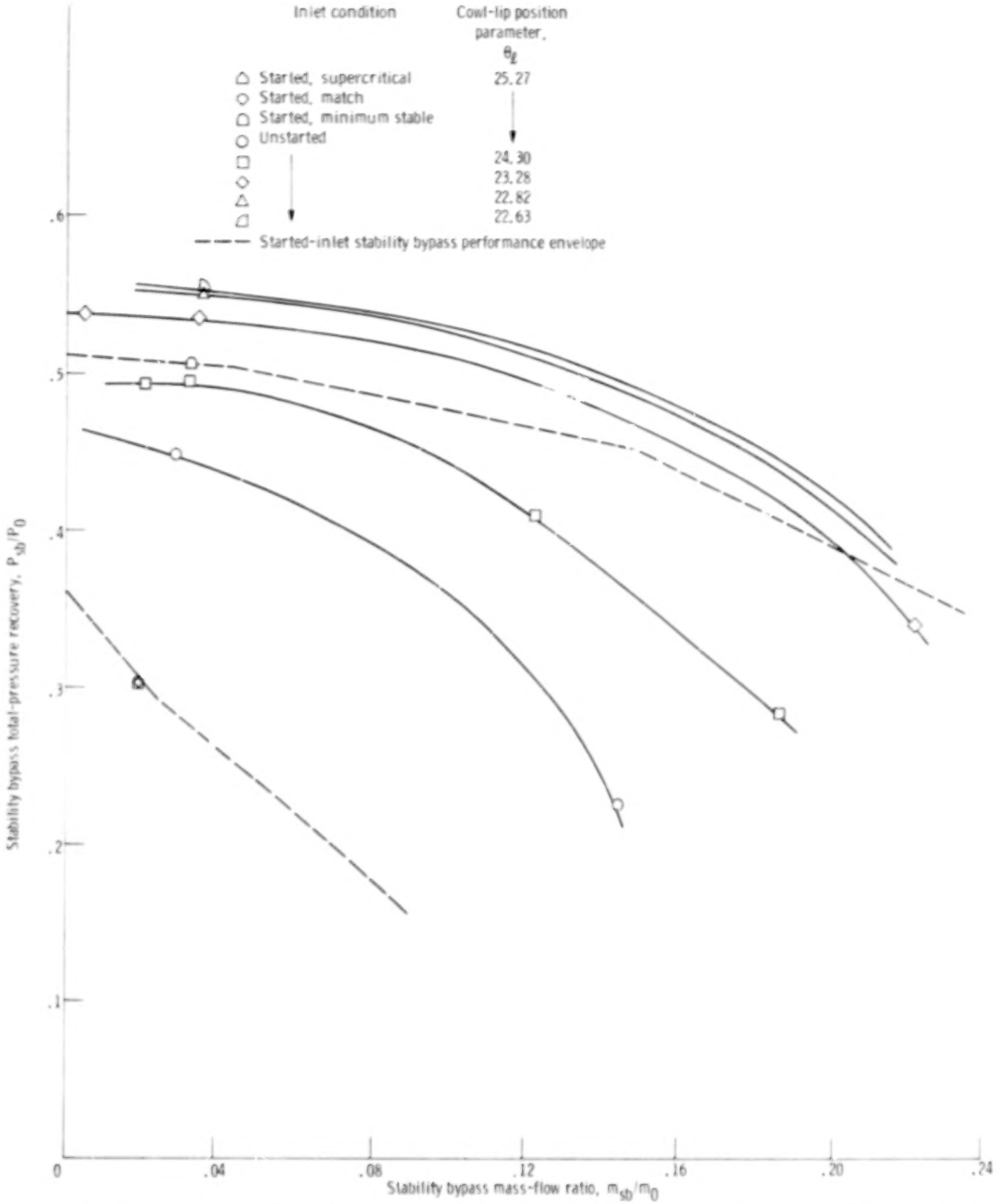

Figure 45. - Inlet-stability bypass system performance for started- and unstarted-inlet conditions. Free-stream Mach number, M_0, 2.5.

CONTENTS

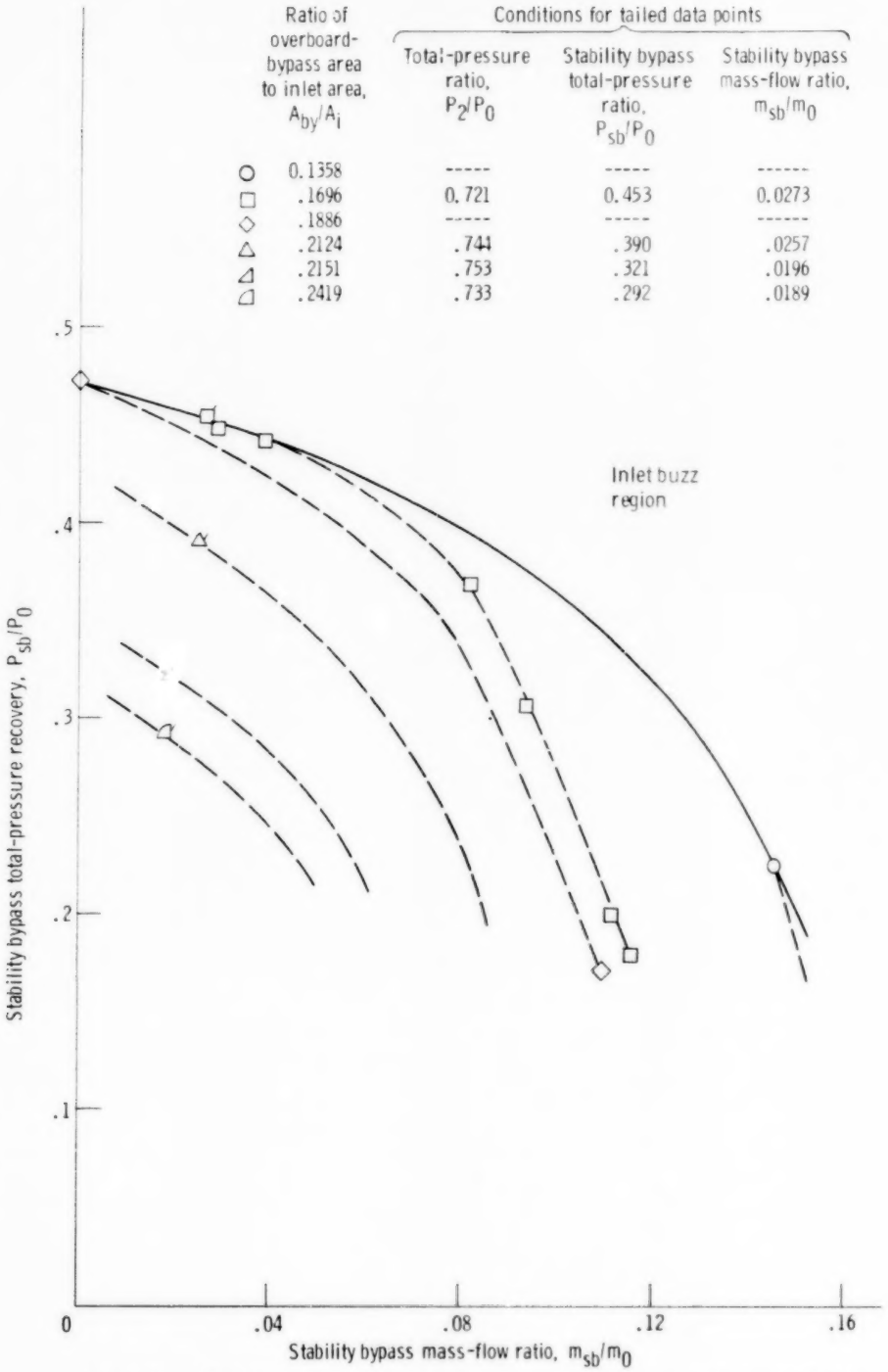

Figure 46. - Effect of varying overboard-bypass area on stability bypass performance of an unstarted inlet with centerbody at design position. Free-stream Mach number, M_0, 2.5; cowl-lip position parameter, θ_ℓ, 25.27.

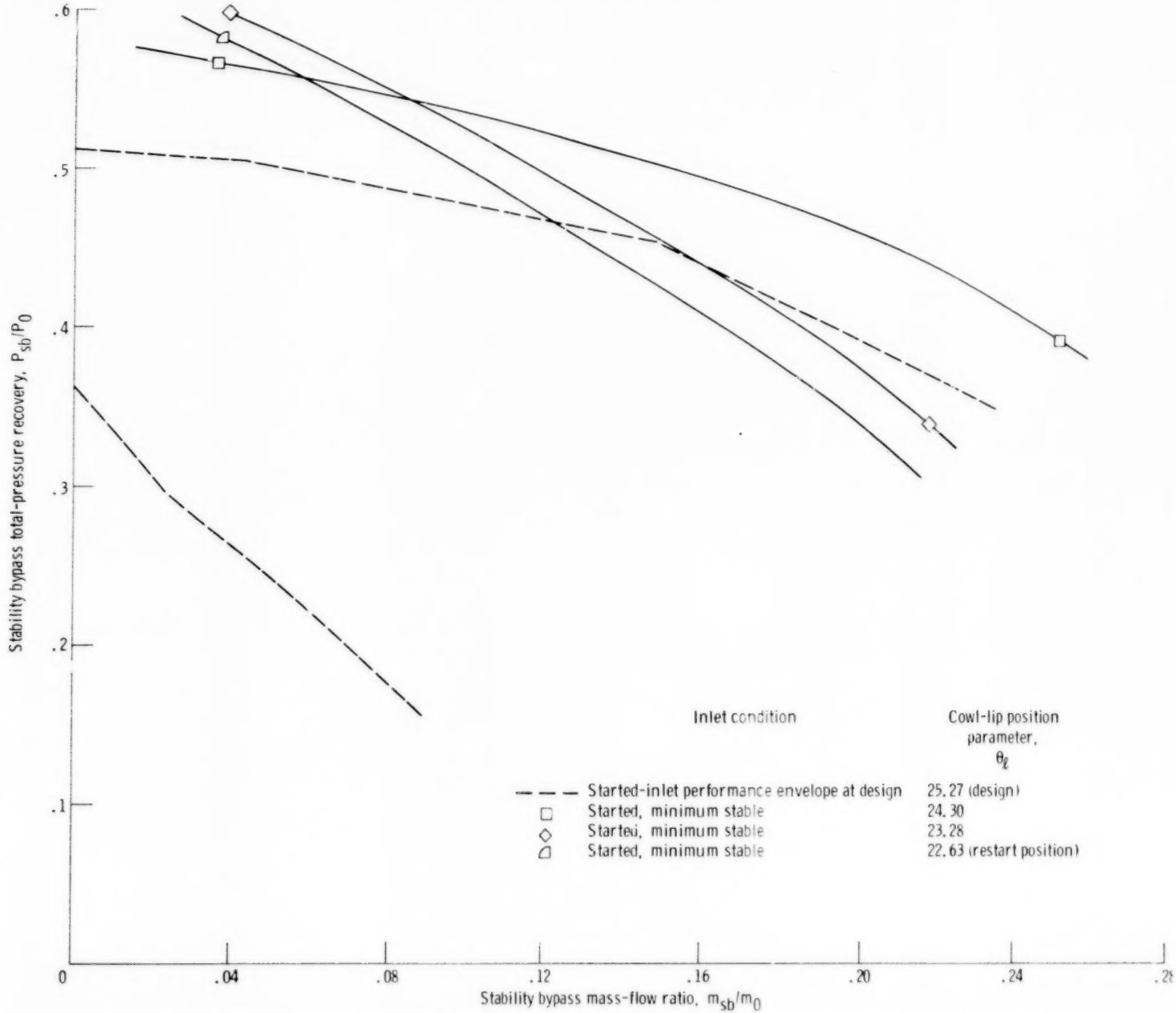

Figure 47. - Effect of centerbody extension on started-inlet stability bypass performance. Free-stream Mach number, M_0, 2.5.

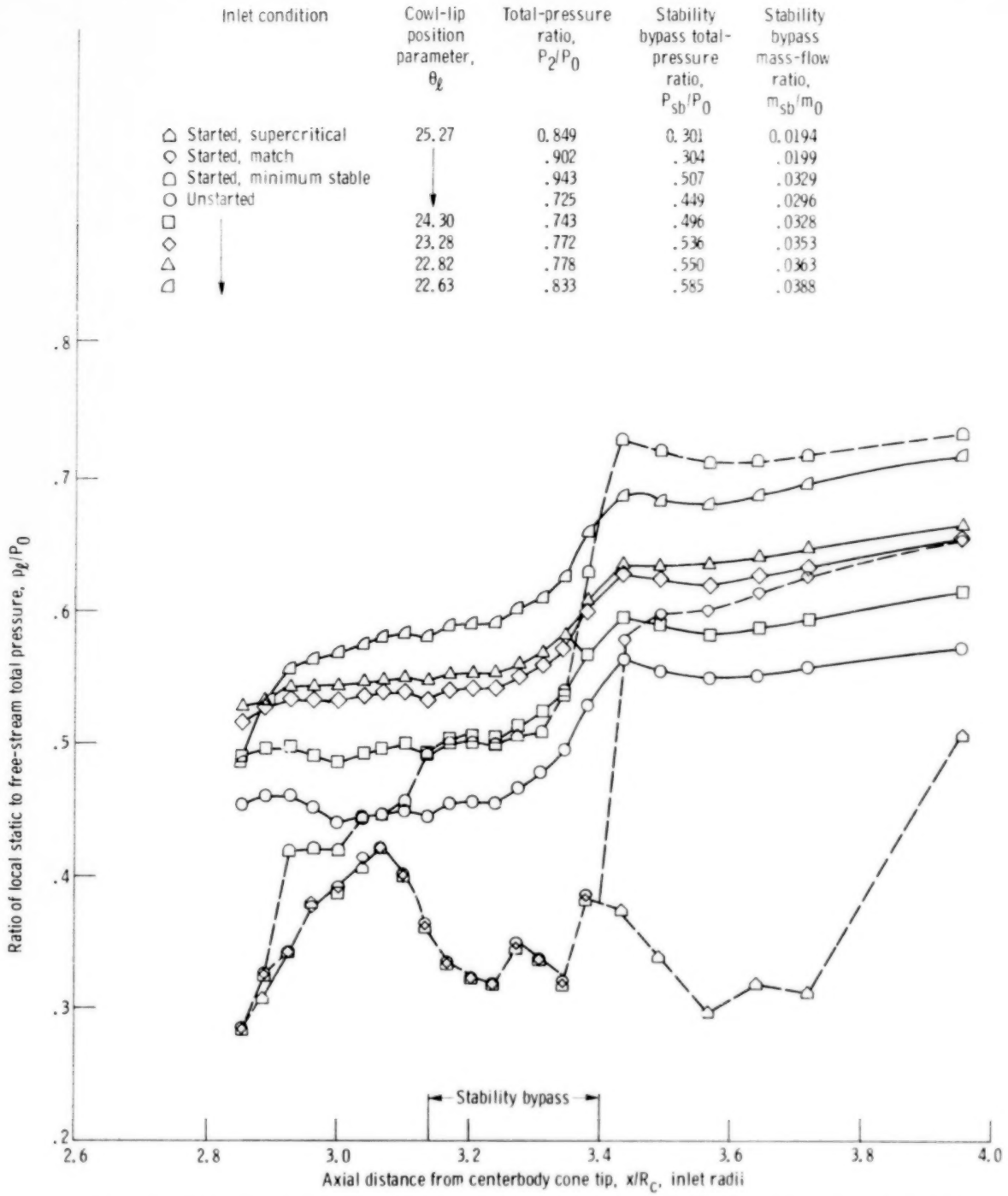

Figure 48. - Cowl surface static-pressure distributions for started- and unstarted-inlet conditions. Free-stream Mach number, M_0, 2.5.

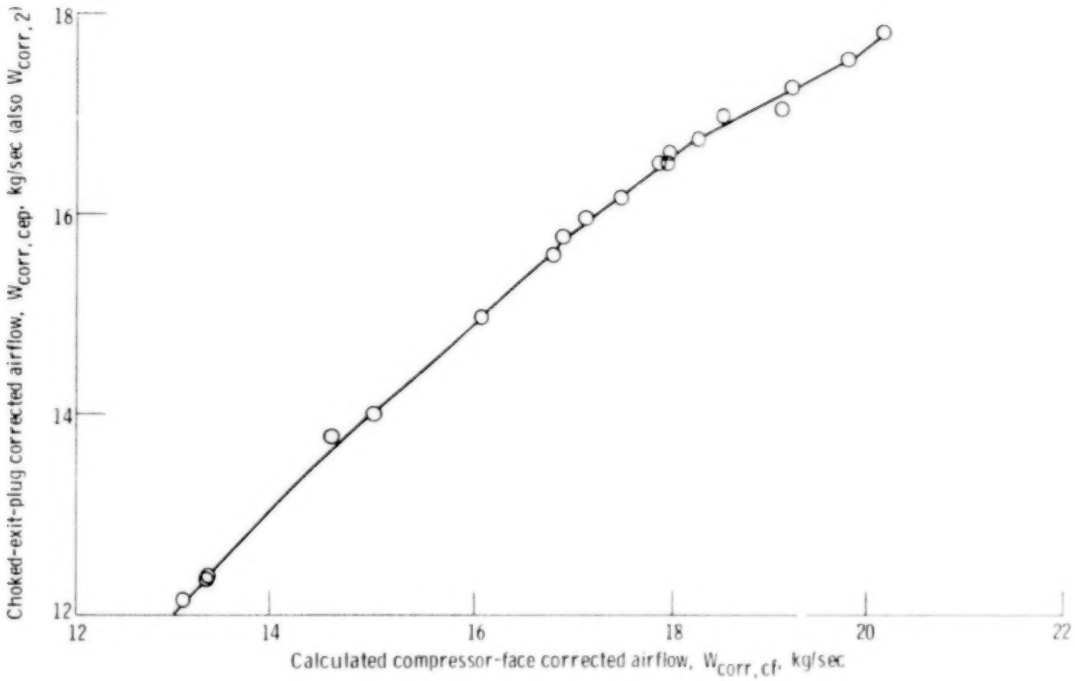

Figure 49. - Compressor-face corrected airflow calibration.

1. Report No.	2. Government Accession No.	3. Recipient's Catalog No.
NASA TP-1531		

4. Title and Subtitle	5. Report Date
DYNAMIC RESPONSE OF A MACH 2.5 AXISYMMETRIC INLET AND TURBOJET ENGINE WITH A POPPET-VALVE-CONTROLLED INLET-STABILITY BYPASS SYSTEM WHEN SUBJECTED TO INTERNAL AND EXTERNAL AIRFLOW TRANSIENTS	January 1980
	6. Performing Organization Code

7. Author(s)	8. Performing Organization Report No.
Bobby W. Sanders	E-9467
	10. Work Unit No.
	505-04

9. Performing Organization Name and Address	11. Contract or Grant No.
National Aeronautics and Space Administration Lewis Research Center Cleveland, Ohio 44135	
	13. Type of Report and Period Covered
12. Sponsoring Agency Name and Address	Technical Paper
National Aeronautics and Space Administration Washington, D.C. 20546	14. Sponsoring Agency Code

15. Supplementary Notes

16. Abstract

The throat of a Mach 2.5 inlet that was attached to a turbojet engine was fitted with a poppet-valve-controlled stability bypass system that was designed to provide a large, stable airflow range. Propulsion system response and stability bypass performance were determined for several transient airflow disturbances, both internal and external. Internal airflow disturbances included reductions in overboard bypass airflow, power lever angle, and primary-nozzle area as well as compressor stall. For reference, data are also included for a conventional, fixed-exit bleed system. The poppet valves greatly increased inlet stability and had no adverse effects on propulsion system performance. Limited unstarted-inlet bleed performance data are presented.

17. Key Words (Suggested by Author(s))	18. Distribution Statement
Air intakes; Supersonic cruise inlets; Shock stability; Inlet bleed; Turbojet engine; Stability bypass	Unclassified - unlimited STAR Category 07

19. Security Classif. (of this report)	20. Security Classif. (of this page)	21. No. of Pages	22. Price*
Unclassified	Unclassified	100	A05

* For sale by the National Technical Information Service, Springfield, Virginia 22161

NASA-Langley, 1980